

© 2014 Rabie Abdullah Abu Saleem

TWO-PHASE TWO-FLUID MODEL SOLVER BASED ON A HIGH-RESOLUTION TOTAL
VARIATION DIMINISHING SCHEME

BY

RABIE ABDULLAH ABU SALEEM

DISSERTATION

Submitted in partial fulfillment of the requirements
for the degree of Doctor of Philosophy in Nuclear, Plasma, and Radiological Engineering
in the Graduate College of the
University of Illinois at Urbana-Champaign, 2014

Urbana, Illinois

Doctoral Committee:

Assistant Professor Tomasz Kozlowski, Chair
Research Scientist Dr. Brian F. Jewett
Professor Rizwan Uddin
Associate Professor Magdi Ragheb

ABSTRACT

A new numerical method and a solver for the two-phase two-fluid model are developed using an innovative high-resolution, Total Variation Diminishing (TVD) scheme. The new scheme is derived first for scalar hyperbolic problems using the method of flux limiters, then extended to the two-phase two-fluid model.

A hybridization of the monotone 1st-order upwind scheme and the Quadratic Upstream Interpolation scheme (QUICK) is implemented using a new flux limiter function. The new function is derived in a systematic manner by imposing conditions necessary to ensure the TVD properties of the resulting scheme. For temporal discretization, the theta method is used, and values for the parameter θ are chosen such that the scheme is unconditionally stable ($1/2 \leq \theta \leq 1$). Finite volume techniques with staggered mesh are then used to develop a solver for the one-dimensional two-phase two-fluid model based on different numerical schemes including the new scheme developed here. Linearized equations of state are used as closure relations for the model, with linearization derivatives calculated numerically using water properties based on the IAPWS IF-97 standard.

Numerical convergence studies were conducted to verify, first, the new numerical scheme and then, the two-phase two-fluid solver. Numerical scheme results are presented for one-dimensional pure advection problem with smooth and discontinuous initial conditions and compared to those of other classical and high-resolution numerical schemes. Convergence rates for the new scheme are examined and shown to be higher compared to those of other schemes. For smooth solutions, the new scheme was found to exhibit a convergence rate of 1.3 and a convergence rate of 0.82 for discontinuous solutions. The two-phase two-fluid model solver is implemented to analyze numerical benchmark problems for verification and testing its abilities to handle discontinuities and fast transients with phase change. Convergence rates are investigated by comparing numerical results to analytical solutions available in literature for the case of the faucet flow problem. The new solver based on the new TVD scheme is shown to exhibit higher-order accuracy compared to other numerical schemes with convergence rate of 0.8. Mass errors are also examined when phase change occurs for the shock tube problem, and compared to those of the 1st-order upwind scheme implemented in common nuclear thermal-hydraulics codes like TRACE and RELAP5. The solver is shown to exhibit numerical stability when implemented to problems with discontinuous solutions and results of the new solver were free of spurious oscillations.

To my beloved parents

Acknowledgments

First and foremost, all my gratefulness is due to God Almighty for guiding me through to be able to complete this work. I would also like to thank my family, especially my parents, for all the support and encouragement, and for being my inspiration and the reason I seek knowledge.

I would like to take this opportunity to express my sincere gratitude towards my advisor Professor Tomasz Kozlowski for his valuable support and patience throughout the entire work of this research. His insight, guidance and encouragement made it possible to put this work together in its present shape.

I would also like to appreciate and thank Dr. Brian Jewett, Professor Rizwan Uddin and Professor Magdi Ragheb for serving on my defense committee. Especially Professor Rizwan, for I started my journey in the University of Illinois under his supervision and following his guidance.

I would also like to thank all my friends who shared with me the good times and the bad times through this journey. Special thanks to Rijan Shrestha and Tamir Rousan for all the continuing genuine support they provided. Finally, I would like to acknowledge all the faculty and staff of NPPE department for their help and guidance.

Table of Contents

<i>LIST OF FIGURES</i>	<i>vii</i>
<i>LIST OF TABLES</i>	<i>x</i>
<i>CHAPTER 1. INTRODUCTION</i>	<i>1</i>
1.1 Two-Phase Flow: Classification and Mathematical Models.....	2
1.1.1 Two-Phase Flow Classification	2
1.1.2 Balance Equations and Mathematical Models	4
1.2 Existing Nuclear Codes and the Semi-Implicit Numerical Method.....	6
1.2.1 Existing Nuclear Codes.....	6
1.2.2 The Semi-Implicit Method.....	8
<i>CHAPTER 2. CONSERVATION LAWS AND SOLUTIONS OF HYPERBOLIC PROBLEMS</i>	<i>10</i>
2.1 Linear Hyperbolic Problems	12
2.2 Non-Linear Hyperbolic Problems	17
<i>CHAPTER 3. REVIEW OF NUMERICAL METHODS FOR HYPERBOLIC PROBLEMS</i>	<i>23</i>
3.1 Numerical Notations	24
3.1.1 Forms of Numerical Schemes	25
3.1.2 Local Truncation Error.....	26
3.1.3 The Courant, Friedrichs and Lewy (CFL) Condition.....	27
3.1.4 Total Variation and Monotonicity.....	29
3.2 Linear Numerical Schemes	31
3.2.1 First-Order Accurate Schemes	31
3.2.2 High-Order Accurate Schemes	36
3.3 Non-Linear Schemes.....	39
3.3.1 Reconstruction-Based Methods	39
3.3.2 Flux Limiter Methods	41
3.4 Temporal Discretization.....	46
3.4.1 The Theta Method.....	46
3.4.2 Semi-Discrete Methods.....	48
<i>CHAPTER 4. HIGH-RESOLUTION TVD SCHEME FOR HYPERBOLIC PROBLEMS</i>	<i>49</i>
4.1 Bounds of the TVD Region	50
4.2 High-Order of Accuracy	52
4.3 Numerical Results.....	55

4.3.1	Smooth Initial Conditions	55
4.3.2	Discontinuous Initial Conditions	60
<i>CHAPTER 5. A SOLVER FOR THE TWO-FLUID MODEL</i>		<i>65</i>
5.1	Mathematical Model	65
5.2	Discretized Equations	68
5.3	Closure Equations	71
5.4	Calculation of Donored Quantities	73
5.4.1	First-Order Upwind.....	73
5.4.2	Second-Order Upwind	74
5.4.3	Flux Limiter Schemes	75
5.5	Non-Linear Solver	76
5.6	Numerical Results and Discussion.....	77
5.6.1	The Faucet Flow Problem.....	77
5.6.2	Edward’s Pipe Problem.....	87
5.6.3	The Shock Tube Problem.....	95
<i>CHAPTER 6. CONCLUSIONS AND RECOMMENDATIONS FOR FUTURE WORK.....</i>		<i>105</i>
6.1	Summary and Conclusions.....	105
6.2	Future Work.....	107
<i>APPENDIX A. MODIFIED EQUATION ANALYSIS FOR THETA METHOD.....</i>		<i>109</i>
<i>APPENDIX B. ALGEBRAIC WORK FOR THE NEW TVD SCHEME.....</i>		<i>115</i>
<i>APPENDIX C. CODE STRUCTURE FOR THE TWO-PHASE TWO-FLUID MODEL SOLVER.....</i>		<i>120</i>
<i>References</i>		<i>125</i>

List of figures

Figure 2.1 Schematic for the characteristic curves.	13
Figure 2.2 Construction of the solution for Riemann problem of a three-equation system.	16
Figure 2.3 Infinitesimal rectangular region in the x-t plane near discontinuity.	19
Figure 2.4 Characteristic curves for different solutions of the Riemann problem	21
Figure 3.1 Numerical domain of dependence for a three-point numerical method.	28
Figure 3.2 Possible solutions for the non-linear scalar Riemann problem.	35
Figure 3.3 TVD region based on the 1 st -order upwind and Lax-Wendroff methods	43
Figure 3.4 Different choices for flux limiters in a TVD region	45
Figure 4.1 Schematic of the TVD region for the new high-order scheme	52
Figure 4.2 Arithmetically averaged limiter function.	54
Figure 4.3 Numerical results for smooth solutions with $\theta=1$	57
Figure 4.4 Numerical results for smooth solutions with $\theta=1/2$	58
Figure 4.5 Spatial convergence rates of the new scheme for smooth solutions	59
Figure 4.6 Numerical results for discontinuous solutions with $\theta=1$	61
Figure 4.7 Numerical results for discontinuous solutions with $\theta=1/2$	62
Figure 4.8 Spatial convergence rates for discontinuous solutions	63
Figure 5.1 Schematic of the staggered cell configuration.	68
Figure 5.2 Illustration of the faucet flow problem	79
Figure 5.3 Results for the 1 st -order-upwind with implicit temporal discretization	80
Figure 5.4 Results for the 1 st -order-upwind with Crank-Nicolson temporal discretization	81

Figure 5.5 Comparison between Implicit and Crank-Nicolson for (N=320)	81
Figure 5.6 Results for the 2 nd -order-upwind with implicit temporal discretization	82
Figure 5.7 Results for the 2 nd -order-upwind with Crank-Nicolson temporal discretization	83
Figure 5.8 Numerical results for new scheme with delta=1 using different values of θ , N=320.....	85
Figure 5.9 Numerical results for different flux limiter functions $\theta=1/2$ and N=320.....	86
Figure 5.10 Convergence of numerical solution for schemes with different limiters.....	86
Figure 5.11 Schematic of the Edward's pipe problem	87
Figure 5.12 Pressure profiles at different times for Edward's pipe problem.....	88
Figure 5.13 Gas void fraction at different times for Edward's pipe problem.....	88
Figure 5.14 Gas velocity profiles at different times for Edward's pipe problem	89
Figure 5.15 Left end pressure for Edward's pipe problem.....	89
Figure 5.16 Pressure profile at t=0.0022 sec for different mesh sizes, $dt = 10 - 5$	90
Figure 5.17 Void fraction profile at t=0.0022 sec for different mesh sizes, $dt = 10 - 5$	91
Figure 5.18 Gas velocity profile at t=0.0022 sec for different mesh sizes, $dt = 10 - 5$	91
Figure 5.19 Pressure history at closed end for different mesh sizes, $dt = 10 - 5$	92
Figure 5.20 Pressure profile at t=0.0022 sec for different time steps, N=40.....	92
Figure 5.21 Void fraction profile at t=0.0022 sec for different time steps, N=40	93
Figure 5.22 Gas velocity profile at t=0.0022 sec for different time steps, N=40.....	93
Figure 5.23 Pressure history at closed end for different time steps, N=40	94
Figure 5.24 Schematic of the shock tube problem.....	95
Figure 5.25 Pressure profile for shock tube problem at time=0.5 ms	97
Figure 5.26 Gas void fraction profile for shock tube problem at time=0.5 ms	97

Figure 5.27 Velocity profiles for shock tube problem at time=0.5 ms	98
Figure 5.28 Internal energy profiles for shock tube problem at time=0.5 ms	98
Figure 5.29 Gas density for shock tube problem at time=0.5 ms	99
Figure 5.30 Pressure profile for shock tube problem at time=0.5 ms for different mesh sizes.....	100
Figure 5.31 Void fraction profile for shock tube problem at time=0.5 ms for different mesh sizes.....	100
Figure 5.32 Gas density profile for shock tube problem at time=0.5 ms for different mesh sizes	101
Figure 5.33 Pressure profile for shock tube problem at time=0.5 ms for different time steps.....	101
Figure 5.34 Void fraction profile for shock tube problem at time=0.5 ms for different time steps.....	102
Figure 5.35 Gas density profile for shock tube problem at time=0.5 ms for different time steps	102
Figure 5.36 Convergence rate for the shock tube problem	104
Figure C.1 Interaction between different blocks of the solver code	124

List of Tables

Table 1.1 Classification of two-phase flow	3
Table 4.1 Spatial convergence rates of different schemes for smooth solution	60
Table 4.2 Spatial convergence rates of different schemes for discontinuous solution	63
Table 5.1 Initial and boundary conditions of the faucet flow problem	79
Table 5.2 Convergence of numerical solution for schemes with different limiters	85
Table 5.3 Initial conditions of the shock tube problem.....	96
Table C.1 Main Blocks	121
Table C.2 Numerical Scheme block	121
Table C.3 State Variables Block.....	122
Table C.4 Donored Quantities Block.....	122
Table C.5 Numerical Fluxes block	123

CHAPTER 1. INTRODUCTION

As a subject of intense interest in many engineering systems, the study of two-phase flow is of great importance in applied research because it is involved in many industrial applications. In the nuclear industry the phenomenon of two-phase flow plays a crucial role, because water in its liquid and gaseous phases is used as both a coolant and a moderator in many types of reactor cores. It also appears in other mechanical parts of the nuclear reactor, such as heat exchangers, condensers and turbines. Consequently, achieving the optimal design for both operation and safety requires a solid understanding of the fundamental aspects of two-phase flow physics and its mathematical models. Modeling of two-phase flows entails several difficulties; difficulties in the mathematical model used to govern the evolution of different properties in space and time, difficulties in physical models describing interfacial interactions, difficulties in the numerical methods used to solve the model and the algebraic equation solver itself used for strongly non-linear discrete equations.

In the last few decades, many researchers dedicated significant effort to overcome the problems associated with modeling of two-phase flow. Because most of the legacy nuclear thermal-hydraulics codes were based on one-dimensional models, the majority of the work targeting the nuclear industry was in that area [1] [2] [3]. Other work was performed in terms of multidimensional analysis (2D, 3D) [4] [5]. Multidimensional analysis of the two-phase flow allows solving for different flow regimes. This entails interface capturing between the two phases using different techniques, such as the Level-Set (LS) method, the Front-Tracking (FT) method and the Volume-Of-Fluid (VOF) method.

This research is aimed at investigating the one-dimensional two-fluid model; its mathematical and numerical problems. For the numerical simulation of the problem, high-order schemes are investigated as a potential replacement for the first-order schemes, and a new high-order scheme is developed. Analysis

for numerical properties is carried out, and a numerical solver based on this analysis is developed, tested and verified using numerical benchmarks and analytical solutions.

The work presented in this research suggests some solutions to the problems associated with numerical modeling of the two-phase two-fluid model. There are other sources of errors and uncertainties in the modeling of two-phase flows. For the two-fluid model, for example, errors in the closure relations can be up to 20% [6]. It is important to mention that these aspects of the problem should be tackled intensively to achieve better modeling of two-phase flows.

This Chapter provides a brief description of two-phase flows; classification and mathematical models. It also discusses the numerical approaches used to simulate the two-phase flow in two of the most common codes used in nuclear industry; TRACE and RELAP5.

1.1 Two-Phase Flow: Classification and Mathematical Models

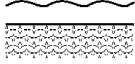
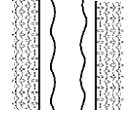

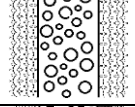
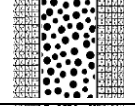
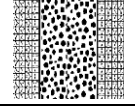
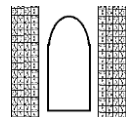
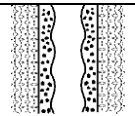
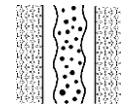
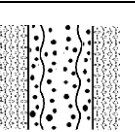
1.1.1 Two-Phase Flow Classification

The difficulty of physical modeling of the two-phase flow arises from the existence of moving and deforming interfaces between the two phases. Fluid properties near these interfaces are discontinuous and flow fields are complicated. Two-phase flow can be classified into different categories based on the nature of the interface. Each category can have different flow regimes (i.e. two-phase interface topology).

Three main categories were identified: Separated flows, mixed or transitional flows and dispersed flows.

This classification is shown in Table 1.1.

Table 1.1 Classification of two-phase flow

Class	Typical regimes	Geometry	Configuration	Examples
Separated flows	Film flow		Film of one phase in another phase	Film condensation Film boiling
	Annular flow		Core of one phase and a film of another phase	Film boiling Boilers
	Jet flow		Jet of one phase in another phase	Atomization Jet condenser
Dispersed flows	Bubbly flow		Gas bubbles in liquid	Chemical reactors
	Droplet flow		Liquid droplets in gas	Spray cooling
	Particulate flow		Solid particles in gas or liquid	Transportation of powder
Mixed or Transitional Flows	Cap, Slug or Churn-turbulent flow		Gas pocket in liquid	Sodium boiling in forced convection
	Bubbly annular flow		Gas bubbles in liquid film with gas core	Evaporators with wall nucleation
	Droplet annular flow		Gas core with droplets and liquid film	Steam generator
	Bubbly droplet annular flow		Gas core with droplets and liquid film with gas bubbles	Boiling nuclear reactor channel

1.1.2 Balance Equations and Mathematical Models

In general, the evolution of a measurable scalar quantity W in a medium of velocity \vec{u} is governed by the conservation relation:

$$\frac{\partial W}{\partial t} + \vec{\nabla} \cdot (W\vec{u}) = S \quad (1.1)$$

and for a vector quantity \vec{W} the conservation relation becomes:

$$\frac{\partial \vec{W}}{\partial t} + \vec{\nabla} \cdot (\vec{W} \times \vec{u}) = S \quad (1.2)$$

Terms on the left-hand side of the equation represent the evolution of the quantity in space and time, and terms on the right-hand side account for the sources and sinks of the measurable quantity.

In a two-phase flow, conservation relations (1.1) and (1.2) are applied to mass, momentum and energy of different phases to obtain a mathematical model. The two-phase model equations used by Yeom and Chang [7] are given by:

$$\frac{\partial(\alpha_g \rho_g)}{\partial t} + \vec{\nabla} \cdot (\alpha_g \rho_g \vec{u}_g) = \Gamma \quad (1.3)$$

$$\frac{\partial(\alpha_l \rho_l)}{\partial t} + \vec{\nabla} \cdot (\alpha_l \rho_l \vec{u}_l) = -\Gamma \quad (1.4)$$

$$\frac{\partial(\alpha_g \rho_g \vec{u}_g)}{\partial t} + \vec{\nabla} \cdot (\alpha_g \rho_g \vec{u}_g \times \vec{u}_g) + \alpha_g \vec{\nabla} p = \vec{F}_g \quad (1.5)$$

$$\frac{\partial(\alpha_l \rho_l \vec{u}_l)}{\partial t} + \vec{\nabla} \cdot (\alpha_l \rho_l \vec{u}_l \times \vec{u}_l) + \alpha_l \vec{\nabla} p = \vec{F}_l \quad (1.6)$$

$$\frac{\partial(\alpha_g e_g)}{\partial t} + \vec{\nabla} \cdot (\alpha_g e_g \vec{u}_g) + \alpha_g \vec{\nabla} \cdot (p \vec{u}_g) = E_g^{gen} + E_g^{exc} \quad (1.7)$$

$$\frac{\partial(\alpha_l e_l)}{\partial t} + \vec{\nabla}(\alpha_l e_l \vec{u}_l) + \alpha_l \vec{\nabla}(p \vec{u}_l) = E_l^{gen} + E_l^{exc} \quad (1.8)$$

The subscripts “*g*” and “*l*” refer to the gas and liquid phases, respectively.

- α is the void fraction.
- ρ is density.
- p is pressure.
- e is the specific internal energy.

As for the source terms on the right-hand side:

- Γ is the phase change rate, for example due to evaporation and condensation.
- \vec{F} accounts for all external forces acting on the fluid, including interfacial forces.
- E^{gen} is the net energy generation and E^{exc} is the net energy exchange with surrounding environment.

In addition to the equations above, there is also the conservation of volume equation:

$$\alpha_g + \alpha_l = 1 \quad (1.9)$$

The 7 equations above, along with two equations of state (one for each phase) yield a closed mathematical system of 9 equations and 9 unknowns ($p, \alpha_g, \alpha_l, u_g, u_l, e_g, e_l, \rho_g, \rho_l$).

A range of approximations is possible to simplify the two-phase model. One possible approximation is to assume the velocities and internal energies of the two phases are equal. This assumption yields the Homogeneous Equilibrium Model (HEM), which simplifies the 9 initial equations into 4 equations. A more general approximation is the drift flux model, where the velocities of the two phases are allowed to be

different. Even more general is the two-fluid model. In this model only pressure is assumed to be equal for the two phases, and all of the 9 equations above are retained. Some researchers consider the closure problems of two-fluid model to be a disadvantage, and favor the drift-flux model to analyze two-phase flow [8]. Yet, the two-fluid model is used in most nuclear thermal-hydraulic codes to date.

1.2 Existing Nuclear Codes and the Semi-Implicit Numerical Method

1.2.1 Existing Nuclear Codes

There are many thermal-hydraulics codes used in the nuclear industry that have the capability to simulate two-phase flows. Two of the most common codes are the **Reactor Excursion and Leak Analysis Program**, version 5 (RELAP5), and **TRAC/RELAP Advanced Computational Engine** (TRACE). Both codes employ the two-fluid model, and use finite volume techniques to solve the partial differential equations.

RELAP5 was developed for the U.S. Nuclear Regulatory Commission (NRC) to simulate the transients of boiling and pressurized water reactors, and analyze large- and small-break Loss-Of-Coolant Accidents (LOCAs). For two-phase flow simulations, RELAP5 uses a one-dimensional, transient, two-fluid model. It can also invoke simpler models like the homogeneous flow and thermal equilibrium models [9]. RELAP5 is probably the most widely used thermal-hydraulics code in the nuclear industry, yet it is expected to be phased out and replaced by TRACE.

TRACE was designed to extend and combine the capabilities of the USA Nuclear Regulatory Commission (USNRC) main system codes; TRAC-P, TRAC-B, RELAP5 and RAMONA. It is capable of analyzing transient and steady-state coupled neutronics/thermal-hydraulics in pressurized and boiling water reactors. It is also designed to perform best-estimate analysis of LOCAs in light water reactors. Models used in

TRACE include three-dimensional two-fluid two-phase flow, non-equilibrium thermodynamics, generalized heat transfer, re-flood, level tracking and reactor kinetics [10].

In terms of two-phase flow physics and numerics, TRACE and RELAP5 have a lot in common. The main similarity is the same two-fluid model and semi-implicit-based numerical methods used in both codes for solving the two-fluid model. A brief discussion of the semi-implicit method is presented in the following section.

In addition, both codes use staggered spatial mesh, where scalar properties (densities, pressure, energies and void fraction) are calculated at cell centers, and vector quantities (velocities) are calculated at the cell boundaries. The mass and energy equations are derived at mesh centers, whereas the momentum conservation equations are derived at mesh interfaces. More on the staggered mesh configuration is discussed in Chapter 5.

Although there are many similarities between the two codes, they differ in some important aspects. One example is the multidimensional capabilities of both codes; RELAP5 has the capability to model 1D flows, while TRACE can be used for 1D and 3D modeling. Another difference is the method used in both codes to improve on the stability of the semi-implicit method. RELAP5 uses the Nearly-Implicit method, while TRACE uses the Stability-Enhancing Two-Step (SETS) method.

The non-linear equations of state are also handled differently in both codes. RELAP5 replaces these equations by a linearized approximation, which is used as a part of the numerical discretization, while TRACE uses an iterative method to utilize the non-linear equations of state directly. RELAP5 uses flow-regime maps for closure relations, TRACE, on the other hand, does not identify specific flow regimes, the constitutive relations are smoothly interpolated for all flow conditions.

1.2.2 The Semi-Implicit Method

This section gives a brief discussion about the Semi-Implicit method used in RELAP5 and TRACE. More numerical fundamentals and concepts will be discussed in Chapter 3.

When explicit methods are used for modeling, the maximum size of the time-step is limited by the time needed for a perturbation (material or pressure wave) to travel along one mesh cell. This is known as the Courant, Friedrichs and Lewy (CFL) limit [10]. Mathematically, the relation between the temporal (Δt) and the spatial (Δx) steps is given by [16]:

$$\Delta t \leq k \frac{\Delta x}{|u| + c} \quad (1.10)$$

Where:

- u is flow velocity.
- c is speed of sound in the medium.
- k is a parameter that depends on the method used, for example $k=1$ for the 1st-order explicit upwind method in one-dimension.

The semi-implicit method relaxes this restriction on the time step by evaluating some terms at new time levels (implicitly). The key ideas of the semi-implicit method implemented in RELAP5 are:

- 1- The numerical scheme should be consistent and conserve mass and energy, so that both are convected from the same cell, and each is evaluated at same time level, that is to say, both of them are evaluated at old time (n).
- 2- Implicit evaluation (at time level $n + 1$) is only used for terms involved in pressure propagation and other phenomena that is known to have small time constants. This means pressure gradient term in the momentum equation, and velocities involved in the mass and energy fluxes.

To illustrate the two concepts above we consider one-dimensional versions of Eqs. (1.3) and (1.5) given by:

$$\frac{\partial(\alpha_g \rho_g)}{\partial t} + \frac{\partial(\alpha_g \rho_g \bar{u}_g)}{\partial x} = \Gamma \quad (1.11)$$

$$\frac{\partial(\alpha_g \rho_g \bar{u}_g)}{\partial t} + \frac{\partial(\alpha_g \rho_g u_g^2)}{\partial x} + \alpha_g \frac{\partial p}{\partial x} = \bar{F}_g \quad (1.12)$$

Following the two guidelines above, the two equations are discretized as follows:

$$\frac{(\alpha_g \rho_g)_i^{n+1} - (\alpha_g \rho_g)_i^n}{\Delta t} + \frac{(\dot{\alpha}_g \dot{\rho}_g)_{i+\frac{1}{2}}^n u_{i+1/2}^{n+1} - (\dot{\alpha}_g \dot{\rho}_g)_{i-\frac{1}{2}}^n u_{i-1/2}^{n+1}}{\Delta x} = \Gamma_i^n \quad (1.13)$$

$$\begin{aligned} & \frac{\alpha_g \rho_g}{\alpha_g \rho_g} \frac{u_{g_{i+1/2}}^{n+1} - u_{g_{i+1/2}}^n}{\Delta t} + \frac{(\alpha_g \rho_g)_{i+1}^n \dot{u}_{g_{i+1}}^{2n} - (\alpha_g \rho_g)_i^n \dot{u}_{g_i}^{2n}}{\Delta x} + \frac{p_{i+1}^{n+1} - p_i^{n+1}}{\Delta x} \\ & = F_{g_i}^n \end{aligned} \quad (1.14)$$

In the previous equations “*i*” is the index for spatial mesh and “*n*” is the index for temporal time step. Because scalar properties (pressure, energies, densities and void fraction) are defined at the cell centers, a value for these properties is needed at the cell interfaces to calculate numerical fluxes (this will be discussed in Chapter 3). These are variables with a “dot” in Eq. (1.13) (called donored quantities in RELAP5 nomenclature). TRACE uses values from adjacent volumes along with a weighting function to calculate the cell interface values. RELAP5 uses the value of the cell center upstream (this is called the upwind method). The same process holds for the momentum equations, where velocities are needed at the cell centers.

CHAPTER 2. CONSERVATION LAWS AND SOLUTIONS OF HYPERBOLIC PROBLEMS

Conservation laws are an important and well known class of hyperbolic problems. They appear in the majority of engineering fields and other scientific disciplines. In this Chapter we will discuss some forms of linear and non-linear conservation laws, their properties and associated problems. Some important concepts are also discussed to get a better understanding of the solution for conservation laws.

Conservation laws arise from the requirement that a measurable property of a closed system (which does not interact with its surroundings) has to remain constant as the system changes. A general form of conservation laws in one dimension is given by:

$$\frac{\partial Q}{\partial t} + \frac{\partial F(Q)}{\partial x} = 0 \quad x \in \mathbb{R}, t > 0 \tag{2.1}$$

$$Q(x, 0) = Q_0(x) \quad x \in \mathbb{R}$$

For a system of m equations:

$$Q = \begin{pmatrix} q_1 \\ q_2 \\ \vdots \\ q_m \end{pmatrix}, \quad F(Q) = \begin{pmatrix} f_1(Q) \\ f_2(Q) \\ \vdots \\ f_m(Q) \end{pmatrix}$$

If the flux function $F(Q)$ is differentiable, this equation can be written in a quasi-linear form as follows:

$$\frac{\partial Q}{\partial t} + F'(Q) \frac{\partial Q}{\partial x} = 0 \tag{2.2}$$

$F'(q)$ is called the Jacobian matrix, and can be written as:

$$A(Q) = F'(Q) = \begin{pmatrix} \frac{\partial f_1}{\partial q_1} & \frac{\partial f_1}{\partial q_2} & \cdots & \frac{\partial f_1}{\partial q_m} \\ \frac{\partial f_2}{\partial q_1} & \frac{\partial f_2}{\partial q_2} & \cdots & \frac{\partial f_2}{\partial q_m} \\ \vdots & \vdots & \ddots & \vdots \\ \frac{\partial f_m}{\partial q_1} & \frac{\partial f_m}{\partial q_2} & \cdots & \frac{\partial f_m}{\partial q_m} \end{pmatrix} \quad (2.3)$$

For the system in Eq. (2.2), there are m eigenvalues (z_k) of the Jacobian matrix (A). These are solutions of the characteristic polynomial resulting from the determinant of the matrix ($A - zI$), where I is the identity matrix. Physically, these eigenvalues represent propagation speeds of information, as will be described later.

A right eigenvector of the matrix A corresponding to an eigenvalue z_k of A is a vector $r^{(k)} = [r_1^{(k)}, r_2^{(k)}, \dots, r_m^{(k)}]$ satisfying $Ar^{(k)} = z_k r^{(k)}$. Similarly, a left eigenvector of the matrix A corresponding to an eigenvalue z_k is a vector $l^{(k)} = [l_1^{(k)}, l_2^{(k)}, \dots, l_m^{(k)}]$ satisfying $l^{(k)}A = z_k l^{(k)}$.

The system in Eq. (2.2) is said to be hyperbolic at any point (x, t) if the Jacobian matrix A has m real eigenvalues and a corresponding set of m linearly independent eigenvectors. A special case is a strictly hyperbolic system, where eigenvalues are all distinct. The two-fluid model does not always satisfy the condition of all real eigenvalues, hence, cannot be assumed hyperbolic for all flow conditions [11][12][13][14].

2.1 Linear Hyperbolic Problems

The advection problem is the simplest case of Eq. (2.2) where $m = 1$. In this problem the vector of variables Q reduces to one variable q , and the flux function $F(Q) = f(q) = \bar{u}q$, where \bar{u} is some constant velocity. The quasi-linear form of this problem is:

$$\frac{\partial q}{\partial t} + \bar{u} \frac{\partial q}{\partial x} = 0 \quad -\infty < x < \infty, t > 0 \quad (2.4)$$

$$q(x, 0) = q_0(x) \quad -\infty < x < \infty$$

This equation represents a pure convection of the scalar property q in a moving fluid of velocity \bar{u} . Because no other forces exist in this problem, one expects the property q to move unchanged in the same direction as \bar{u} . With this conclusion, the solution can be written as:

$$q(x, t) = q_0(x - \bar{u}t) \quad (2.5)$$

Equation (2.5) shows that the solution remains constant along the parallel lines $x = x_0 + \bar{u}t$, also called *characteristic curves* (see Figure 2.1).

The Riemann problem

Now, we consider a special case of the advection problem in Eq.(2.4), with a piecewise constant initial condition, given by:

$$q_0(x) = \begin{cases} q_L & x < 0 \\ q_R & x > 0 \end{cases} \quad (2.6)$$

Equations (2.4) and (2.6) are called the *Riemann problem*. This kind of problems is very important for understanding different numerical schemes for hyperbolic equations.

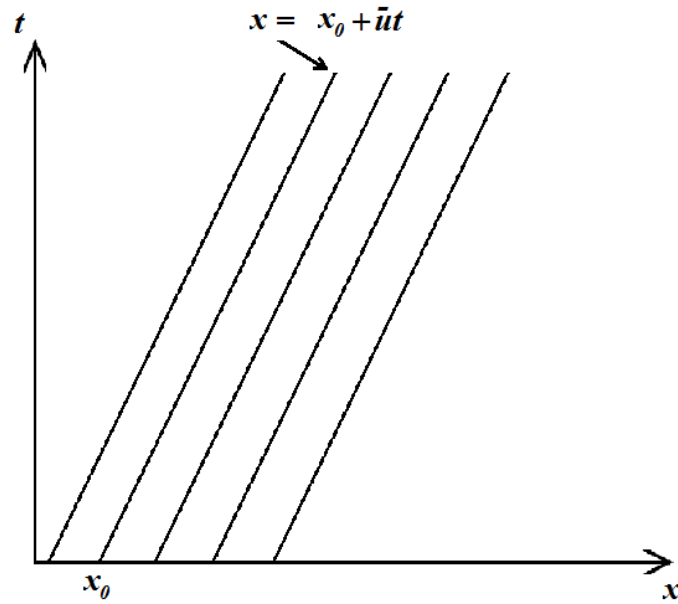


Figure 2.1 Schematic for the characteristic curves.

In this problem the discontinuity appearing in the initial condition is expected to propagate along the characteristic curves. This can be expressed mathematically as:

$$q(x, t) = \begin{cases} q_L & x - \bar{u}t < 0 \\ q_R & x - \bar{u}t > 0 \end{cases} \quad (2.7)$$

The advection problem discussed above can be extended to a system of linear equations. Here, we consider a linear case of Eq. (2.2), where $A = F'(Q)$ is a matrix of constant entries, independent of Q . Assuming a strictly hyperbolic system, i.e. distinct real eigenvalues, the system can be diagonalized and can be expressed in a form of decoupled system of equations.

If we consider the matrix R with its columns consisting of eigenvectors $r^{(k)}$, $k = 1, 2, \dots, m$ of A , then we can write:

$$A = RDR^{-1} \quad (2.8)$$

where D is a diagonal matrix, and its diagonal entries are the eigenvalues of A . We can define a new set of characteristic variables W :

$$W = R^{-1}Q \quad (2.9)$$

Using Eqs. (2.8) and (2.9) we can write the linear system (Eq. (2.2)) as:

$$\frac{\partial W}{\partial t} + D \frac{\partial W}{\partial x} = 0 \quad (2.10)$$

The system above is a decoupled system of m scalar equations, with each equation given by:

$$\frac{\partial w^k}{\partial t} + z_k \frac{\partial w^k}{\partial x} = 0 \quad (2.11)$$

where w^k is the characteristic variable corresponding to the k^{th} characteristic. The solution of the equation above is a wave traveling at characteristic speed z_k (similar to the simple advection problem). These speeds define the characteristic curves $x(t) = x_0 + z_k t$. Along these curves solution of Eq. (2.11) is constant, so if we have:

$$W_0(x) = R^{-1}Q_0(x)$$

The solution for w^k at any point (x, t) is given by:

$$w^k(x, t) = w^k(x - z_k t, 0) = w_0^k(x - z_k t)$$

Finally, the solution of the original system is a linear combination of the solutions of the decoupled system, given as:

$$Q = RW \quad (2.12)$$

Now we consider the Riemann problem for the case of a linear hyperbolic system, with a piecewise constant initial condition, given by:

$$Q_0(x) = \begin{cases} Q_L & x < 0 \\ Q_R & x > 0 \end{cases} \quad (2.13)$$

If we use the notation of characteristic variables, we can define (compare with Eq. (2.12)):

$$Q_L = \sum_{k=1}^m w_L^k r^k \quad \text{and} \quad Q_R = \sum_{k=1}^m w_R^k r^k \quad (2.14)$$

so we obtain an initial condition for the characteristic variables as:

$$w_0^k(x) = \begin{cases} w_L^k & x < 0 \\ w_R^k & x > 0 \end{cases} \quad (2.15)$$

and the solution for the decoupled system in Eq. (2.11) becomes (compare with Eq. (2.7)):

$$w^k(x, t) = \begin{cases} w_L^k & x < z_k t \\ w_R^k & x > z_k t \end{cases} \quad (2.16)$$

To obtain a solution for the original variables of Riemann's problem, we need to consider waves that satisfy the upper and lower conditions of Eq. (2.16) separately. This can be expressed mathematically as follows:

$$Q(x, t) = \sum_{k: z^k < x/t} w_R^k r^k + \sum_{k: z^k > x/t} w_L^k r^k \quad (2.17)$$

Figure 2.2 shows the construction of the solution Q_r^* for a linear system of three equations at a point (x', t') given by: $Q_r^* = w_l^1 r^1 + w_r^2 r^2 + w_r^3 r^3$. Similarly, we calculate $Q_l^* = w_l^1 r^1 + w_l^2 r^2 + w_l^3 r^3$.

There are two main observations we can conclude from Eq. (2.17):

- 1- Solution at any point between the lines $x = z^k t$ and $x = z^{k+1} t$ is constant and has the same combination of characteristic variables.
- 2- Once it crosses the k^{th} characteristic, the solution corresponding to w^k jumps from w_L^k to w_R^k , the other characteristic variables remain constant. This causes a jump in the solution Q , and this jump is given by $(w_R^k - w_L^k) r^k$.

From the second observation, we notice that the jump in the solution is an eigenvector of matrix A , because it is a scalar multiple of r^k . A generalization of this conclusion is useful for solving the Riemann problem for non-linear cases, as we will see later. This is referred to as the *Rankine-Hugoniot jump condition* [15].

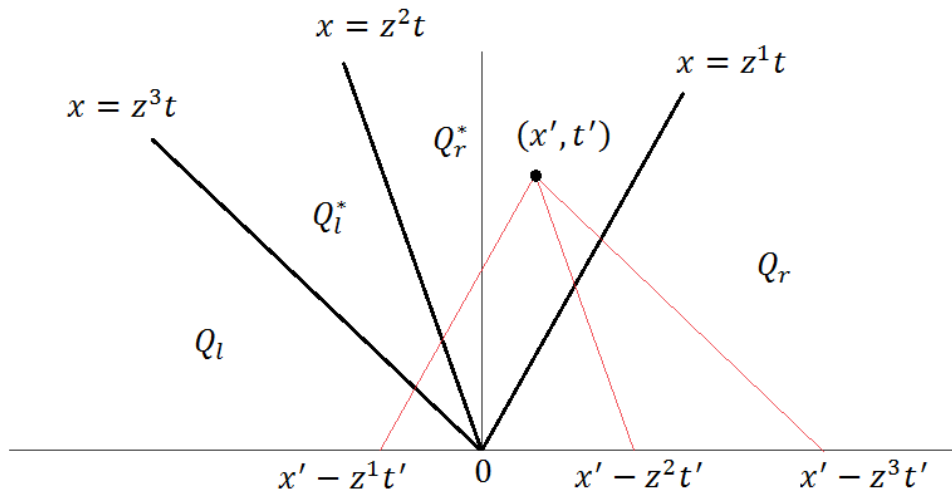


Figure 2.2 Construction of the solution for Riemann problem of a three-equation system.

2.2 Non-Linear Hyperbolic Problems

Before we move to non-linear systems, we shall start with a simple case of one equation ($m = 1$), in quasilinear form:

$$\frac{\partial q}{\partial t} + a(q) \frac{\partial q}{\partial x} = 0 \quad -\infty < x < \infty, t > 0 \quad (2.18)$$

$$q(x, 0) = q_0(x) \quad -\infty < x < \infty$$

where $a(q) = f'(q)$. It can be shown that the solution q is constant along the curves satisfying $\frac{dx}{dt} = a(q)$, $x(0) = x_0$. This means the slopes of characteristic curves are constants, and yield straight lines of the form $x = x_0 + a(q(x_0))t$. The slopes (being dependent on the solution) will not be the same for different characteristic curves, which causes a deformation of the solution. This is different from the linear case where information was moving along the characteristics unchanged.

The fact that characteristic curves have different slopes implies either an intersection or a divergence in the x - t plane. The possibility of intersection means multiple values of the solution at some points; hence, the solution will be discontinuous at these points, even for a smooth initial condition. Equation (2.1) in its conservative form ceases to be valid at points of discontinuity, and we need to admit the *integral form* of the conservation law to allow for discontinuities to exist.

Let us assume discontinuity exists at $x_s = x_s(t)$ in the x - t plane, and the solution $q(x, t)$ and the flux $f(q)$ are continuous and smooth elsewhere. If we zoom into that point and consider the rectangle shown in Figure 2.3, we can apply the integral form of the conservation law and obtain *weak solutions* that satisfy the integral form rather than differential form:

$$\int_{x_1}^{x_1+\Delta x} q(x, t_1 + \Delta t) dx - \int_{x_1}^{x_1+\Delta x} q(x, t_1) dx =$$
(2.19)

$$\int_{t_1}^{t_1+\Delta t} f(q(x_1, t)) dt - \int_{t_1}^{t_1+\Delta t} f(q(x_1 + \Delta x, t)) dt$$

Carrying out the integration above and assuming constant values of q and $f(q)$ on the wedges (see Figure 2.3), we get:

$$\Delta x(q_r - q_l) = \Delta t(f(q_l) - f(q_r))$$

If we define the propagation speed of discontinuity $s = -\Delta x/\Delta t$, we get:

$$s(q_r - q_l) = f(q_r) - f(q_l)$$
(2.20)

In general, this speed is not constant because the solution to the left and the right of the discontinuity changes with time. A generalization of this result for a system of equations yields the Rankine-Hugoniot jump condition discussed before, namely:

$$A(q_r - q_l) = s(q_r - q_l)$$
(2.21)

where A is the Jacobian matrix, and the shock speed s is an eigenvalue of A .

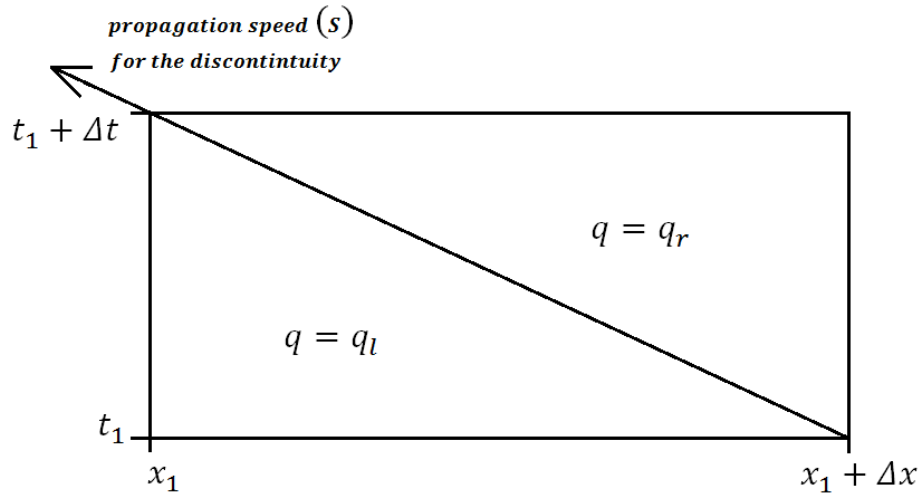


Figure 2.3 Infinitesimal rectangular region in the x - t plane near discontinuity.

An example of non-linear conservation law is the *Inviscid Burger equation*, namely:

$$\frac{\partial q}{\partial t} + q \frac{\partial q}{\partial x} = 0 \quad (2.22)$$

In this equation, q is fluid velocity. Now, we consider the Riemann problem of Burger's equation (Eq. (2.22)) with the piecewise constant initial condition (Eq. (2.6)).

We discussed before, that solutions of non-linear hyperbolic equations depend on initial conditions. This is due to the fact that slopes of the characteristic curves depend on the solution, which in turn is a propagation of initial conditions.

In case of Eq. (2.22) these slopes are given by $q(x_0)$. Because of this, we need to consider two different cases for the solution:

$$1- q_L > q_R$$

In this case the slopes for $x < 0$ are greater than those for $x > 0$. As a result characteristic curves will intersect at time $t = 0$ causing the creation of a shock wave at $x = 0$. This wave propagates with a speed s .

The solution anywhere away from this shock is piecewise and is given by:

$$q(x) = \begin{cases} q_L & x < st \\ q_R & x > st \end{cases} \quad (2.23)$$

The propagation speed s is calculated using Eq. (2.20) to be: $s = (q_L + q_R)/2$. We notice this is simply the average of characteristic speeds on the two sides.

$$2- q_L < q_R$$

We know the solution is constant along characteristic curves, thus we conclude the following about the solution:

$$q(x) = \begin{cases} q_L & \frac{x}{t} < q_L \\ q_R & \frac{x}{t} > q_R \end{cases} \quad (2.24)$$

This solution is missing the part for $q_L < \frac{x}{t} < q_R$. In this region two different scenarios are possible for the characteristic curves:

- a- An *expansion shock* is forming between the two sets of characteristics, with a speed: $s = (q_L + q_R)/2$. This scenario yields the same solution as in Eq. (2.23).

b- A formation of a family of characteristics with slopes ranging between slope values of the left and right sides. This kind of solution is called a *rarefaction wave* and the complete solution in this case is given by:

$$q(x) = \begin{cases} q_L & \frac{x}{t} < q_L \\ \frac{x}{t} & q_L < \frac{x}{t} < q_R \\ q_R & \frac{x}{t} > q_R \end{cases} \quad (2.25)$$

Figure 2.4 shows the three different solutions discussed above. We can see from the example of Burger's equation, that a weak solution for the conservation law is not a unique solution. To be able to decide which solution is more sensible, additional conditions have to be imposed, these conditions are known as the *entropy conditions*.

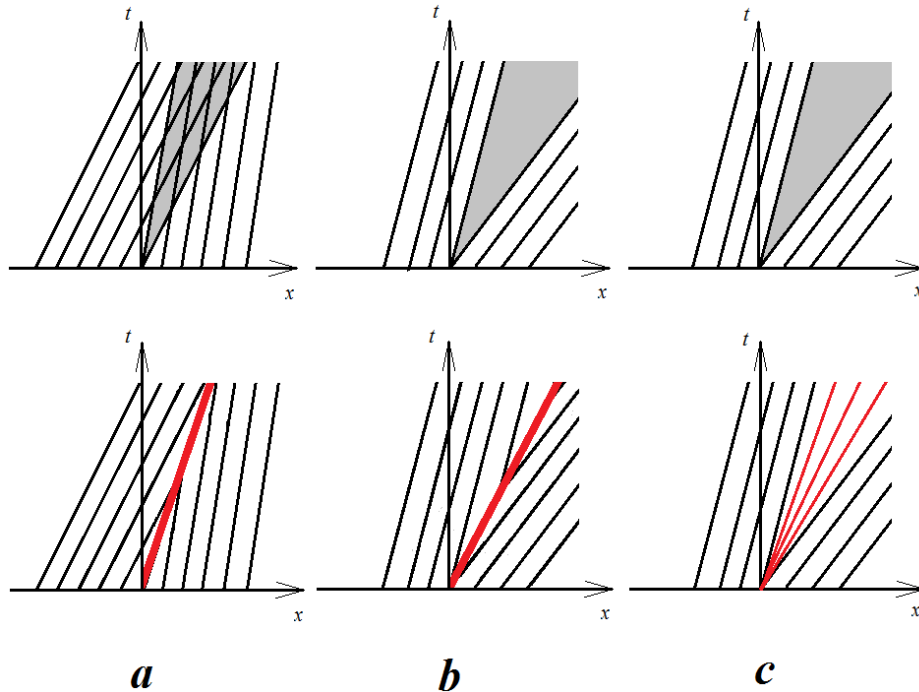


Figure 2.4 Characteristic curves for different solutions of the Riemann problem
 (a) Shock wave (b) Expansion shock (c) Rarefaction wave

One entropy condition is the *Lax entropy condition* [15]. For Eq. (2.22), a discontinuity propagating with speed s should satisfy:

$$f'(q_L) > s > f'(q_R) \quad (2.26)$$

This condition rules out the expansion shock in the solution of Burger's equation.

In many numerical methods, solving the Riemann problem for a non-linear system is a crucial part of the numerical algorithm. Leveque [15] describes a three steps strategy for solving the Riemann problem for such systems:

- 1- Determination whether each of the m waves is a shock wave or a rarefaction wave, a proper entropy condition has to be used.
- 2- Calculation for intermediate states between different waves.
- 3- Determination of the solution structure through any rarefaction wave.

To solve for shock waves, Leveque uses the Rankine-Hugoniot jump condition in Eq. (2.20) on the speed of propagation. For rarefaction waves Leveque uses the property that they are similarity solutions of the equations (constant along every line $x/t = \text{constant}$). For more details on how to solve the Riemann problem of a non-linear system of equations we suggest the reader to consult Leveque's book [15].

CHAPTER 3. REVIEW OF NUMERICAL METHODS FOR HYPERBOLIC PROBLEMS

Developing stable numerical schemes for modeling hyperbolic problems has been an intense research area for decades. This field of study poses several challenging difficulties. One of the most important difficulties is the existence of discontinuities and the formation of different types of shocks in the solution. As discussed in Chapter 2, discontinuities appear in the solution of non-linear equations, even with smooth initial conditions.

Special attention should be paid to the treatment of discontinuous solutions and shock propagation. There have been many approaches for dealing with these discontinuities, one of which is adding artificial viscosity term to the scheme. Addition of artificial viscosity can be achieved by either explicitly adding additional differential terms or implicitly within the numerical scheme used, such as first-order schemes which are known to be dissipative and able to smear the solution around discontinuities. Other approaches consider these dissipative schemes only at the regions of discontinuities, and adopt higher order schemes elsewhere. Another approach that has been developed for high-order accurate schemes is the Godunov's scheme, where the Riemann problem (exact or approximate) is solved at the cell interfaces at each time step. This Chapter includes a brief discussion on these different approaches and other numerical schemes.

There have been many classifications for the numerical methods used for hyperbolic problems. In this Chapter we will consider the classification based on the linearity of the scheme. The first section of this Chapter will be a brief discussion of some crucial concepts necessary for understanding of numerical schemes. The second part includes a discussion of linear and non-linear numerical schemes, and methods of temporal discretization.

3.1 Numerical Notations

Eq. (2.1) can be written in a scalar form:

$$\frac{\partial q}{\partial t} + \frac{\partial f(Q)}{\partial x} = 0 \quad -\infty < x < \infty, t > 0 \quad (3.1)$$

To allow for discontinuities along a discretized spatial and temporal domain, we need to admit weak solutions for Eq. (3.1). To explain this, we consider the control volume $C_i = [x_{i-1/2}, x_{i+1/2}]$, with $\Delta x_i = (x_{i+1/2} - x_{i-1/2})$. Similarly we define $T_{n+1/2} = [t_n, t_{n+1}]$, and $\Delta t = (t_{n+1} - t_n)$. Integrating Eq. (3.1) over $C_i \times T_{n+1/2}$ and dividing by Δx_i we obtain:

$$\begin{aligned} & \frac{1}{\Delta x_i} \int_{x_{i-1/2}}^{x_{i+1/2}} q(x, t_{n+1}) dx - \frac{1}{\Delta x_i} \int_{x_{i-1/2}}^{x_{i+1/2}} q(x, t_n) dx \\ & + \frac{\Delta t}{\Delta x_i} \left(\frac{1}{\Delta t} \int_{t_n}^{t_{n+1}} f(q(x_{i+1/2}, s)) ds - \frac{1}{\Delta t} \int_{t_n}^{t_{n+1}} f(q(x_{i-1/2}, s)) ds \right) = 0 \end{aligned} \quad (3.2)$$

If we define the following:

$$q_i^n \approx \frac{1}{\Delta x_i} \int_{x_{i-1/2}}^{x_{i+1/2}} q(x, t_n) dx \quad (3.3)$$

$$\mathcal{F}_{i\pm 1/2}^n \approx \frac{1}{\Delta t} \int_{t_n}^{t_{n+1}} f(q(x_{i\pm 1/2}, s)) ds \quad (3.4)$$

$$\lambda = \frac{\Delta t}{\Delta x_i} \quad (3.5)$$

we can write a general numerical scheme in its conservative form as:

$$q_i^{n+1} = q_i^n - \lambda (\mathcal{F}_{i+1/2}^n - \mathcal{F}_{i-1/2}^n) \quad (3.6)$$

Different ways of calculating the numerical fluxes $\mathcal{F}_{i\pm 1/2}^n$ yield different numerical schemes. This will be discussed in the following sections.

3.1.1 Forms of Numerical Schemes

In addition to the conservative form of Eq. (3.6), there are many other forms to represent numerical schemes for solving Eq. (3.1). Some of these forms are:

- the general form:

$$q_i^{n+1} = H(q_{i-k}^n, q_{i-k+1}^n, \dots, q_i^n, \dots, q_{i+k}^n) \quad (3.7)$$

- the incremental form:

$$q_i^{n+1} = q_i^n - D_{i-1/2} \Delta q_{i-1/2} + C_{i+1/2} \Delta q_{i+1/2} \quad (3.8)$$

- the viscous form:

$$q_i^{n+1} = q_i^n - \frac{1}{2} \lambda [f(q_{i+1}^n) - f(q_{i-1}^n)] + \frac{1}{2} (d_{i+1/2} \Delta q_{i+1/2} - d_{i-1/2} \Delta q_{i-1/2}) \quad (3.9)$$

where

$$\Delta q_{i-1/2} = q_i - q_{i-1}$$

$$\Delta q_{i+1/2} = q_{i+1} - q_i$$

$$D_{i-1/2} = D(q_{i-k}, \dots, q_{i+k})$$

$$C_{i+1/2} = C(q_{i-k}, \dots, q_{i+k})$$

and $d_{i\pm 1/2}$ is called the viscosity coefficient. These forms will be useful when we discuss the properties of different numerical schemes.

3.1.2 Local Truncation Error

For a numerical scheme, the local truncation error is a measure of the quality of approximating a partial differential equation (PDE) by a difference equation at a single time step. If we consider a scheme in its general form (Eq. (3.7)), we can write the numerical operator (L_a) that satisfies the difference equation as follows:

$$L_a(q_i) = q_i^{n+1} - H(q_{i-k}^n, q_{i-k+1}^n, \dots, q_i^n, \dots, q_{i+k}^n) = 0 \quad (3.10)$$

If L_a is applied to the exact solution $q(x, t)$ of the PDE at time t_n and location x_i , the value on the right-hand side of Eq. (3.10) will be different from zero. This value quantifies the local truncation error (τ_i^n) of the scheme, namely:

$$\tau_i^n = \frac{1}{\Delta t} L_a(q(x_i, t_n)) \neq 0 \quad (3.11)$$

Assuming the solution $q(x, t)$ of Eq. (3.1) to be smooth, we can use Taylor series expansion about the point (x_i, t_n) , and substitute in Eq. (3.11). With some algebraic manipulation we can solve for the truncation error of the scheme. In general:

$$\tau_i^n = \frac{\partial q(i\Delta x, n\Delta t)}{\partial t} + \frac{\partial f(q(i\Delta x, n\Delta t))}{\partial x} + O(\Delta t)^k + O(\Delta x)^m \quad (3.12)$$

k and m are integers based on the scheme used. The first two terms on the right-hand side of Eq. (3.12) vanish, because $q(x, t)$ is a solution of the original PDE. Therefore, the truncation error is given by:

$$\tau_i^n = O(\Delta t)^k + O(\Delta x)^m \quad (3.13)$$

Equation (3.13) implies that the numerical scheme is of the order of accuracy k in time and m in space. It also implies that the numerical scheme is consistent with Eq. (3.1) if and only if $\tau_t^n \rightarrow 0$ as both the spatial and temporal mesh sizes approach zero.

3.1.3 The Courant, Friedrichs and Lewy (CFL) Condition

The CFL condition is a stability condition that was first derived by Courant et al. [16]. The condition dictates that the numerical method should be used in such a way that the information can propagate at the correct physical speeds. In other words:

“For a numerical method to be convergent, the numerical domain of dependence for the difference equation has to contain the true domain of dependence of the partial differential equation, at least in the limit as Δt and Δx go to zero”

To illustrate the statement above, we study the scalar advection case of Eq. (2.4). We already know the exact solution of this equation is given by $q(x, t) = q_0(x - \bar{u}t)$. This implies that at any point (x_i, t_n) the solution depends on the initial data at the spatial location $x_i - \bar{u}t_n$, which is referred to as the domain of dependence of the point (x_i, t_n) .

Let's consider a three point numerical method, where the solution at any time step depends on the previous solution at the same cell and two neighboring cells. This is illustrated in Figure 3.1.

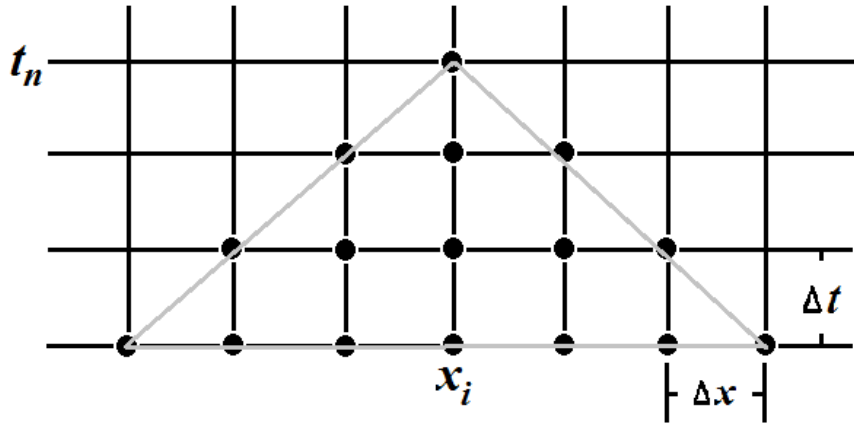


Figure 3.1 Numerical domain of dependence for a three-point numerical method.

One observation from Figure 3.1 is that the solution at any point (x_i, t_n) in the numerical domain depends on the solutions at all points between $(x_i - \frac{t_n}{\Delta t} \Delta x)$ and $(x_i + \frac{t_n}{\Delta t} \Delta x)$. If we apply the CFL condition above we require:

$$x_i - \frac{t_n}{\Delta t} \Delta x \leq x_i - \bar{u} t_n \leq x_i + \frac{t_n}{\Delta t} \Delta x$$

By defining the Courant number v , this can be simplified into:

$$v = \left| \frac{\bar{u} \Delta t}{\Delta x} \right| \leq 1 \quad (3.14)$$

For a system of equations the CFL condition is dictated by the maximum eigenvalue of the Jacobian matrix discussed in Chapter 2.

3.1.4 Total Variation and Monotonicity

A numerical scheme of the general form (Eq. (3.7)) is called a *monotone scheme* if the operator H is non-decreasing for all its arguments, namely:

$$\frac{\partial}{\partial q_k^n} H(q_{i-l}^n, q_{i-l+1}^n, \dots, q_i^n, \dots, q_{i+r}^n) \geq 0 \quad (3.15)$$

for any k in the spatial domain. According to Harten [17], a weak solution for a scalar version of Eq. (3.1) has the following monotonicity property:

- 1- No new local extrema in x direction may be created.
- 2- The value of a local minimum is non-decreasing and the value of the local maximum is non-increasing.

Based on the two properties above monotone schemes are desired because they have the property of not introducing oscillations with new extrema, particularly near discontinuities.

Another important notion that gives a measure for oscillations due to a numerical scheme is the *Total Variation* (TV). For a differentiable function $q(x, t)$, the total variation at a given time (t_0) is defined as [15]:

$$TV(q(x, t_0)) = \int_{-\infty}^{\infty} \left| \frac{\partial q(x, t_0)}{\partial x} \right| dx \quad (3.16)$$

If we consider the simple advection problem with flux function given by:

$$f(q) = \bar{u}q \quad (3.17)$$

the exact solution for this problem moves unchanged with a constant speed \bar{u} . This dictates the total variation to be constant in time, namely:

$$TV(q(x, t_1)) = TV(q(x, t_2))$$

for any t_1 and $t_2 > 0$. For a given piecewise grid function $q(i, n)$ that approximates the exact solution $q(x, t)$, the total variation is given by:

$$TV(q^n) = \sum_{i=-\infty}^{\infty} |q_i^n - q_{i-1}^n| \quad (3.18)$$

A numerical method is called *Total Variation Diminishing (TVD)* if the total variation does not increase due to the numerical operator H in Eq. (3.7), i.e.:

$$TV(q^{n+1}) \leq TV(q^n) \quad (3.19)$$

For a numerical scheme in the incremental form (Eq. (3.8)), this condition is satisfied if [18]:

$$D_{i-1/2} \geq 0, C_{i+1/2} \geq 0 \text{ and } 0 \leq D_{i-1/2} + C_{i+1/2} \leq 1 \quad (3.20)$$

On the relation between monotonicity and total variation, Harten suggests that a monotone scheme has a non-increasing TV, and a scheme with non-increasing TV preserves monotonicity [17].

3.2 Linear Numerical Schemes

A *linear scheme* for solving the linear advection equation can be written in the form:

$$q_i^{n+1} = \sum_{k=-b}^{k=d} c_k q_{i+k}^n \quad (3.21)$$

The coefficients c_k in Eq. (3.21) are constants and do not depend on the solution. There are many classical linear schemes available in literature to solve hyperbolic equations. These schemes can be classified into monotone first-order schemes and non-monotone high-order schemes. In this section we will present the main schemes of the two families.

3.2.1 First-Order Accurate Schemes

In this section we shall discuss some linear numerical schemes that are first-order accurate. These schemes are constructed by choosing different expressions for the numerical flux $\mathcal{F}_{i+1/2}^n$ in the conservative form (Eq. (3.6)). Most of these schemes are known to be dissipative and cause smearing in the solution for hyperbolic problems. This dissipation is shown mathematically for the next two example schemes.

The Lax-Friedrichs method

The Lax-Friedrichs method is a three-point scheme with first-order accuracy in space and time. The numerical flux for this scheme given by:

$$\mathcal{F}_{i+1/2}^n = \frac{1}{2} [f(q_i^n) + f(q_{i+1}^n)] - \frac{\Delta x}{2\Delta t} (q_{i+1}^n - q_i^n) \quad (3.22)$$

If we substitute this flux into the conservative form (Eq. (3.6)) we obtain the following scheme:

$$q_i^{n+1} = \frac{1}{2} (q_{i+1}^n + q_{i-1}^n) - \frac{\Delta t}{2\Delta x} [f(q_{i+1}^n) - f(q_{i-1}^n)] \quad (3.23)$$

The Lax-Friedrichs scheme is known to be diffusive. It has an implicit numerical viscosity that is useful for solving problems with discontinuities. To quantify the numerical viscosity of the Lax-Friedrichs scheme we use the modified equation approach. In this approach we seek a PDE for which the numerical approximation q_i^n due to the numerical scheme is an exact solution. The resulting equation is called the *Modified Differential Equation* (MDE) for the numerical scheme of interest. For the simple advection case (Eq. (2.4)), we can use this approach to find the modified equation for the Lax-Friedrichs scheme to be:

$$\frac{\partial q}{\partial t} + \bar{u} \frac{\partial q}{\partial x} = \left(\frac{\Delta x^2}{2\Delta t} - \frac{\Delta t}{2} \bar{u}^2 \right) \frac{\partial^2 q}{\partial x^2} \quad (3.24)$$

If we use the definition of Courant number in Eq. (3.14), we obtain:

$$\frac{\partial q}{\partial t} + \bar{u} \frac{\partial q}{\partial x} = \frac{\Delta x \bar{u}}{2} \left(\frac{1}{v} - v \right) \frac{\partial^2 q}{\partial x^2} \quad (3.25)$$

This is an advection-diffusion equation with the diffusion coefficient $\frac{\Delta x \bar{u}}{2} \left(\frac{1}{v} - v \right)$. This coefficient vanishes as the mesh size is refined. The interpretation here is that the Lax-Friedrichs scheme is at least second-order accurate for the advection-diffusion equation (Eq. (3.24)). The scheme has an implicit numerical viscosity when used to solve the advection equation, this causes the smearing of the solution near discontinuities.

The first-order upwind method

As discussed before, hyperbolic problems have the property that the initial data propagates along the characteristic curves. The upwind method uses this property to construct a numerical scheme that is dependent on the direction of the flow velocity. If we consider the non-linear advection equation:

$$\frac{\partial q}{\partial t} + \frac{\partial f(q)}{\partial x} = 0 \quad (3.26)$$

The information will propagate along the characteristic curves with a speed $a(q) = \frac{\partial f}{\partial q}$. Based on that, the numerical flux for the first-order upwind scheme is given by:

$$\mathcal{F}_{i+1/2}^n = \begin{cases} f(q_i^n) & \text{if } a_{i+1/2} > 0 \\ f(q_{i+1}^n) & \text{if } a_{i+1/2} < 0 \end{cases} \quad (3.27)$$

and the characteristic speed $a_{i+1/2}$ is defined as:

$$a_{i+1/2} = \begin{cases} \frac{f(q_{i+1}^n) - f(q_i^n)}{q_{i+1}^n - q_i^n} & \text{if } q_{i+1}^n \neq q_i^n \\ \left. \frac{\partial f}{\partial q} \right|_{q=q_i^n} & \text{if } q_{i+1}^n = q_i^n \end{cases} \quad (3.28)$$

The numerical flux above yields the following scheme:

$$q_i^{n+1} = q_i^n - \frac{\Delta t}{2\Delta x} [f(q_{i+1}^n) - f(q_{i-1}^n) - |a_{i+1/2}|(q_{i+1}^n - q_i^n) + |a_{i-1/2}|(q_i^n - q_{i-1}^n)] \quad (3.29)$$

For a simple advection problem with positive speed $\bar{u} > 0$, the scheme is simply:

$$q_i^{n+1} = q_i^n - \frac{\bar{u}\Delta t}{\Delta x} [q_i^n - q_{i-1}^n]$$

The first-order upwind method is a dissipative method and it has an implicit numerical viscosity. To quantify this viscosity we can apply the modified equation approach as we did for the Lax-Friedrichs method. The modified differential equation for the case of simple advection with positive speed is:

$$\frac{\partial q}{\partial t} + \bar{u} \frac{\partial q}{\partial x} = \frac{\Delta x \bar{u}}{2} (1 - \nu) \frac{\partial^2 q}{\partial x^2} \quad (3.30)$$

We can see that the numerical viscosity term vanishes as the mesh is refined, assuming that the Courant number is a fixed constant. We can also see that the viscosity coefficient for the first-order upwind method is less than that of the Lax-Friedrichs method, which means less dissipation.

The first-order upwind method is based on the original work of Courant et. al [19], where the authors developed the Courant-Isaacson-Rees (CIR) methods. These methods can be used for a system of equations, and the upwind direction is chosen based on the signs of the eigenvalues of the Jacobian matrix of the system.

The Godunov's method

This method was first proposed by Godunov [20] as a first-order accurate method. The idea behind this method is to reconstruct a piecewise constant function for the q_i^n solution in each cell based on the average q_i^n at the cell centers. Then, the solution is evolved to the next time step by solving the resulting Riemann problem at each cell interface. The method, as discussed by Leveque [15] has three main steps:

- 1- Solving the Riemann problem at $x_{i\pm 1/2}$ to find $q_{i\pm 1/2}^n$.
- 2- Defining the numerical fluxes $\mathcal{F}_{i\pm 1/2}^n = f(q_{i\pm 1/2}^n)$.
- 3- Applying the conservative form (Eq. (3.6)) of the numerical scheme to evolve the solution in time.

For a simple advection problem (Eq. (2.4)), Godunov's method simplifies into the first-order upwind method. For non-linear equations, the solution depends on the type of discontinuity and its speed s . Figure 3.2 shows five different possibilities for the solution at the cell face $x_{i+1/2}$. For cases (a) and (c), the discontinuity is moving to the left, and $q_{i+1/2}^n = q_{i+1}^n$. For the cases (b) and (e) the discontinuity is moving to the right, and $q_{i+1/2}^n = q_i^n$. For the case (d), the rarefaction wave spreads on the two sides of $x = x_{i+1/2}$, and the solution at the interface is given by the solution for the rarefaction wave q_s^n .

Based on this discussion, the flux function can be given as:

$$\mathcal{F}_{i+1/2}^n = \begin{cases} f(q_i^n) & \text{if } q_i^n > q_s^n \text{ and } s > 0 \\ f(q_{i+1}^n) & \text{if } q_{i+1}^n < q_s^n \text{ and } s < 0 \\ f(q_s^n) & \text{if } q_i^n < q_s^n < q_{i+1}^n \end{cases} \quad (3.31)$$

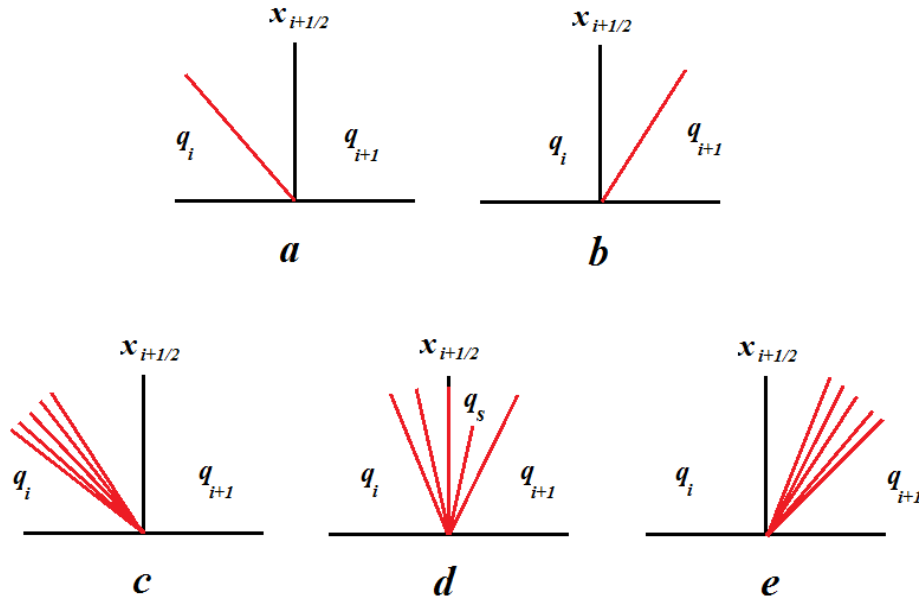


Figure 3.2 Possible solutions for the non-linear scalar Riemann problem

The piecewise constant reconstruction used in Godunov's method yields a first-order accurate scheme. Other schemes use higher order piecewise polynomials for reconstruction, which results in higher order schemes. Some of these schemes will be discussed later.

3.2.2 High-Order Accurate Schemes

Second-order upwind method

The second-order upwind method is also called the *Linear Upwind Differencing* method (LUD). It is similar to the 1st-order upwind method in the sense that it uses numerical fluxes based on the direction of the characteristic speeds. On the other hand, this method uses information of two neighboring cells instead of one, which results in a second-order accurate scheme.

The flux for this method is simply $\mathcal{F}_{i+1/2}^n = f(q_{i+1/2}^n)$, and the solution approximation $q_{i+1/2}^n$ at the cell interface is given by:

$$q_{i+1/2}^n = \begin{cases} \frac{3}{2}q_i^n - \frac{1}{2}q_{i-1}^n & \text{if } a_{i+1/2} > 0 \\ \frac{3}{2}q_{i+1}^n - \frac{1}{2}q_{i+2}^n & \text{if } a_{i+1/2} < 0 \end{cases} \quad (3.32)$$

This method is known to be dispersive. This dispersion can be shown by studying the modified differential equation for the scheme as follows.

Consider the test wave function $q_{test} = e^{i(\omega t + \beta x)}$, where ω is the frequency and β is the wave number. If we substitute this into Eq. (2.4) we obtain the relation:

$$\frac{\omega}{\beta} = -\bar{u}$$

This is known as the *dispersion relation* for the partial differential equation. It shows that for any wave-like solution, all waves travel with the same constant speed ($-\bar{u}$) regardless of their wave number. The modified differential equation for the LUD scheme is:

$$\frac{\partial q}{\partial t} + \bar{u} \frac{\partial q}{\partial x} = \bar{u} \frac{\Delta x^2}{3} \frac{\partial^3 q}{\partial x^3}$$

If we substitute the test wave function into this equation and simplify, we get the dispersion relation:

$$\frac{\omega}{\beta} = -\bar{u} + \bar{u} \frac{\Delta x^2}{3} \beta^2$$

This means that the wave speed is no longer constant and depends on the wave number and a coefficient $\frac{\Delta x^2}{3}$, which vanishes as the mesh size is refined. This causes short waves (waves with large wave numbers) to travel with a speed less than the one expected from Eq. (2.4).

The Lax-Wendroff method

This method is a result of Lax and Wendroff's work [21]. It is second-order accurate in both space and time, and it is based on a Taylor series expansion in time. The scheme is given by:

$$q_i^{n+1} = q_i^n - \frac{\Delta t A}{2\Delta x} (q_{i+1}^n - q_{i-1}^n) + \frac{\Delta t^2 A^2}{2\Delta x^2} (q_{i+1}^n - 2q_i^n + q_{i-1}^n) \quad (3.33)$$

This scheme can be regarded as a finite volume scheme in a conservative form with the numerical flux:

$$\mathcal{F}_{i+1/2}^n = \frac{A}{2} [q_{i+1}^n + q_i^n] - \frac{\Delta t A^2}{2\Delta x} (q_{i+1}^n - q_i^n) \quad (3.34)$$

For a system of non-linear equations this scheme can be extended in different ways, one of which is the Richtmyer Two-Step Lax-Wendroff method. The first step in this approach is to calculate the solution approximation at the interface after half a time step (at $t_{n+1/2}$), and the second step is to use the numerical flux $f(q_{i+1/2}^{n+1/2})$ in the conservative form (Eq. (3.6)). This is defined as follows:

$$q_{i+1/2}^{n+1/2} = \frac{1}{2} (q_{i+1}^n + q_i^n) - \frac{\Delta t}{2\Delta x} [f(q_{i+1}^n) - f(q_i^n)]$$

$$\mathcal{F}_{i+1/2}^n = f(q_{i+1/2}^{n+1/2})$$

$$q_i^{n+1} = q_i^n - \frac{\Delta t}{\Delta x} (\mathcal{F}_{i+1/2}^n - \mathcal{F}_{i-1/2}^n)$$

It can be shown that the Richtmyer Two-Step Lax-Wendroff method reduces to the standard Lax-Wendroff method for a system of linear equations.

The Quadratic Upstream Interpolation for Convective Kinematics (QUICK) method

This scheme was introduced by Leonard [22] as a stable scheme based on quadratic upstream interpolation of the approximate solution at neighboring cells. In his paper he found that stability cannot be guaranteed with a scheme based on central difference, so he suggested upstream difference methods for problems with convection terms. Hence, the QUICK scheme is meant to possess both good accuracy and the stable property of upstream schemes.

The flux for this method is $\mathcal{F}_{i+1/2}^n = f(q_{i+1/2}^n)$, and the solution approximation $q_{i+1/2}^n$ at the cell interface is given by:

$$q_{i+1/2}^n = \begin{cases} \frac{1}{2}(q_i^n + q_{i+1}^n) - \frac{1}{8}(q_{i-1}^n + q_{i+1}^n - 2q_i^n) & \text{if } a_{i+1/2} > 0 \\ \frac{1}{2}(q_i^n + q_{i+1}^n) - \frac{1}{8}(q_{i+2}^n + q_i^n - 2q_{i+1}^n) & \text{if } a_{i+1/2} < 0 \end{cases} \quad (3.35)$$

This can be interpreted as the unstable central difference method with a correction term corresponding to the upstream-weighted curvature. This kind of interpolation yields a third-order accuracy in space.

3.3 Non-Linear Schemes

Godunov proved that monotonicity cannot be achieved with linear schemes of order higher than one when they are used to solve the advection equation. This is referred to as *Godunov's order barrier theorem*, and it states that [20]:

“Linear numerical schemes for solving the advection equation, having the property of not generating new extrema (monotone scheme), can be at most first-order accurate.”

This implies that the only high-order accurate monotone schemes possible are non-linear schemes, where the coefficients c_k in Eq. (3.21) are not constant, and depend on the solution itself. In this section we present two families of non-linear schemes used to overcome the contradiction between high-order accuracy and monotonicity of Godunov's theorem: the reconstruction-based methods and the flux limiter methods.

3.3.1 Reconstruction-Based Methods

To better understand this family of schemes we recall the first-order Godunov's scheme. With this scheme, we used a constant piecewise reconstruction for the solution in each cell based on the averages q_i^n at cell centers. A better approximation can be achieved by higher-order piecewise polynomial $p_i(x)$ in spatial cell $[x_{i-1/2}, x_{i+1/2}]$. This kind of reconstruction achieves a better recovery of the information lost in the averaging process done in Eq. (3.2). The choice of such polynomial is restricted by two conditions:

- 1- It has to be conservative, meaning it satisfies the definition: $q_i^n = \frac{1}{\Delta x_i} \int_{i-1/2}^{i+1/2} q(x, t_n) dx$.
- 2- It has to maintain the non-oscillatory property. This can be attained by either imposing a TVD condition or imposing an Essentially Non-Oscillatory (ENO) property.

Based on the two requirements above, numerical methods can be constructed in many ways depending on the choice of the polynomial $p_i(x)$. Some of the methods are discussed next.

One of the ways of constructing the polynomial $p_i(x)$ is called the *TVD slopes method* or the *slope limiter method*. For such methods the polynomial $p_i(x)$ is given by:

$$p_i(x) = q_i^n + (x - x_i)\Delta_i \quad (3.36)$$

A limitation is prescribed on the slope Δ_i such that the resulting numerical scheme is TVD. There are many TVD slopes in literature; here we list two of them.

The minmod slope

If we define $\Delta_{i+1/2} = \frac{q_{i+1}^n - q_i^n}{\Delta x}$ and $\Delta_{i-1/2} = \frac{q_i^n - q_{i-1}^n}{\Delta x}$, the minmod slope is given by:

$$\Delta_i^{\minmod} = \minmod(\Delta_{i-1/2}, \Delta_{i+1/2})$$

with the minmod function defined as

$$\minmod(x, y) = \begin{cases} x & \text{if } |x| \leq |y| \text{ and } xy > 0 \\ y & \text{if } |x| > |y| \text{ and } xy > 0 \\ 0 & \text{if } xy < 0 \end{cases}$$

The Monotonized Central-difference (MC) slope

$$\Delta_i^{MC} = \minmod\left(\frac{1}{2}(\Delta_{i+1/2} + \Delta_{i-1/2}), 2\Delta_{i+1/2}, 2\Delta_{i-1/2}\right)$$

Many numerical methods are based on the concept of slope limiters, for example the MUSCL family of numerical schemes [23].

Another way of reconstructing the polynomial $p_i(x)$ is called the non-linear reconstruction. This type of reconstruction uses polynomials of order higher than one. One example of numerical methods that use the non-linear reconstruction is the Piecewise Parabolic Method (PPM) [24].

Another type of reconstruction-based methods suggested by Harten and Osher [25] [26] is called the Essentially Non-Oscillatory (ENO) method. This method does not necessarily maintain a *TVD* property; instead it diminishes the number of local extremas. Consequently the values of local extremas are not required to be damped at each time step.

ENO methods are reconstruction based methods, for which piecewise polynomials are reconstructed for each individual cell based on the average value of the solution in the cell of interest and its neighboring cells, all together are called the numerical stencil. The more cells contained in the numerical stencil the higher the order of the reconstructed polynomial and, consequently, the higher the order of the numerical scheme. The idea of the method is to choose among all candidate stencils so that discontinuous cells are excluded from the stencil as long as that is possible. The chosen stencil is then used for the reconstruction process.

Another method based on the ENO method is called the Weighted Essentially Non-Oscillatory (WENO) method [27]. In this method a convex combination of all the candidate stencils is used for the reconstruction process. This combination is based on a weighted average of candidate stencils, in which the weighting factors depend on the smoothness of the solution in each candidate stencil. Because a combination of all candidate stencils is used rather than one stencil, the WENO method improves the order of accuracy of the ENO method in smooth regions. Different numerical schemes for temporal discretization can be used with the ENO and WENO methods. One popular way is to use the Runge-Kutta method [28].

3.3.2 Flux Limiter Methods

The flux limiter approach is a non-linear scheme based on a combination of a dissipative 1st-order scheme and a higher-order accurate scheme [29]. The idea is to combine the monotonicity of first-order accurate schemes and the accuracy of higher-order linear schemes by using the former near discontinuities and the

latter in smooth regions. Examples of this approach are the works done by Harten [17], Sweby [30] and Kadalbajoo [31]. The numerical scheme in a conservative form is given by:

$$q_i^{n+1} = q_i^n - \lambda(\mathcal{F}_{i+1/2}^{TVD^n} - \mathcal{F}_{i-1/2}^{TVD^n}) \quad (3.37)$$

The TVD numerical flux in Eq. (3.37) is given by:

$$\mathcal{F}_{i\pm 1/2}^{TVD} = \mathcal{F}_{i\pm 1/2}^{LO} + \varphi_{i\pm 1/2}[\mathcal{F}_{i\pm 1/2}^{HI} - \mathcal{F}_{i\pm 1/2}^{LO}] \quad (3.38)$$

where $\mathcal{F}_{i\pm 1/2}^{LO}$ is the numerical flux associated with a first-order scheme and $\mathcal{F}_{i\pm 1/2}^{HI}$ is the numerical flux associated with a higher order scheme. For $\varphi_{i\pm 1/2} = 0$ this reduces to the first-order accurate scheme, and for $\varphi_{i\pm 1/2} = 1$ it reproduces the high-order accurate scheme. The limiter function $\psi_{i\pm 1/2}$ is chosen such that the scheme in Eq. (3.37) is *TVD*

To illustrate this method we consider the numerical flux $\mathcal{F}_{i\pm 1/2}^{LO}$ associated with the 1st-order upwind scheme, and the numerical flux $\mathcal{F}_{i\pm 1/2}^{HI}$ associated with the Lax-Wendroff scheme. Both are taken for the case of a scalar advection equation:

$$\mathcal{F}_{i+1/2}^{LO} = \begin{cases} \bar{u}q_i^n & \text{if } \bar{u} > 0 \\ \bar{u}q_{i+1}^n & \text{if } \bar{u} < 0 \end{cases} \quad (3.39)$$

$$\mathcal{F}_{i+1/2}^{HI} = \frac{\bar{u}}{2}(1+v)q_i^n + \frac{\bar{u}}{2}(1-v)q_{i+1}^n \quad (3.40)$$

where v is the courant number defined in Eq. (3.14).

The next step is to find the *TVD* region for the limiter function $\varphi_{i+1/2}$ that depends on the smoothness of the solution, i.e. $\varphi_{i+1/2} = \varphi(r_{i+1/2})$. We define the smoothness parameter:

$$r_{i+1/2} = \begin{cases} \frac{\Delta q_{i-1/2}}{\Delta q_{i+1/2}} = \frac{q_i^n - q_{i-1}^n}{q_{i+1}^n - q_i^n} & \text{if } \bar{u} > 0 \\ \frac{\Delta q_{i+3/2}}{\Delta q_{i+1/2}} = \frac{q_{i+2}^n - q_{i+1}^n}{q_{i+1}^n - q_i^n} & \text{if } \bar{u} < 0 \end{cases} \quad (3.41)$$

If we substitute Eqs. (3.39) and (3.40) into Eq. (3.38), then into Eq. (3.37), we can use the definition of the smoothness parameter in Eq. (3.41) to rewrite the scheme into an incremental form. We can use the conditions in Eq. (3.20) to find the *TVD* region shown in Figure 3.3

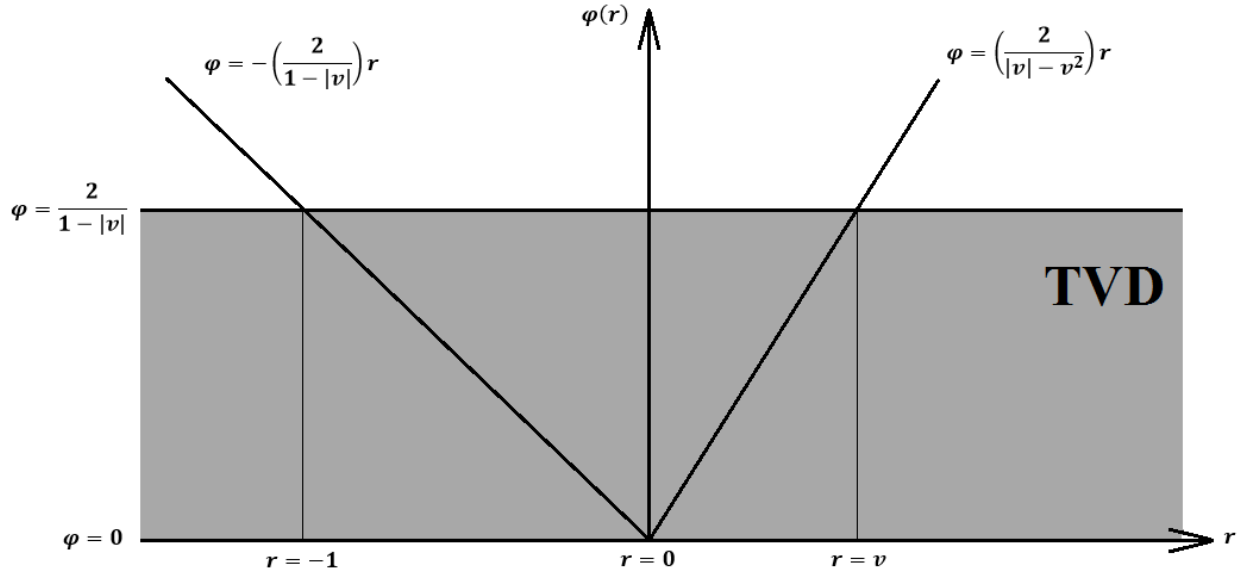


Figure 3.3 *TVD* region based on the 1st-order upwind and Lax-Wendroff methods

Any limiter function contained within the shaded *TVD* region in Figure 3.3 yields a *TVD* numerical scheme, yet not all *TVD* limiters are good limiters.

Some flux limiter functions shown by other researchers to work well are listed below:

The SUPERBEE limiter

$$\varphi(r)^{SUPERBEE} = \begin{cases} 0 & \text{if } r \leq 0 \\ 2r & \text{if } 0 \leq r \leq \frac{1}{2} \\ 1 & \text{if } \frac{1}{2} \leq r \leq 1 \\ r & \text{if } 1 \leq r \leq 2 \\ 2 & \text{if } r \geq 2 \end{cases}$$

The VANLEER limiter

$$\varphi(r)^{VANLEER} = \begin{cases} 0 & \text{if } r \leq 0 \\ \frac{2r}{1+r} & \text{if } r \geq 0 \end{cases}$$

The VANALBADA limiter

$$\varphi(r)^{VANALBADA} = \begin{cases} 0 & \text{if } r \leq 0 \\ \frac{r(1+r)}{1+r^2} & \text{if } r \geq 0 \end{cases}$$

The MINBEE limiter

$$\varphi(r)^{MINBEE} = \begin{cases} 0 & \text{if } r \leq 0 \\ r & \text{if } 0 \leq r \leq 1 \\ 1 & \text{if } r \geq 1 \end{cases}$$

All the limiter functions above share the property that $\varphi(1) = 1$. This means that for smooth regions the scheme reduces to the second-order Lax-Wendroff scheme. Figure 3.4 shows the four different limiter functions in the TVD region for a Courant number of 0.3.

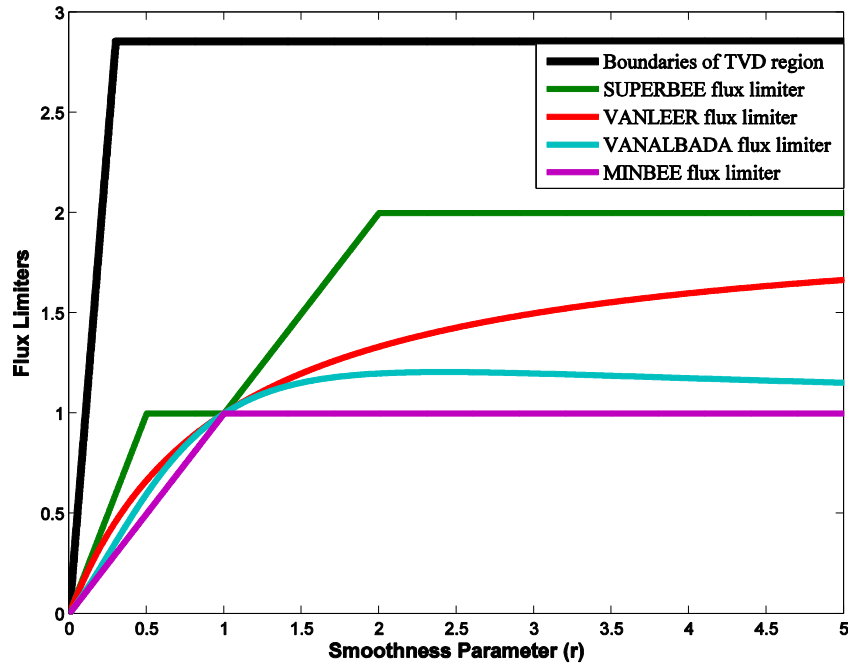


Figure 3.4 Different choices for flux limiters in a TVD region with Courant number = 0.3

Another family of flux limiters was suggested by Kadalbajoo and Kumar [31]. Their limiter was based on a first-order upwind scheme and second-order upwind scheme. The limiter is given by:

$$\varphi(r)^{KUMAR} = \begin{cases} 0 & \text{if } r \leq 0 \\ \min\left(2, \frac{2}{r}, \frac{1+\gamma}{r+\gamma}\right) & \text{if } r > 0 \end{cases}$$

where $\gamma \in [0, \infty]$.

Flux limiter methods can be based on other first-order accurate schemes, such as the Lax-Friedrich scheme, rather than the 1st-order upwind scheme. The same approach is followed to define the *TVD* region. More on this can be found in [23].

The analysis above was made for a scalar conservation equation. For non-linear system of equations the problem is more complicated, however the concept of flux limiters can be extended in an empirical way, as suggested by Toro [23].

3.4 Temporal Discretization

Most of the numerical schemes discussed so far are based on a first-order explicit discretization in time. Many options are available to obtain higher accuracy in time. In this section we discuss some of these options.

3.4.1 The Theta Method

This method is also called the generalized Crank-Nicolson method. It is based on a weighted average of explicit and implicit terms in the difference equation. For the simple advection equation (Eq. (2.4)) with the definitions in Eqs. (3.3), (3.4) and (3.5) the theta method is given by:

$$q_i^{n+1} = q_i^n - \lambda[\theta(\mathcal{F}_{i+1/2}^{n+1} - \mathcal{F}_{i-1/2}^{n+1}) + (1 - \theta)(\mathcal{F}_{i+1/2}^n - \mathcal{F}_{i-1/2}^n)] \quad (3.42)$$

θ is a positive number, $\theta \in [0,1]$, and the numerical fluxes $\mathcal{F}_{i\pm 1/2}$ in Eq. (3.42) are calculated using one of the numerical schemes discussed before.

Equation (3.42) represents a family of schemes characterized by θ . Different schemes can be obtained for different values of θ . Explicit scheme is obtained for $\theta = 0$, the implicit scheme for $\theta = 1$ and the Crank-

Nicolson scheme for $\theta = 1/2$. The theta method is unconditionally stable for any choice of $\theta \in [1/2, 1]$ [32][33].

Attributes of the theta method can be studied by carrying out the modified equation analysis. Such analysis reveals information about the order of accuracy of the method, its dissipation and dispersion properties. Here, the modified equation analysis was done for the cases of first-order upwind scheme and second-order upwind scheme. Analysis was conducted for the scalar advection problem with positive velocity. Details for this analysis are presented in Appendix A.

The modified equation for the theta method with the first-order upwind space discretization is given by:

$$\frac{\partial q}{\partial t} + \bar{u} \frac{\partial q}{\partial x} = \left(\frac{\bar{u}\Delta x}{2} + \bar{u}^2 \Delta t \left(\theta - \frac{1}{2} \right) \right) \frac{\partial^2 q}{\partial x^2} \quad (3.43)$$

and for the case of second-order upwind scheme:

$$\frac{\partial q}{\partial t} + \bar{u} \frac{\partial q}{\partial x} = \bar{u}^2 \Delta t \left(\theta - \frac{1}{2} \right) \frac{\partial^2 q}{\partial x^2} + \left(\frac{\bar{u}\Delta x^2}{3} - \frac{\bar{u}^3 \Delta t^2}{2} \left(\theta - \frac{1}{3} \right) \right) \frac{\partial^3 q}{\partial x^3} \quad (3.44)$$

The first observation to notice about the modified differential equations above is that all terms involving Δt exist for any choice of θ except for the case of Crank-Nicolson method ($\theta = 1/2$). This means that the theta method is first-order in time except for the case of Crank-Nicolson method, which is second-order in time.

Another observation is the dissipation properties of the two schemes shown by terms on the right-hand side with second derivative in space. The dissipation coefficient for the first-order upwind scheme can be presented as two parts: due to the spatial discretization given by $\left(\frac{\bar{u}\Delta x}{2} \right)$, and due to temporal discretization given by $\bar{u}^2 \Delta t \left(\theta - \frac{1}{2} \right)$. For the second-order upwind scheme, dissipation occurs only due to temporal

discretization with the coefficient $\bar{u}^2 \Delta t \left(\theta - \frac{1}{2} \right)$. Therefore, for both schemes dissipation due temporal discretization ceases to exist with $\theta = 1/2$ (Crank-Nicolson method).

Equation (3.44) shows that the second-order upwind scheme poses dispersion properties as well, with a dispersion coefficient of $\left(\frac{\bar{u} \Delta x^2}{3} - \frac{\bar{u}^3 \Delta t^2}{2} \left(\theta - \frac{1}{3} \right) \right)$.

3.4.2 Semi-Discrete Methods

All numerical schemes considered up to this point are fully discretized in both space and time. Another way to handle time discretization is the semi-discrete method. In this method the problem is discretized in space only and is left continuous in time. This leads to a system of ordinary differential equations in time called the semi-discrete equations. This system of ordinary differential equations can be solved using any standard numerical method, including the implicit, explicit and Crank-Nicolson method discussed before.

CHAPTER 4. HIGH-RESOLUTION TVD SCHEME FOR HYPERBOLIC PROBLEMS

In this Chapter we propose a new high-resolution scheme for hyperbolic problems. The main idea is to use a combination of the first-order accurate upwind scheme and the third-order QUICK scheme using a flux limiter function derived in a systematical approach. The generalized Crank-Nicolson method (theta method) is used for temporal discretization. Bounds for the high-order *TVD* region are given for the limiter function such that the resulting scheme is *TVD*. The scheme is applied to a simple advection problem with smooth and discontinuous solutions, and convergence rates are analyzed and compared to those obtained from well-known classical and high-resolution schemes.

First, we consider Eq. (2.4) and implement the numerical scheme in Eq. (3.42) with a numerical flux

$\mathcal{F}_{i\pm 1/2} = \mathcal{F}_{i\pm 1/2}^{TVD}$, where:

$$\mathcal{F}_{i\pm 1/2}^{TVD} = \mathcal{F}_{i\pm 1/2}^{1st} + \varphi_{i\pm 1/2}[\mathcal{F}_{i\pm 1/2}^{QUICK} - \mathcal{F}_{i\pm 1/2}^{1st}] \quad (4.1)$$

$\mathcal{F}_{i\pm 1/2}^{1st}$ is the numerical flux associated with a 1st-order upwind scheme and $\mathcal{F}_{i\pm 1/2}^{QUICK}$ is the numerical flux associated with 3rd-order QUICK scheme. Both numerical fluxes depend on the direction of characteristic speeds and consequently obey the hyperbolicity property of the problem. The limiter function $\varphi_{i\pm 1/2}$ is chosen such that the scheme is *TVD*.

4.1 Bounds of the TVD Region

To find the bounds of the *TVD* region of the scheme we consider the explicit formulation of the theta method ($\theta = 0$), and we apply it to the linear scalar equation, namely:

$$\frac{\partial q}{\partial t} + u \frac{\partial q}{\partial x} = 0$$

For this equation the numerical flux due to the 1st-order upwind scheme is defined as:

$$\mathcal{F}_{i+1/2}^{1st} = \begin{cases} uq_i & u > 0 \\ uq_{i+1} & u < 0 \end{cases} \quad (4.2)$$

and for the 3rd-order QUICK scheme:

$$\mathcal{F}_{i+1/2}^{QUICK} = \begin{cases} \frac{u}{8}(6q_i + 3q_{i+1} - q_{i-1}) & u > 0 \\ \frac{u}{8}(6q_{i+1} + 3q_i - q_{i+2}) & u < 0 \end{cases} \quad (4.3)$$

For the case $u > 0$, if we substitute the numerical fluxes into Eq. (4.1) and then into Eq. (3.42), and using $\theta = 0$, we obtain the following scheme:

$$q_i^{n+1} = q_i^n - v \left[(q_i - q_{i-1}) + \varphi_{i+1/2} \left[\frac{1}{8}(6q_i + 3q_{i+1} - q_{i-1}) - q_i \right] - \varphi_{i-1/2} \left[\frac{1}{8}(6q_{i-1} + 3q_i - q_{i-2}) - q_{i-1} \right] \right] \quad (4.4)$$

where $v = (u\Delta t/\Delta x)$ is the Courant number.

With additional algebraic manipulation, this can be written as:

$$q_i^{n+1} = q_i^n - v \left[1 + \frac{\varphi_{i+1/2}}{8} \left[\frac{3}{r_i} + 1 \right] - \frac{\varphi_{i-1/2}}{8} [3 + r_{i-1}] \right] \Delta q_{i-1/2} \quad (4.5)$$

where $r_i = \frac{\Delta q_{i-1/2}}{\Delta q_{i+1/2}}$ is referred to as the smoothness parameter. This is a numerical scheme written in an

incremental form (Eq. (3.8)) with the following parameters:

$$D_{i-1/2} = \left(v \left[1 + \frac{\varphi_{i+1/2}}{8} \left[\frac{3}{r_i} + 1 \right] - \frac{\varphi_{i-1/2}}{8} [3 + r_{i-1}] \right] \right), \quad C_{i+1/2} = 0 \quad (4.6)$$

Implementing the conditions for the scheme to be *TVD* (Eq. (3.20)), we obtain the following inequality:

$$-8 \leq \varphi_{i+1/2} \left[\frac{3}{r_i} + 1 \right] - \varphi_{i-1/2} [3 + r_{i-1}] \leq 8 \left(\frac{1-v}{v} \right) \quad (4.7)$$

At this point we impose another restriction to our scheme by requiring $0 \leq v \leq 1/2$. This yields the following:

$$|\varphi_{i+1/2}(3 + r_i)/r_i - \varphi_{i-1/2}(3 + r_{i-1})| \leq 8 \quad (4.8)$$

For our scheme to be *TVD* at the extreme points in the solution, we must have $\varphi(r) = 0$ for $r < 0$. This condition, along with Eq. (4.8) can be satisfied within the bounds:

$$0 \leq \left(\varphi_{i+1/2}(3 + r_i)/r_i, \varphi_{i-1/2}(3 + r_{i-1}) \right) \leq 8 \quad (4.9)$$

Eq. (4.9) defines the *TVD* region shaded in grey in Figure 4.1. This region is bounded by the function

$\varphi(r) = \min \left[\frac{8r}{3+r}, \frac{8}{3+r} \right]$. The same *TVD* region can be obtained for the case of negative advection velocity

(details for the case of $u < 0$ can be found in Appendix B). For the numerical scheme to be *TVD*, the limiter function has to be bounded by the *TVD* area of Figure 4.1.

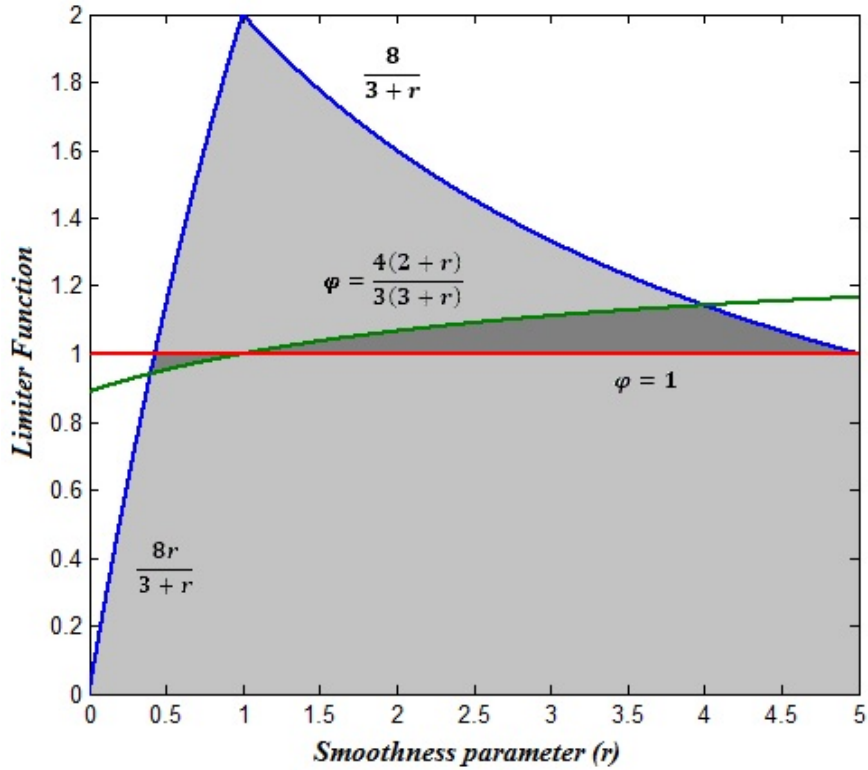


Figure 4.1 Schematic of the *TVD* region for the new high-order scheme

4.2 High-Order of Accuracy

Equation (4.1) suggests that maximizing the flux limiter increases the anti-diffusivity of the scheme (because the 1st-order scheme is the diffusive one). This means that a flux limiter function corresponding to the upper boundary of the *TVD* region yields the least diffusive scheme possible. Nevertheless, choosing

such a limiter does not guarantee the highest possible order of accuracy. To ensure high-order of accuracy we require one additional condition; the limiter function should be chosen such that the scheme in Eq. (4.5) is 3rd-order accurate whenever possible. To impose this constraint, we investigate another numerical scheme; the 3rd-order upwind scheme. Due to this scheme, the numerical fluxes for Eq. (2.4) are defined as:

$$\mathcal{F}_{i+1/2}^u = \begin{cases} \frac{u}{6}(5q_i - q_{i-1} + 2q_{i+1}) & u > 0 \\ \frac{u}{6}(5q_{i+1} - q_{i+2} + 2q_i) & u < 0 \end{cases} \quad (4.10)$$

The discretization for the advection equation (Eq. (2.4)) due to this scheme (for $u > 0$) is given by:

$$q_i^{n+1} = q_i^n - \frac{\Delta t}{\Delta x} u \left[\frac{5q_i - q_{i-1} + 2q_{i+1}}{6} - \frac{5q_{i-1} - q_{i-2} + 2q_i}{6} \right] \quad (4.11)$$

With algebraic manipulation (details can be found in Appendix B), it can be shown that this scheme is equivalent to the scheme in Eq. (4.5) when the flux limiter function is chosen to be $\varphi = \frac{4(2+r)}{3(3+r)}$. Hence, we define the region shaded with dark gray in Figure 4.1 as the desired 3rd-order *TVD* region for our scheme.

To guarantee all the imposed conditions are satisfied, we derive a family of flux limiters lying in the 3rd-order *TVD* region whenever possible. Any flux function in that region can be expressed as an arithmetic average of two limiter functions:

- 1- $\varphi = 1$, corresponding to the QUICK scheme.
- 2- $\varphi = \frac{4(2+r)}{3(3+r)}$, corresponding to the 3rd-order upwind scheme, namely:

$$\varphi^* = 1 + \frac{\delta(r-1)}{3(3+r)}, \quad 0 < \delta < 1 \quad (4.12)$$

Intersection points r_1^* and r_2^* are found to be $r_1^* = \frac{9-\delta}{21-\delta}$ and $r_2^* = \frac{\delta+15}{\delta+3}$ (see Figure 4.2). We can see that for any chosen value of δ , the limiter function satisfies our condition for smooth regions $\varphi^*(1) = 1$. The arithmetic average and the intersection points are shown in Figure 4.2.

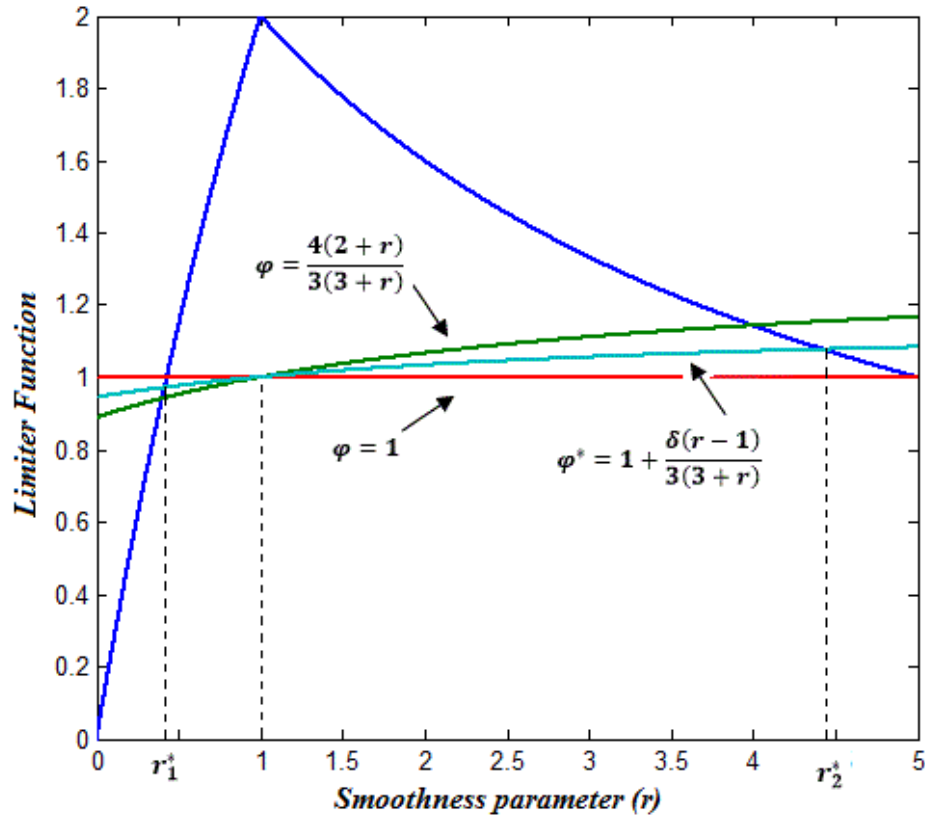


Figure 4.2 Arithmetically averaged limiter function

Based on the above, we propose the following new family of flux limiters characterized by the parameter δ :

$$\varphi(r) = \begin{cases} 0 & r < 0 \\ \frac{8r}{3+r} & 0 < r < r_1^* \\ 1 + \frac{\delta(r-1)}{3(3+r)} & r_1^* < r < r_2^* \\ \frac{8}{3+r} & r_2^* < r \end{cases} \quad (4.13)$$

Equation (4.13) shows that the proposed limiter function is continuous and bounded for any value of the smoothness parameter r . It also satisfies the condition for smooth regions $\varphi(1) = 1$. The flux limiter functions in Eq. (4.13) lie in the *TVD* region for any choice of δ , hence, the resulting numerical scheme is *TVD*.

4.3 Numerical Results

In this section we present two sets of numerical results, one for the case of smooth solutions, and the other for discontinuous solutions. Both sets of results are shown for the case of pure advection with positive velocity. Results from the proposed scheme are also compared to those from well-known numerical schemes.

4.3.1 Smooth Initial Conditions

For this set of results we consider the simple advection equations (Eq. (2.4)) with a smooth initial condition given by:

$$q_0(x) = 0.5 + 0.3\sin(2\pi x) \quad (4.14)$$

Boundary conditions for this problem are periodic with a convection velocity $u = 1 \text{ m/s}$ on a 1 m domain. Total time of the simulation was set to 1 sec, so that the exact solution at the end of the simulation is the same as the initial condition.

Figure 4.3 shows a comparison of the new scheme with other classical schemes and existing high-resolution schemes for the case of implicit time discretization ($\theta = 1$). Comparison was made for a grid size of 0.05 m and a Courant number of 0.2.

Excessive dissipation of the 1st-order upwind scheme can be observed and the solution is smeared out due to the inherent numerical viscosity of the scheme. For the two higher order linear schemes (2nd-order upwind and Lax-Wendroff schemes) dissipative errors were minimized, but the signal in the numerical solution was either leading or lagging due to the dispersion errors. This dispersive nature of the error was discussed in terms of the modified equation analysis in the previous Chapter (see Section 3.4.1).

On the other hand, more satisfactory results can be observed when implementing high-resolution schemes with different flux limiters. The new scheme with $\delta = 0$ resulted in the best numerical solution as compared to other schemes.

Figure 4.4 shows a comparison of the same set of schemes for the case of Crank-Nicolson time discretization ($\theta = 1/2$). By examining the modified equation in Eq. (3.44), one can notice that the dissipative error terms cease to exist for the case of $\theta = 1/2$. This explains the reduction in dissipation for the high-order linear schemes (2nd-order upwind and Lax-Wendroff). On the other hand, our new scheme continues to produce the best results as compared to other schemes.

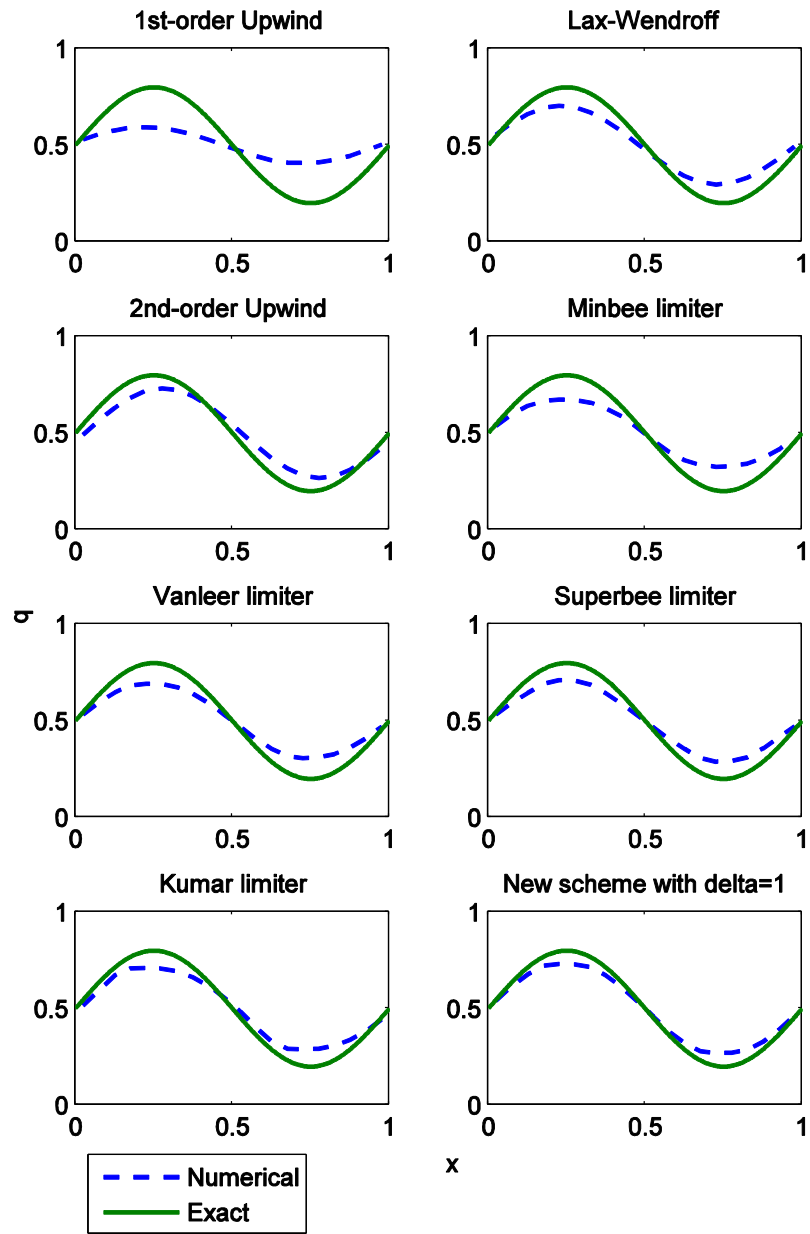


Figure 4.3 Numerical results for smooth solutions with $\theta=1$

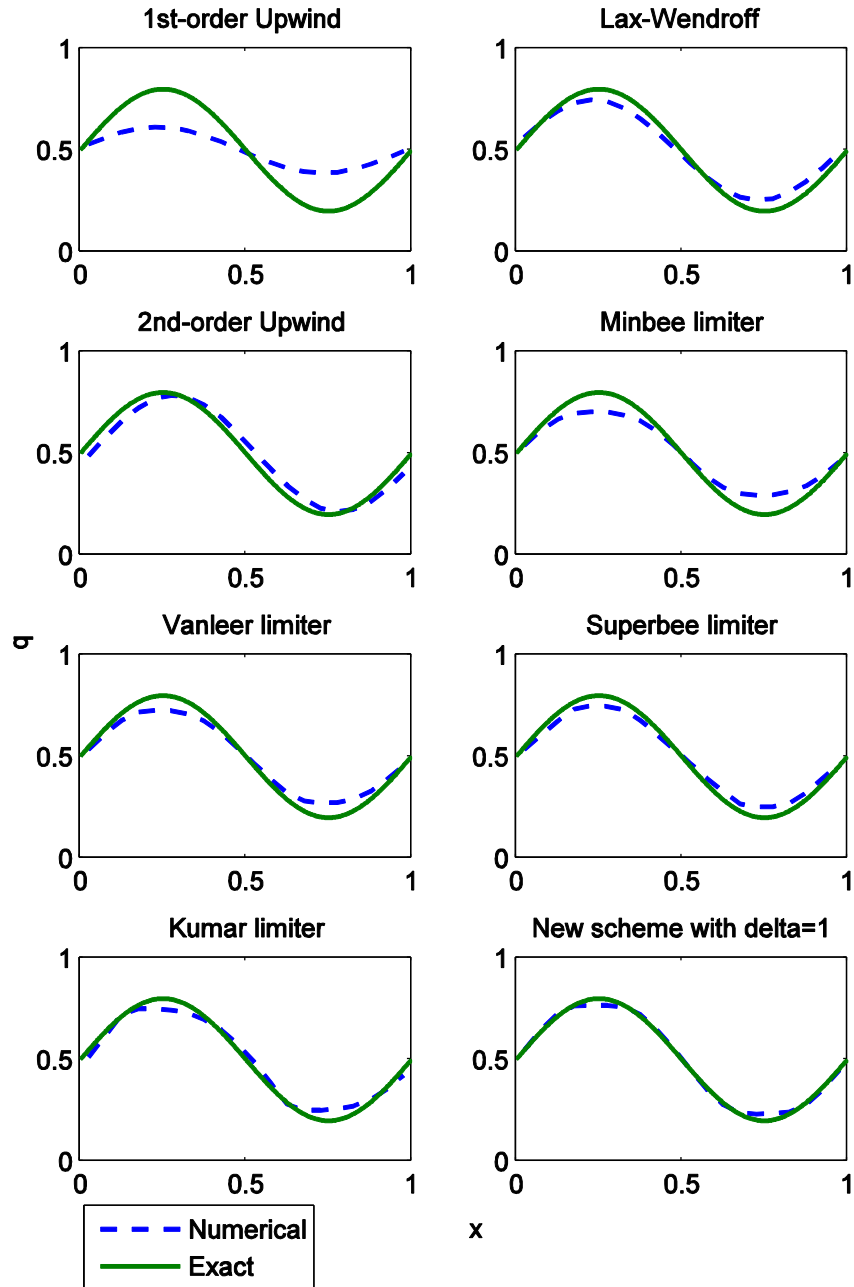


Figure 4.4 Numerical results for smooth solutions with $\theta=1/2$

The exact solution was used to determine the accuracy and convergence rate of considered numerical schemes. Accuracy was assessed on the basis of the L_1 norm, defined as:

$$L_1 = \frac{1}{N} \sum_{i=1}^N |q_N(x_i) - q_E(x_i)| \quad (4.15)$$

where N is the number of cells and $q_N(x_i)$ is the numerical solution at the i^{th} cell. Convergence rate is represented by a log-log plot of the norm of the error versus mesh size.

Figure 4.5 shows results of the spatial convergence for the case $\theta = 1/2$. Convergence rates for several considered schemes are listed in Table 4.1. The results show competitive rate of convergence for the new scheme as compared to the other schemes.

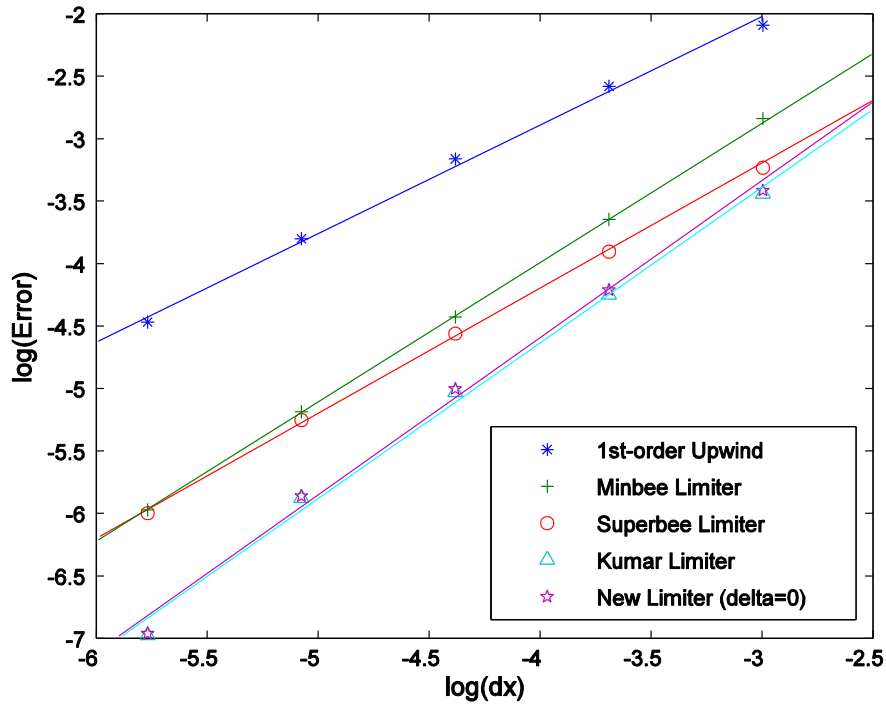


Figure 4.5 Spatial convergence rates of the new scheme for smooth solutions

Table 4.1 Spatial convergence rates of different schemes for smooth solution

Numerical Scheme	Convergence Rate
1 st -order upwind	0.86
Minbee limiter	1.1
Superbee	0.99
Kumar limiter	1.3
New limiter with $\delta = 0$	1.3

4.3.2 Discontinuous Initial Conditions

For this set of results we consider Eq. (2.4) with a discontinuous initial condition given by:

$$q_0(x) = \begin{cases} 0.3 & \text{for } 0.0 < x < 0.4 \\ 0.8 & \text{for } 0.4 < x < 0.6 \\ 0.3 & \text{for } 0.6 < x < 1.0 \end{cases} \quad (4.16)$$

Boundary conditions for this problem are periodic with a convection velocity $u = 1 \text{ m/s}$ on a 1 m domain, and the time of the simulation is 1 sec.

Two sets of results are shown: implicit time discretization ($\theta = 1$) is shown in Figure 4.6, and Crank-Nicolson time discretization is shown in Figure 4.7. Comparison is made for a grid size of 0.0125 m and Courant number of 0.2 .

Results show significantly more dissipation for the case of implicit discretization. For the 2nd-order upwind scheme and the Lax-Wendroff scheme, dispersion error appears in the form of overshoots and undershoots. For the Lax-Wendroff scheme, these oscillations were damped for the case of $\theta = 1$ due to dissipation. High-resolution schemes, including the new scheme, give better results capturing the discontinuity, especially for the case with $\theta = 1/2$ where dissipation is reduced.

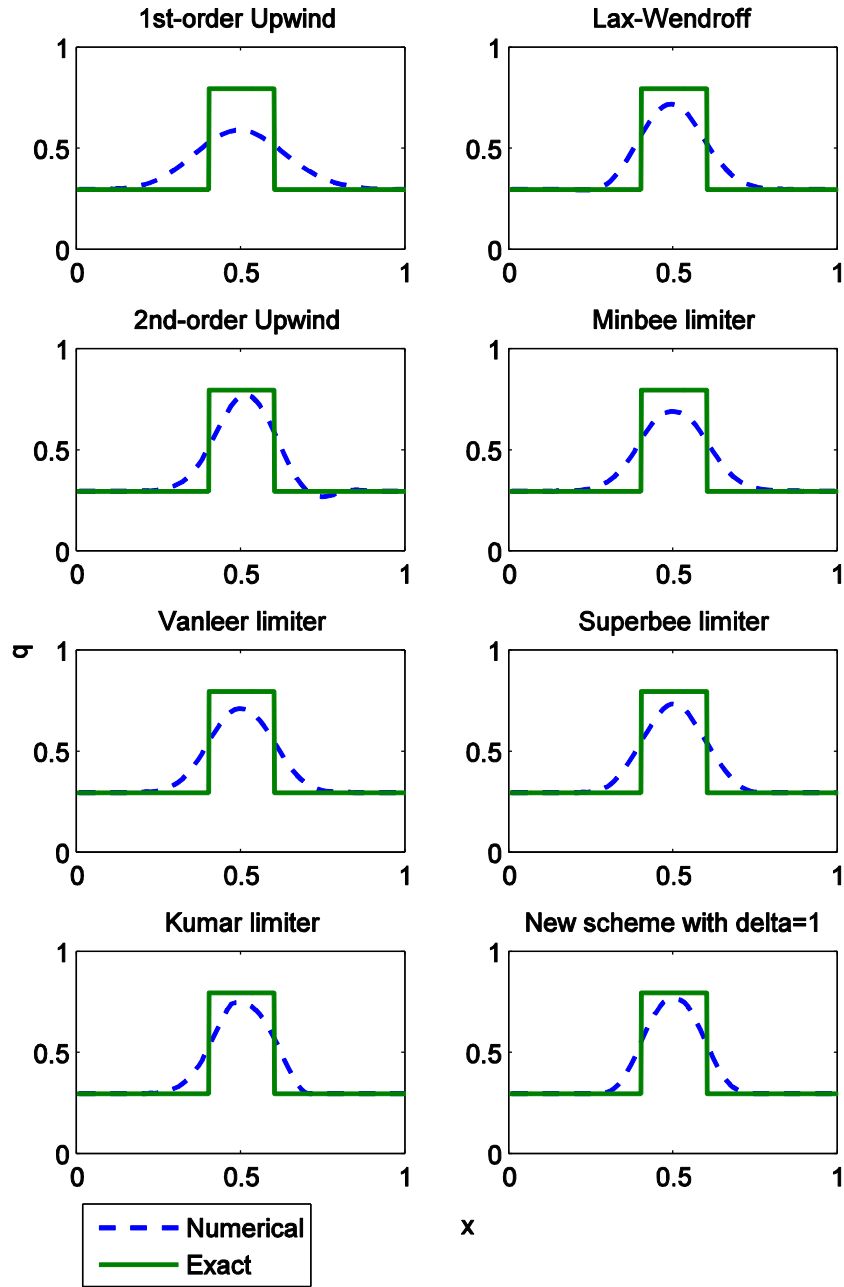


Figure 4.6 Numerical results for discontinuous solutions with $\theta=1$

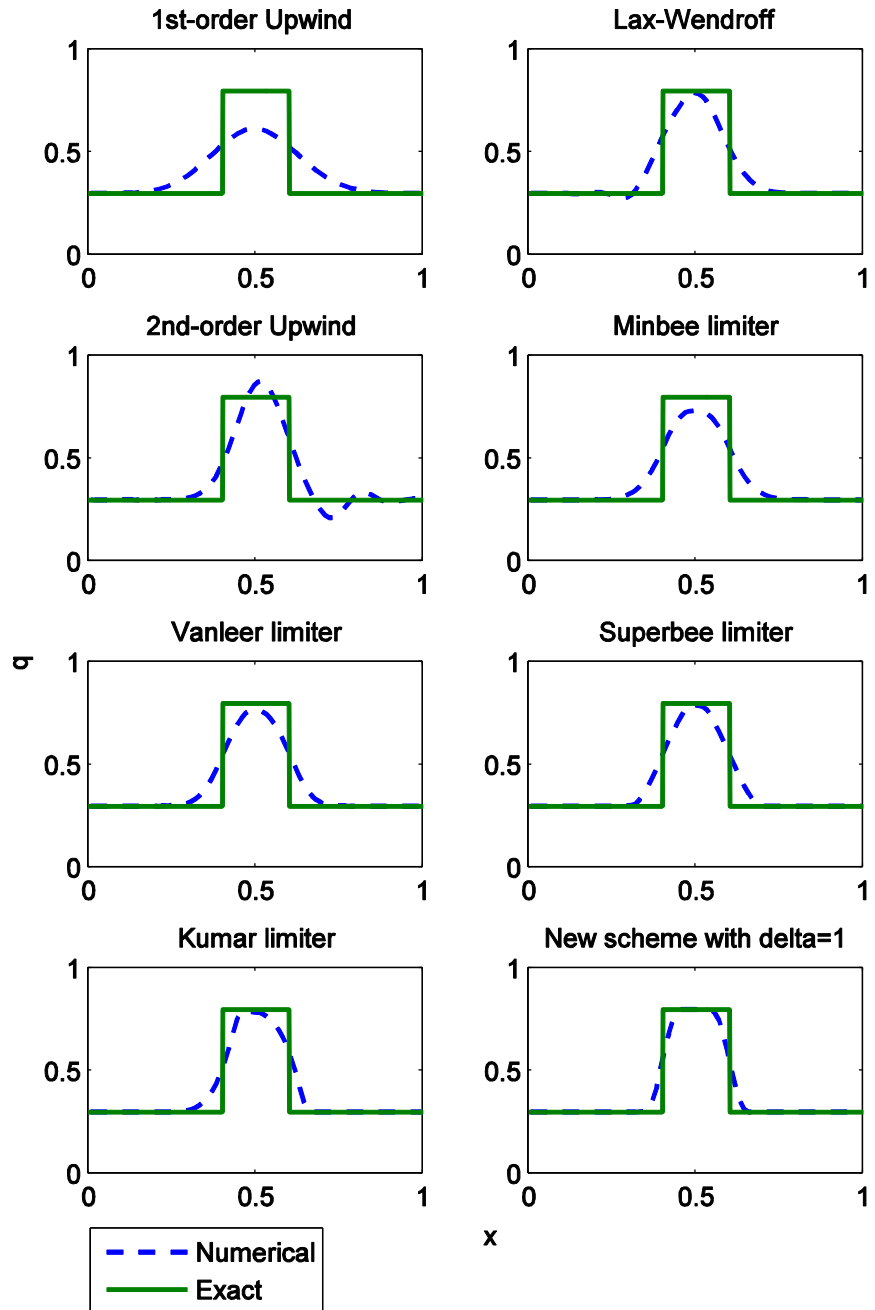


Figure 4.7 Numerical results for discontinuous solutions with $\theta=1/2$

Figure 4.8 shows results of the spatial convergence study for the considered schemes. Results of this study are listed in Table 4.2. We can observe better rate of convergence for the new scheme compared to other schemes.

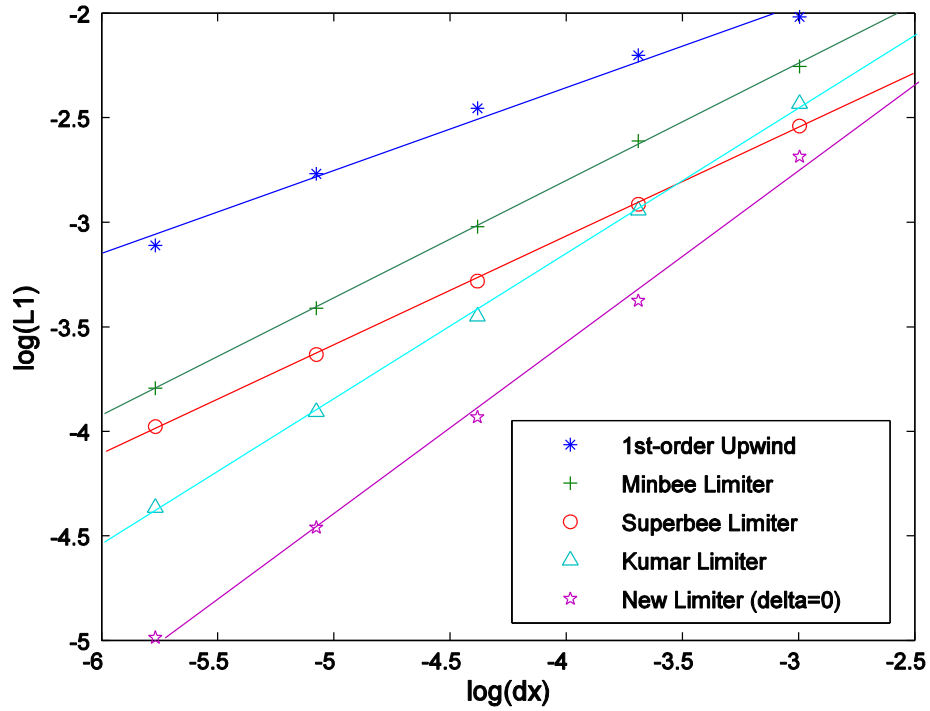


Figure 4.8 Spatial convergence rates for discontinuous solutions

Table 4.2 Spatial convergence rates of different schemes for discontinuous solution

Numerical Scheme	Convergence Rate
1 st -order upwind	0.40
Minbee limiter	0.56
Superbee limiter	0.52
Kumar limiter	0.70
New limiter with $\delta = 0$	0.82

We can see that the proposed scheme exhibits the best convergence rate compared to other considered schemes. High-resolution schemes based on 2nd-order Lax-Wendroff discretization exhibit a convergence rate of about 1.0 for smooth solutions and 0.5 for discontinuous solutions. On the other hand, the new scheme based on the 3rd-order QUICK discretization exhibits a convergence rate of about 1.3 for smooth solutions and 0.8 for discontinuous solutions. In the case of discontinuous solutions, the new method derived in this thesis shows the best convergence rate of all schemes investigated here and more importantly exhibits no spurious oscillations.

CHAPTER 5. A SOLVER FOR THE TWO-FLUID MODEL

In this Chapter we implement the numerical techniques discussed in Chapters 3 and 4 to the six equation two-fluid model employed by RELAP5 and TRACE. We present the discrete equations of the model along with its closure relations. Temporal discretization is based on the theta method with different techniques implemented for spatial discretization including the new scheme developed in Chapter 4. Numerical results due to different schemes are presented and compared for three benchmark problems.

5.1 Mathematical Model

The two-phase flow mathematical model is obtained by applying conservation relations to mass, momentum and energy of different phases separately. The model employed by RELAP5 and TRACE is based on the standard one-dimensional two-fluid model [9]. This model exhibits a single pressure for both phases. The following two equations represent the conservation of mass for gas and liquid phases respectively:

$$\frac{\partial(\alpha_g \rho_g)}{\partial t} + \frac{\partial(\alpha_g \rho_g u_g)}{\partial x} = \Gamma_g \quad (5.1)$$

$$\frac{\partial(\alpha_l \rho_l)}{\partial t} + \frac{\partial(\alpha_l \rho_l u_l)}{\partial x} = -\Gamma_g \quad (5.2)$$

In these equations:

- α_g and α_l are void fractions for gas and liquid phases, respectively.
- ρ_g and ρ_l , are gas and liquid densities.

- u_g and u_l are gas and liquid velocities.
- Γ_g is the interfacial mass transfer, and it is equal in magnitude and opposite in sign between the two phases. Γ_g is given by [1]:

$$\Gamma_g = -\frac{H_{ig}a_{int}(T_s - T_g) + H_{il}a_{int}(T_s - T_l)}{h_g^* - h_l^*} \quad (5.3)$$

In this equation:

- a_{int} is the interfacial area between the two phases.
- T_g and T_l are gas and liquid temperatures, respectively.
- T_s is saturation temperature.
- H_{ig} and H_{il} are the heat transfer coefficients of gas and liquid phases with the interface.

The phasic mass transfer enthalpies of the two phases (h_g^* and h_l^*) are calculated as follows:

$$h_g^* = \begin{cases} h_{gs} & \text{if } \Gamma_g > 0 \\ h_g & \text{Otherwise} \end{cases} \quad (5.4)$$

$$h_l^* = \begin{cases} h_l & \text{if } \Gamma_g > 0 \\ h_{ls} & \text{Otherwise} \end{cases}$$

h_g and h_l are the phasic enthalpies of gas and liquid, respectively. h_{gs} and h_{ls} are the phasic saturation enthalpies.

Conservation of momentum is also applied to each phase separately, to obtain the following two equations for the gas and liquid phases, respectively:

$$\begin{aligned} \frac{\alpha_g \rho_g \partial(u_g)}{\partial t} + \alpha_g \rho_g u_g \frac{\partial(u_g)}{\partial x} + \alpha_g \frac{\partial p}{\partial x} - \alpha_g \rho_g G \\ = -a_{int} FI |u_g - u_l| (u_g - u_l) - \Gamma_g (u_{int} - u_g) \end{aligned} \quad (5.5)$$

$$\begin{aligned} \frac{\alpha_l \rho_l \partial(u_l)}{\partial t} + \alpha_l \rho_l u_l \frac{\partial(u_l)}{\partial x} + \alpha_l \frac{\partial p}{\partial x} - \alpha_l \rho_l G \\ = a_{int} FI |u_g - u_l| (u_g - u_l) + \Gamma_g (u_{int} - u_l) \end{aligned} \quad (5.6)$$

In the equations above G is the gravity acceleration and p is the pressure of the system. The term with the interfacial friction coefficient (FI) accounts for momentum losses due to interfacial friction. These losses are equal in magnitude and opposite in sign for the two phases. Terms including Γ in the momentum equations account for the momentum lost or gained by the new mass appearing at the interfacial velocity (u_{int}).

Conservation of energy is also applied to each phase separately. This yields the following two equations for gas and liquid phases, respectively:

$$\frac{\partial(\alpha_g \rho_g e_g)}{\partial t} + \frac{\partial(\alpha_g \rho_g e_g u_g)}{\partial x} + p \frac{\partial \alpha_g}{\partial t} + p \frac{\partial(\alpha_g u_g)}{\partial x} = H_{ig} a_i (T_s - T_g) + \Gamma_g h_g^* \quad (5.7)$$

$$\frac{\partial(\alpha_l \rho_l e_l)}{\partial t} + \frac{\partial(\alpha_l \rho_l e_l u_l)}{\partial x} + p \frac{\partial \alpha_l}{\partial t} + p \frac{\partial(\alpha_l u_l)}{\partial x} = H_{il} a_i (T_s - T_l) - \Gamma_g h_l^* \quad (5.8)$$

In these equations, e_g and e_l are the specific energies for gas and liquid phases, respectively. Finally, conservation of volume is applied:

$$\alpha_g + \alpha_l = 1 \quad (5.9)$$

and as a closure for the system, we use two additional equations of state for both phases in the form:

$$\rho_j = f(p, e_j) \quad (5.10)$$

$j = \text{“}g\text{”}$ for gas and $\text{“}l\text{”}$ for liquid. The 7 equations above, along with the two equations of state yield a closed mathematical system of 9 equations and 9 unknowns: $p, \alpha_j, \rho_j, e_j, u_j$, where $j \in \{g, l\}$.

5.2 Discretized Equations

In this section we introduce the discrete equations for the two-fluid model presented in previous section. Numerical methods used to obtain the discrete equations are finite volume based on a staggered mesh. In this configuration scalar properties (pressure, energies, densities and void fraction) are defined at cell centers and the vector properties (velocities) are defined at cell faces. Figure 5.1 shows a schematic of the cell configuration for this type of discretization.

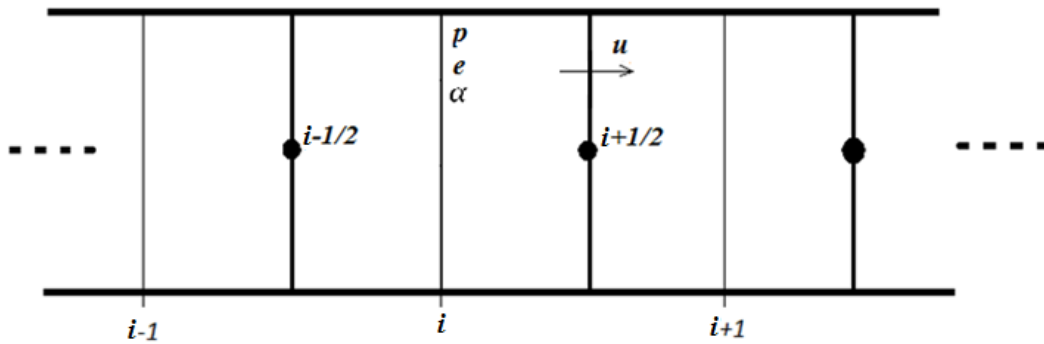


Figure 5.1 Schematic of the staggered cell configuration

Based on the above, we use the formulation of the theta method to write discrete equations in a residual form similar to Mousseau’s work [1]. In the following set of equations superscripts $\text{“}n\text{”}$ and $\text{“}n + 1\text{”}$

represent the old and new time steps, respectively. The temporal discretization depends on the value of θ as discussed in Chapter 3. The subscripts containing “ i ” determine the spatial position.

1- Residuals from the conservation of mass: calculated at cell centers and given as:

$$rescg = \frac{\Delta x}{\Delta t} (\alpha_{g,i}^{n+1} \rho_{g,i}^{n+1} - \alpha_{g,i}^n \rho_{g,i}^n) + (1 - \theta) F_{cg}^n + \theta F_{cg}^{n+1} \quad (5.11)$$

$$rescl = \frac{\Delta x}{\Delta t} (\alpha_{l,i}^{n+1} \rho_{l,i}^{n+1} - \alpha_{l,i}^n \rho_{l,i}^n) + (1 - \theta) F_{cl}^n + \theta F_{cl}^{n+1} \quad (5.12)$$

where F_{cg} and F_{cl} are the mass numerical fluxes given by:

$$F_{cg}^{n+1} = ((\dot{\rho}\alpha)_{g,i+1/2}^{n+1} u_{g,i+1/2}^{n+1} - (\dot{\rho}\alpha)_{g,i-1/2}^{n+1} u_{g,i-1/2}^{n+1}) - \Delta x \Gamma_{g,i}^{n+1} \quad (5.13)$$

$$F_{cl}^{n+1} = ((\dot{\rho}\alpha)_{l,i+1/2}^{n+1} u_{l,i+1/2}^{n+1} - (\dot{\rho}\alpha)_{l,i-1/2}^{n+1} u_{l,i-1/2}^{n+1}) + \Delta x \Gamma_{g,i}^{n+1} \quad (5.14)$$

2- Residuals from the conservation of momentum: calculated at cell faces, and given as:

$$resmg = \frac{\Delta x}{\Delta t} (\overline{\alpha\rho})_{g,i+1/2}^{n+1/2} (u_{g,i+1/2}^{n+1} - u_{g,i+1/2}^n) + (1 - \theta) F_{mg}^n + \theta F_{mg}^{n+1} \quad (5.15)$$

$$resml = \frac{\Delta x}{\Delta t} (\overline{\alpha\rho})_{l,i+1/2}^{n+1/2} (u_{l,i+1/2}^{n+1} - u_{l,i+1/2}^n) + (1 - \theta) F_{ml}^n + \theta F_{ml}^{n+1} \quad (5.16)$$

where F_{mg} and F_{ml} are the momentum numerical fluxes given by:

$$\begin{aligned} F_{mg}^{n+1} = & \overline{(\alpha\rho)}_{g,i+1/2}^{n+1} u_{g,i+1/2}^{n+1} (\dot{u}_{g,i+1}^{n+1} - \dot{u}_{g,i}^{n+1}) + \bar{\alpha}_{g,i+1/2}^{n+1} (p_{i+1}^{n+1} - p_i^{n+1}) \\ & - \Delta x \overline{(\alpha\rho)}_{g,i+1/2}^{n+1} G + \Delta x \bar{\Gamma}_{g,i+1/2}^{n+1} (u_{int,i+1/2}^{n+1} - u_{g,i+1/2}^{n+1}) \\ & + \Delta x (\bar{\alpha}_{int}^{n+1} F I^{n+1}) (u_{g,i+1/2}^{n+1} - u_{l,i+1/2}^{n+1}) |u_{g,i+1/2}^{n+1} - u_{l,i+1/2}^{n+1}| \end{aligned} \quad (5.17)$$

$$\begin{aligned}
F_{ml}^{n+1} &= \overline{(\alpha\rho)}_{l,i+1/2}^{n+1} u_{l,i+1/2}^{n+1} (\dot{u}_{l,i+1}^{n+1} - \dot{u}_{l,i}^{n+1}) + \bar{\alpha}_{l,i+1/2}^{n+1} (p_{l,i+1}^{n+1} - p_l^{n+1}) \\
&\quad - \Delta x \overline{(\alpha\rho)}_{l,i+1/2}^{n+1} G - \Delta x \bar{\Gamma}_{g,i+1/2}^{n+1} (u_{int,i+1/2}^{n+1} - u_{l,i+1/2}^{n+1}) \\
&\quad - \Delta x (\bar{a}_{int}^{n+1} F_I^{n+1}) (u_{g,i+1/2}^{n+1} - u_{l,i+1/2}^{n+1}) |u_{g,i+1/2}^{n+1} - u_{l,i+1/2}^{n+1}|
\end{aligned} \tag{5.18}$$

3- Residuals from the conservation of energy: calculated at cell centers and given as:

$$\begin{aligned}
reseg &= \frac{\Delta x}{\Delta t} (\alpha_{g,i}^{n+1} \rho_{g,i}^{n+1} e_{g,i}^{n+1} - \alpha_{g,i}^n \rho_{g,i}^n e_{g,i}^n) + \frac{\Delta x p_i^{n+1/2}}{\Delta t} (\alpha_{g,i}^{n+1} - \alpha_{g,i}^n) \\
&\quad + (1 - \theta) F_{eg}^n + \theta F_{eg}^{n+1}
\end{aligned} \tag{5.19}$$

$$\begin{aligned}
resel &= \frac{\Delta x}{\Delta t} (\alpha_{l,i}^{n+1} \rho_{l,i}^{n+1} e_{l,i}^{n+1} - \alpha_{l,i}^n \rho_{l,i}^n e_{l,i}^n) + \frac{\Delta x p_i^{n+1/2}}{\Delta t} (\alpha_{l,i}^{n+1} - \alpha_{l,i}^n) \\
&\quad + (1 - \theta) F_{el}^n + \theta F_{el}^{n+1}
\end{aligned} \tag{5.20}$$

where F_{eg} and F_{el} are the energy numerical fluxes given by:

$$\begin{aligned}
F_{eg}^{n+1} &= ((\rho\dot{\alpha}e)_{g,i+1/2}^{n+1} u_{g,i+1/2}^{n+1} - (\rho\dot{\alpha}e)_{g,i-1/2}^{n+1} u_{g,i-1/2}^{n+1}) \\
&\quad + p_i^{n+1} (\dot{\alpha}_{g,i+1/2}^{n+1} u_{g,i+1/2}^{n+1} - \dot{\alpha}_{g,i-1/2}^{n+1} u_{g,i-1/2}^{n+1}) \\
&\quad - \Delta x H_{ig}^{n+1} a_{int}^{n+1} (T_{s,i}^{n+1} - T_{g,i}^{n+1}) - \Delta x \Gamma_{g,i}^{n+1} h_{g,i}^{*n+1}
\end{aligned} \tag{5.21}$$

$$\begin{aligned}
F_{el}^{n+1} &= ((\rho\dot{\alpha}e)_{l,i+1/2}^{n+1} u_{l,i+1/2}^{n+1} - (\rho\dot{\alpha}e)_{l,i-1/2}^{n+1} u_{l,i-1/2}^{n+1}) \\
&\quad + p_i^{n+1} (\dot{\alpha}_{l,i+1/2}^{n+1} u_{l,i+1/2}^{n+1} - \dot{\alpha}_{l,i-1/2}^{n+1} u_{l,i-1/2}^{n+1}) \\
&\quad - \Delta x H_{il}^{n+1} a_{int}^{n+1} (T_{s,i}^{n+1} - T_{l,i}^{n+1}) + \Delta x \Gamma_{g,i}^{n+1} h_{l,i}^{*n+1}
\end{aligned} \tag{5.22}$$

A quantity with an over-bar is an arithmetically averaged quantity:

$$\bar{\Phi}_{i+1/2} = \frac{\Phi_i + \Phi_{i+1}}{2} \tag{5.23}$$

Because scalar properties (pressure, energies, densities and void fraction) are defined at cell centers, a value for these properties is needed at cell interfaces in order to calculate numerical fluxes. These are the variables with a “dot” in Eqs. (5.13), (5.14), (5.21) and (5.22). These quantities are called donored quantities in RELAP5 nomenclature. Same thing holds for momentum numerical fluxes in Eqs. (5.17) and (5.18), where velocities are needed at cell centers.

Order of accuracy for our discretization depends on the method used to calculate the donored quantities in numerical fluxes. There are many numerical schemes one can apply to calculate these donored quantities. For this research, results from 1st-order upwind scheme, second-order upwind scheme and flux limiter schemes (including the new scheme developed in Chapter 4) are shown. This will be discussed in next sections.

5.3 Closure Equations

In order to close the discrete system of equations discussed in the previous section, equations of state are needed. These equations relate densities and temperatures of the two phases to other state variables (pressure and internal energy). The linearized equations of state for densities are:

$$\rho_{g,i}^{n+1} = \rho_{g,i}^n + \left(\frac{\partial \rho_g}{\partial p} \right)_n (p_i^{n+1} - p_i^n) + \left(\frac{\partial \rho_g}{\partial e_g} \right)_n (e_{g,i}^{n+1} - e_{g,i}^n) \quad (5.24)$$

$$\rho_{l,i}^{n+1} = \rho_{l,i}^n + \left(\frac{\partial \rho_l}{\partial p} \right)_n (p_i^{n+1} - p_i^n) + \left(\frac{\partial \rho_l}{\partial e_l} \right)_n (e_{l,i}^{n+1} - e_{l,i}^n) \quad (5.25)$$

for saturation temperature and phasic temperatures of gas and liquid:

$$T_{s,i}^{n+1} = T_{s,i}^n + \left(\frac{\partial T}{\partial p} \right)_n (p_i^{n+1} - p_i^n) \quad (5.26)$$

$$T_{g,i}^{n+1} = T_{g,i}^n + \left(\frac{\partial T}{\partial p} \right)_n (p_i^{n+1} - p_i^n) + \left(\frac{\partial T_g}{\partial e_g} \right)_n (e_{g,i}^{n+1} - e_{g,i}^n) \quad (5.27)$$

$$T_{l,i}^{n+1} = T_{l,i}^n + \left(\frac{\partial T}{\partial p} \right)_n (p_i^{n+1} - p_i^n) + \left(\frac{\partial T_l}{\partial e_l} \right)_n (e_{l,i}^{n+1} - e_{l,i}^n) \quad (5.28)$$

for saturation enthalpies and specific enthalpies of the two phases:

$$h_{gs,i}^{n+1} = h_{gs,i}^n + \left(\frac{\partial h_{gs}}{\partial p} \right)_n (p_i^{n+1} - p_i^n) \quad (5.29)$$

$$h_{ls,i}^{n+1} = h_{ls,i}^n + \left(\frac{\partial h_{ls}}{\partial p} \right)_n (p_i^{n+1} - p_i^n) \quad (5.30)$$

$$h_{g,i}^{n+1} = e_{g,i}^{n+1} + \frac{p_i^{n+1}}{\rho_{g,i}^{n+1}} \quad (5.31)$$

$$h_{l,i}^{n+1} = e_{l,i}^{n+1} + \frac{p_i^{n+1}}{\rho_{l,i}^{n+1}} \quad (5.32)$$

All derivatives in the previous equations are calculated numerically using water properties. Water properties used in this research are based on the International Association for Properties of Water and Steam Industrial Formulation 1997 (IAPWS IF-97) standard. XSteam, an implementation MatLab code of the IAPWS IF-97 standard formulation by Magnus Holmgren [34], is used to obtain all necessary water properties.

The closure relations discussed here can be substituted directly into Eqs. (5.11) - (5.22) to reduce the number of unknown variables to six, namely: pressure, void fraction, gas and liquid velocities and internal energies of the two phases.

5.4 Calculation of Donored Quantities

As mentioned before, the order of accuracy of our discretized equations depends on the numerical scheme used to calculate donored quantities in the numerical fluxes. There are many numerical schemes one can apply to calculate these donored quantities. In this research, results for the 1st-order upwind scheme, second-order upwind scheme and flux limiter schemes (including the new scheme developed in Chapter 4) are shown.

5.4.1 First-Order Upwind

For a scalar quantity Φ (this can be ρ , e , p or α) calculated at the center of the i^{th} cell, donored quantities at cell faces are defined as follows:

$$\dot{\Phi}_{i+1/2} = \frac{1}{2} \left[(\Phi_i + \Phi_{i+1}) + \frac{|u_{i+1/2}|}{u_{i+1/2}} (\Phi_i - \Phi_{i+1}) \right] \quad (5.33)$$

Similarly, for a velocity u calculated at the face of the i^{th} cell, the donored quantity at the cell center is defined as:

$$\dot{u}_i = \frac{1}{2} \left[(u_{i-1/2} + u_{i+1/2}) + \frac{|u_{i+1/2}|}{u_{i+1/2}} (u_{i-1/2} - u_{i+1/2}) \right] \quad (5.34)$$

As an example, donored gas density ($\dot{\rho}_{g_{i+1/2}}$), and donored gas velocity (\dot{u}_{g_i}) are given as:

$$\dot{\rho}_{g_{i+1/2}} = \frac{1}{2} \left[(\rho_{g_i} + \rho_{g_{i+1}}) + \frac{|u_{i+1/2}|}{u_{i+1/2}} (\rho_{g_i} - \rho_{g_{i+1}}) \right]$$

$$\dot{u}_{g_i} = \frac{1}{2} \left[(u_{g_{i-1/2}} + u_{g_{i+1/2}}) + \frac{|u_{i+1/2}|}{u_{i+1/2}} (u_{g_{i-1/2}} - u_{g_{i+1/2}}) \right]$$

Since the 1st-order upwind scheme is a monotone scheme, we expect the solution due to this discretization to be free of non-physical numerical oscillations. However, the solution is expected to be smeared due to excessive dissipation of the scheme.

5.4.2 Second-Order Upwind

For a scalar quantity Φ calculated at the center of the i^{th} cell, donored quantities at cell faces are defined as follows:

$$\begin{aligned} \dot{\Phi}_{i+1/2} = & \frac{1}{4} [(3\Phi_i + 3\Phi_{i+1} - \Phi_{i-1} - \Phi_{i+2}) \\ & + \frac{|u_{i+1/2}|}{u_{i+1/2}} (3\Phi_i - 3\Phi_{i+1} - \Phi_{i-1} + \Phi_{i+2})] \end{aligned} \quad (5.35)$$

Similarly, for a velocity u calculated at the face of the i^{th} cell, the donored quantity at the cell center is defined as:

$$\begin{aligned} \dot{u}_i = & \frac{1}{4} [(3u_{i-1/2} + 3u_{i+1/2} - u_{i-3/2} - u_{i+3/2}) \\ & + \frac{|u_{i+1/2}|}{u_{i+1/2}} (3u_{i-1/2} - 3u_{i+1/2} - u_{i-3/2} + u_{i+3/2})] \end{aligned} \quad (5.36)$$

As an example, the donored quantity $(\dot{\alpha\rho})_{g,i+1/2}$, and the donored gas velocity $(\dot{u})_{g,i}$ are given as:

$$\begin{aligned} (\dot{\alpha\rho})_{g,i+1/2} = & \frac{1}{4} [(3(\alpha\rho)_{g_i} + 3(\alpha\rho)_{g_{i+1}} - (\alpha\rho)_{g_{i-1}} - (\alpha\rho)_{g_{i+2}}) \\ & + \frac{|u_{i+1/2}|}{u_{i+1/2}} (3(\alpha\rho)_{g_i} - 3(\alpha\rho)_{g_{i+1}} - (\alpha\rho)_{g_{i-1}} + (\alpha\rho)_{g_{i+2}})] \end{aligned}$$

$$\dot{u}_{g_i} = \frac{1}{4} \left[\left(3u_{g_{i-1/2}} + 3u_{g_{i+1/2}} - u_{g_{i-3/2}} - u_{g_{i+3/2}} \right) + \frac{|u_{i+1/2}|}{u_{i+1/2}} \left(3u_{g_{i-1/2}} - 3u_{g_{i+1/2}} - u_{g_{i-3/2}} + u_{g_{i+3/2}} \right) \right]$$

The 2nd-order upwind scheme is expected to yield more accurate results as compared to 1st-order upwind. However, the scheme is non-monotone, and according to Godunov's barrier theorem it is expected to exhibit non-physical oscillations near discontinuities.

5.4.3 Flux Limiter Schemes

The flux limiter approach is based on a combination of a monotone 1st-order scheme and a higher-order accurate scheme. The two schemes are combined in a way such that the 1st-order scheme is used near discontinuities to prevent spurious oscillations, and the high-order scheme is used elsewhere to obtain the highest order of accuracy possible. The weighted interpolation between the two schemes depends on the smoothness of the solution. Because the smoothness parameter is calculated for a given variable, and depends on the characteristics of the solution, it is harder to implement the flux limiter approach to a system of non-linear equations like the two-fluid model. One way to implement flux limiter methods to a system of non-linear equations is to approach the problem in an empirical manner. In this research we consider the empirical approach suggested by Torro [23]. His approach for a system of m variables is based on calculating the smoothness parameters for each variable ($q = q_k, k = 1, 2, \dots, m$) in the system:

$$r_{i+1/2}^L = \frac{\Delta q_{i-1/2}}{\Delta q_{i+1/2}} = \frac{q_i - q_{i-1}}{q_{i+1} - q_i} \quad (5.37)$$

$$r_{i+1/2}^R = \frac{\Delta q_{i+3/2}}{\Delta q_{i+1/2}} = \frac{q_{i+2} - q_{i+1}}{q_{i+1} - q_i} \quad (5.38)$$

Then, the value for the flux limiter function is calculated as follows:

$$\varphi(r) = \min_k \left[\min \left(\varphi(r_{i+1/2}^L), \varphi(r_{i+1/2}^R) \right) \right] \quad (5.39)$$

The flux limiter φ in Eq. (5.39) is a function of the smoothness parameter. There are many different forms of flux limiters. In this Chapter we investigate the new scheme developed in Chapter 4 along with three other limiters discussed in Chapter 3: the Minbee limiter function, the Superbee limiter function and Kumar's limiter function.

Results from Eq. (5.39) are then applied to all m flux components. For the two-phase problem we have the following variables:

$$q = \begin{pmatrix} \alpha_g \\ p \\ u_g \\ u_l \\ e_g \\ e_l \end{pmatrix} \quad (5.40)$$

The residual form discussed in Section 5.2 can be written using the following form for the flux terms:

$$F = F^{1st} + \varphi(r)(F^{High} - F^{1st})$$

F^{1st} is the numerical flux using the monotone 1st-order upwind scheme, F^{High} is the numerical flux using the higher order accurate scheme.

5.5 Non-Linear Solver

For a discrete domain of N cells, Eqs. (5.11), (5.12), (5.15), (5.16), (5.19) and (5.20) form a system of $6N$ non-linear algebraic equations with $6N$ unknowns. The unknowns are $\alpha_{g,i}^{n+1}$, p_i^{n+1} , $u_{g,i+1/2}^{n+1}$, $u_{l,i+1/2}^{n+1}$, $e_{g,i}^{n+1}$

and $e_{l,i}^{n+1}$ for $i \in [1,2,3,\dots,N]$. These equations need to be solved simultaneously by non-linear algebraic equations solver. In this research, a solver by Kelley [35] is used. The solver uses Newton's method with a direct factorization of the Jacobian. Because the goal of this research is improvement of the numerical method rather than the non-linear solver, we use the non-linear solver without any modifications. More information about this solver can be found in [35].

5.6 Numerical Results and Discussion

In this section we implement the new high-order numerical method derived in this thesis to numerically solve the two-fluid model. The solver is then employed to different benchmark problems that entail two-phase flows. Numerical results are presented for three types of problems: the faucet flow problem, Edward's pipe problem and the shock tube problem. The solver was developed in MatLab computing language. More details on the structure of the code can be found in Appendix C.

5.6.1 The Faucet Flow Problem

The faucet flow benchmark problem has been used for decades as a tool for verification of numerical methods for two-phase problems. In this problem, the fluid accelerates through the spatial domain under the effect of gravity, and the initial profile of the void fraction is moved out of the domain under this acceleration. With this convection of the void fraction profile, there is also a moving discontinuity in the profile. This feature of the void fraction profile makes it a very good test for the dissipative properties of the numerical scheme and its stability near discontinuities. This problem has an analytical solution for the case of negligible pressure variation and no interfacial and wall interactions. This analytical solution is compared to numerical solutions for verification purposes.

The spatial domain of this problem consists of a vertical tube of length L m. This tube contains a uniform column of liquid moving with initial velocity u_l m/s in a vapor annulus with initial velocity u_g m/s. The initial volume fraction of water is α_l^0 . Initial pressure (p_0) is uniform at saturation temperature. At the tube inlet the liquid volume fraction (α_l^{in}), liquid velocity (u_l^{in} m/s), and vapor velocity (u_g^{in} m/s) are kept constant. Outlet pressure is maintained constant at p_0 , and a gravity field (G) is applied at the start of the simulation. The problem is illustrated in Figure 5.2.

The analytical solution for the void fraction is given by [36]:

$$\alpha_g(x, t) = \begin{cases} 1 - \frac{\alpha_l^0 u_l}{\sqrt{2Gx + u_l^2}} & x \leq u_l t + \frac{Gt^2}{2} \\ 1 - \alpha_l^0 & \text{Otherwise} \end{cases} \quad (5.41)$$

The numerical schemes discussed earlier are applied to discretize the two-fluid model as presented in previous sections of this Chapter. The analytical solution in Eq. (5.41) assumes no phase transfer between the two phases, hence Γ_g in the model was set to zero. Table 5.1 contains the list of initial and boundary conditions for the problem.

Numerical results from this simulation are shown for three types of schemes: 1st-order upwind scheme, 2nd-order upwind scheme and flux limiter schemes, including the new flux limiter scheme derived in this thesis.

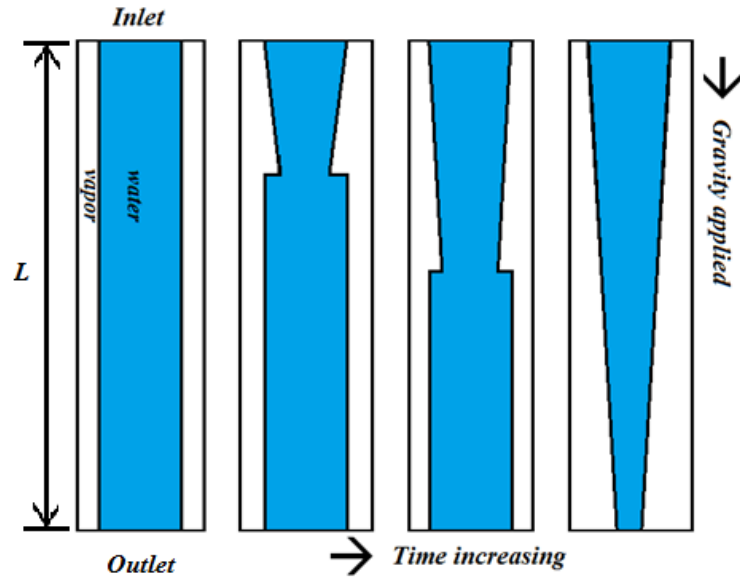


Figure 5.2 Illustration of the faucet flow problem

Table 5.1 Initial and boundary conditions of the faucet flow problem

Tube length L	1m
Initial and boundary liquid velocities u_l, u_l^{in}	10 m/s
Initial and boundary gas velocities u_g, u_g^{in}	10 m/s
Initial and boundary volume fraction of liquid $\alpha_l^0, \alpha_l^{in}$	0.8
Initial and boundary pressure p_0, p_0^{out}	1.5 bars
Gravity acceleration G	9.8 m/s^2

1st-Order and 2nd-Order Upwind Schemes

For this set of results we consider two cases: the implicit discretization ($\theta = 1$) and the Crank-Nicolson discretization ($\theta = 1/2$). Simulation time was set to 0.045 seconds with a time step of size 10^{-4} seconds. All results for the first-order upwind scheme are characterized by a lack for any spurious oscillations. However, the solution is smeared as compared to the second-order upwind scheme. Figure 5.3 shows results for the first-order upwind scheme with implicit method for different mesh sizes: $N=40, 80, 160$ and 320 . Figure 5.4 shows results for the Crank-Nicolson method with the same mesh sizes. It can be observed that Crank-Nicolson method is less dissipative than the implicit method. This result was expected from the modified equation analysis discussed in Chapter 3. The numerical solution for the two methods is compared for $N=320$ in Figure 5.5.

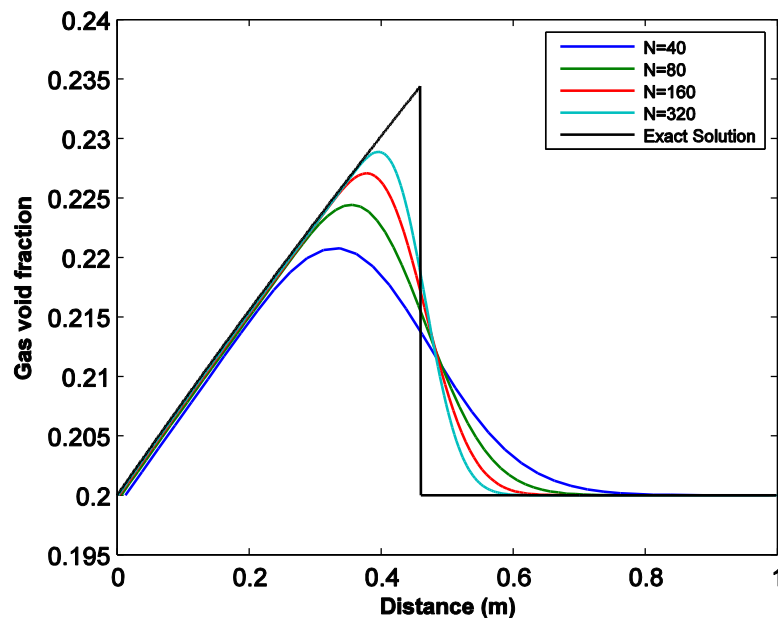


Figure 5.3 Results for the 1st-order-upwind with implicit temporal discretization

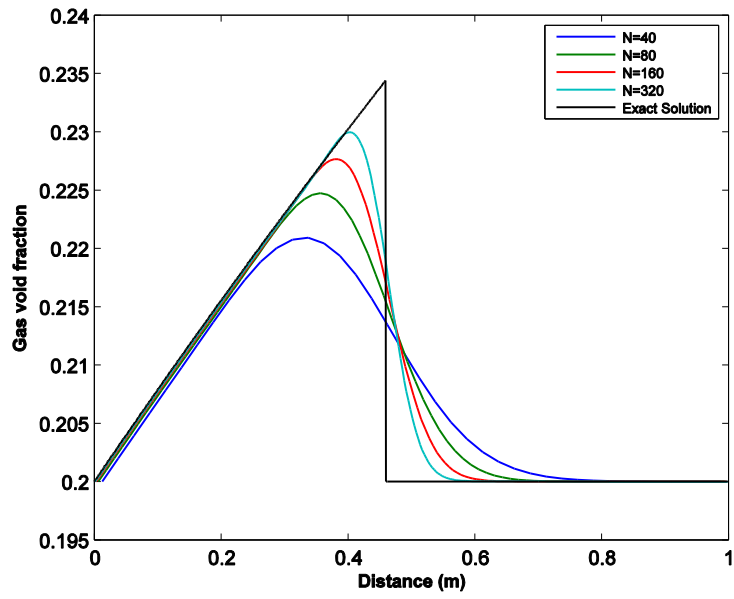


Figure 5.4 Results for the 1st-order-upwind with Crank-Nicolson temporal discretization

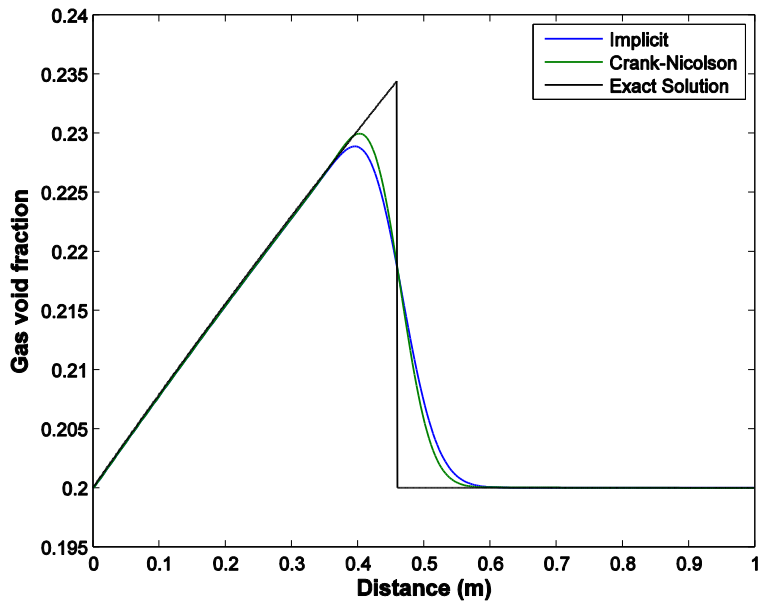


Figure 5.5 Comparison between Implicit and Crank-Nicolson for (N=320)

For the 2nd-order upwind scheme, spurious oscillations appear in the numerical solution for any choice of θ , even fully implicit ($\theta = 1$). Figure 5.6 shows the numerical solution for the implicit case ($\theta = 1$) with different mesh sizes. Figure 5.7 shows the numerical solution for the Crank-Nicolson case ($\theta = 1/2$). It is observed that dissipation causes a reduction in the oscillation amplitudes for implicit discretization, which is not the case for Crank-Nicolson, where dissipation is negligible.

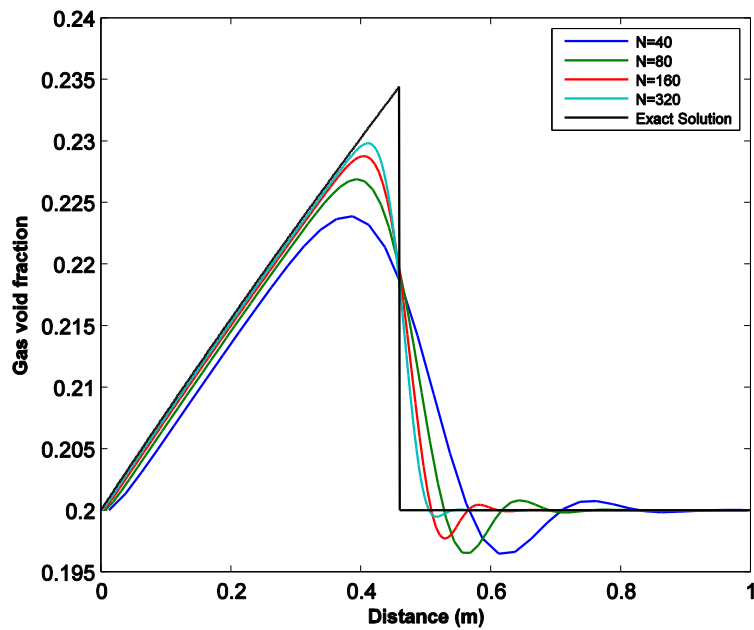


Figure 5.6 Results for the 2nd-order-upwind with implicit temporal discretization

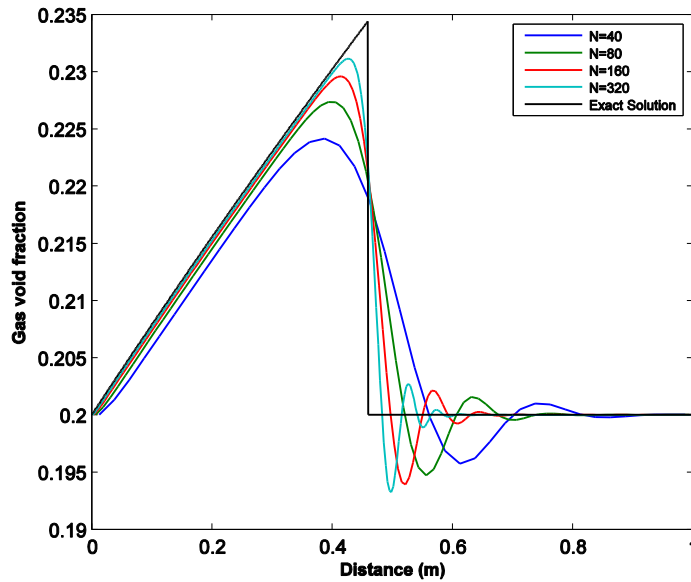


Figure 5.7 Results for the 2nd-order-upwind with Crank-Nicolson temporal discretization

Flux-Limiter Schemes

As discussed earlier, application of this method for a system of non-linear equations is based on an empirical approach. The smoothness parameters defined in Eq. (5.37) and Eq. (5.38) were calculated for all the variables in Eq. (5.40), and it was found that using smoothness parameters based on void fraction (α) leads to the best results. Hence all results from flux limiter schemes shown in this section are based on void fraction being used to calculate the smoothness parameters.

Different combinations of limiters and θ values were investigated to reach the best numerical solution. In practice, different limiters led to results with little qualitative difference. A scheme based on the Minbee limiter was found to be the most dissipative among flux limiter schemes. Changing the value of θ resulted in slightly different results, with implicit method ($\theta = 1$) more dissipative than the Crank-Nicolson method ($\theta = 1/2$). The numerical solutions were free of spurious oscillations for all cases, as expected. Figure

5.8 shows numerical results due to the new scheme with $\delta = 1$ for different choices of θ . It shows better results for the Crank-Nicolson method ($\theta = 1/2$), where dissipation is minimal.

Figure 5.9 shows numerical results for four different schemes: 1st-order upwind scheme, Minbee flux limiter scheme, Superbee flux limiter scheme and the new scheme with $\delta = 1$. All results are shown with $\theta = 1/2$. Results from the 1st-order upwind scheme are the most smeared as compared to other schemes. Results from the Minbee limiter seem to be more smeared than the other two limiters, and the new scheme yields numerical solution that is the closest to the exact one.

The exact solution in Eq. (5.41) was used to determine the accuracy of numerical schemes. Accuracy was assessed on the basis of the L_1 norm, discussed in Section 4.3.1. Convergence rate is represented by a log-log plot of the norm of the error versus the mesh size. Figure 5.10 shows the results of the space convergence study. The 1st-order upwind scheme converges with the order of 0.52, the Minbee limiter converges with the order of 0.67 and the new scheme with $\delta = 0$ converges with the order of 0.80. The complete results are shown in Table 5.2.

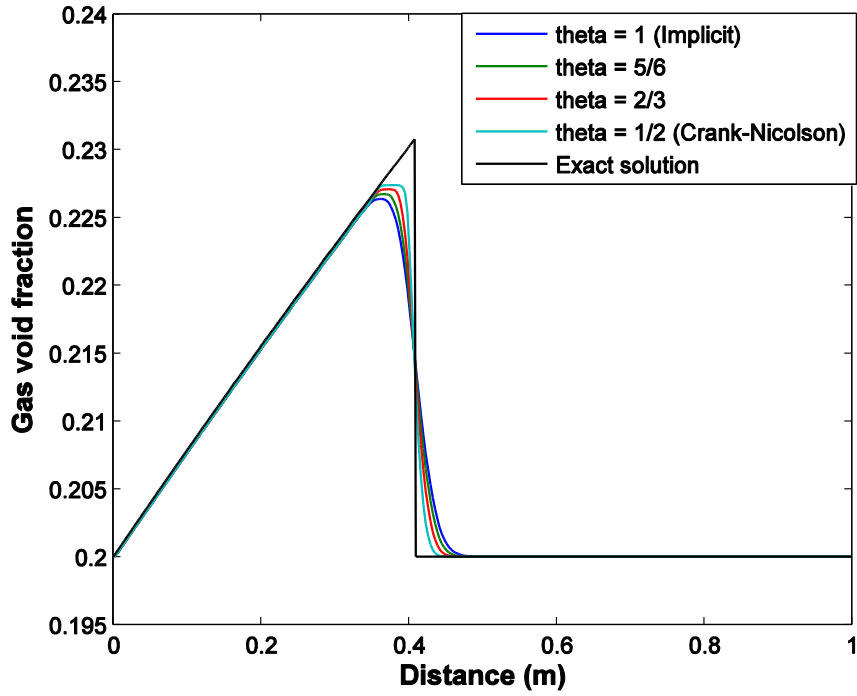


Figure 5.8 Numerical results for new scheme with $\delta=1$ using different values of θ , $N=320$

Table 5.2 Convergence of numerical solution for schemes with different limiters

Numerical Scheme	Convergence Rate
1 st -order upwind	0.52
Minbee limiter	0.67
Superbee limiter	0.74
Kumar limiter	0.73
New limiter with $\delta = 1$	0.78
New limiter with $\delta = 0$	0.80

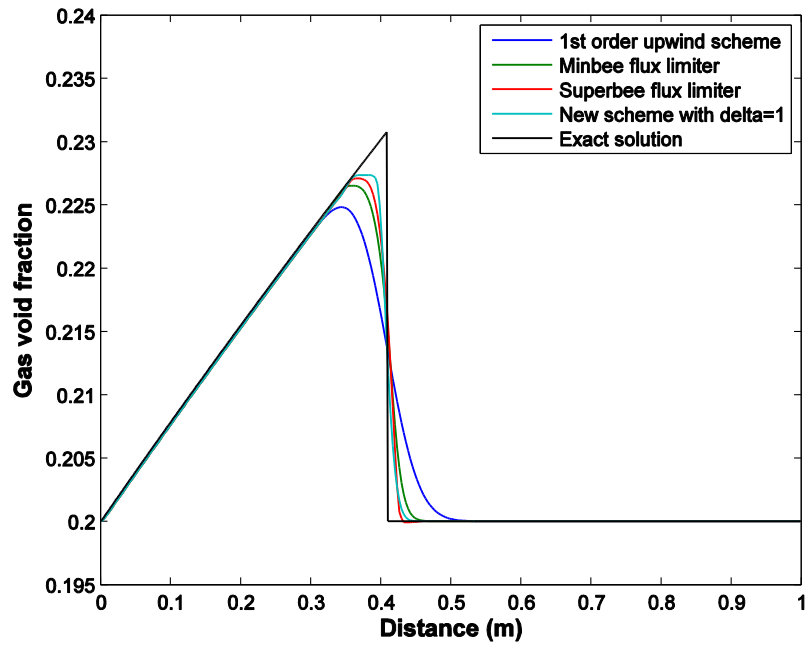


Figure 5.9 Numerical results for different flux limiter functions $\theta=1/2$ and $N=320$

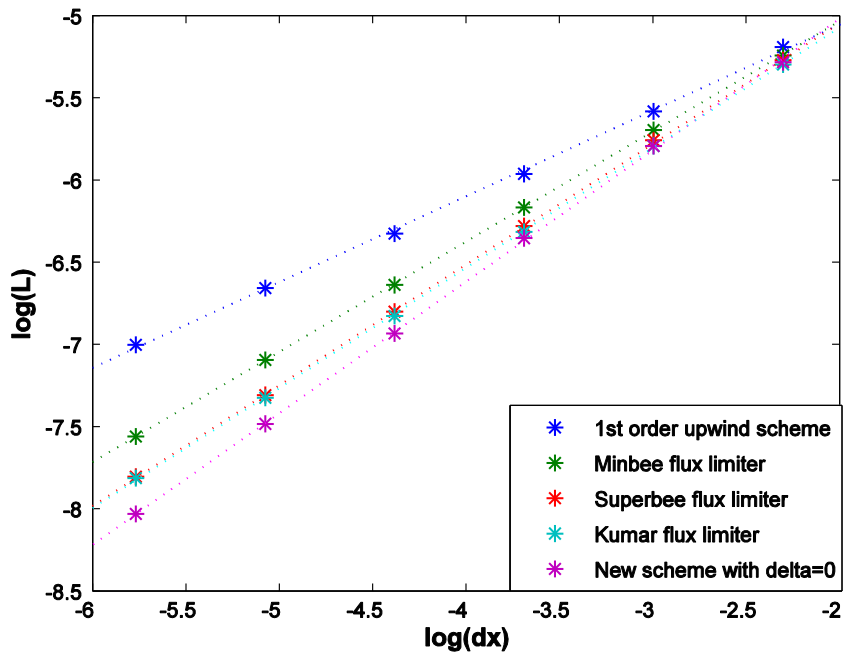


Figure 5.10 Convergence of numerical solution for schemes with different limiters

5.6.2 Edward's Pipe Problem

Another benchmark that has been used for safety studies of nuclear reactors is the Edward's pipe problem [37]. This problem mimics an accident where sudden depressurization of water happens. When the pressure of liquid water drops below the saturation value in a sudden manner, it leads to an instantaneous phase change in the form of evaporation, this phenomenon is called flashing [38].

The setup for this problem consists of a 1 m pipe containing liquid water and steam at a saturation pressure of 10 MPa. The left end of the pipe is closed, and the right end is opened to atmospheric pressure at the beginning of the simulation. Initial gas void fraction in the pipe is set to 0.01. The spatial domain of the problem was divided into 50 cells and the size of the time step used was set to 10^{-5} seconds. A schematic of the Edward's pipe problem is shown in Figure 5.11.

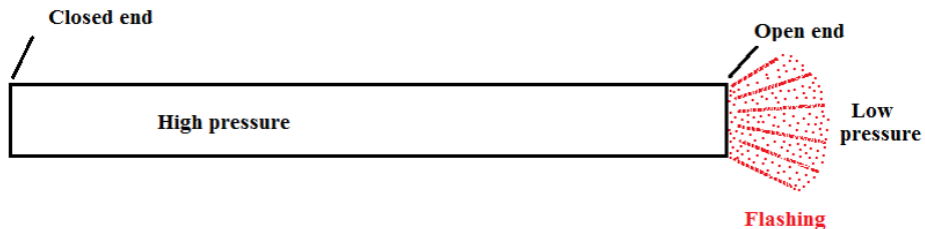


Figure 5.11 Schematic of the Edward's pipe problem

Solution profiles for pressure, void fraction and gas velocity at different time instances are presented in Figure 5.12, Figure 5.13 and Figure 5.14, respectively. Figure 5.15 shows the predicted values for the pressure history at the closed end.

A rarefaction wave propagates during the first 5 ms of the transient starting from the open end of the pipe towards the closed end, resulting in a rapid depressurization of water as shown in Figure 5.12. As a consequence of this depressurization, flashing happens leading to an increase in void fraction as shown in Figure 5.13.

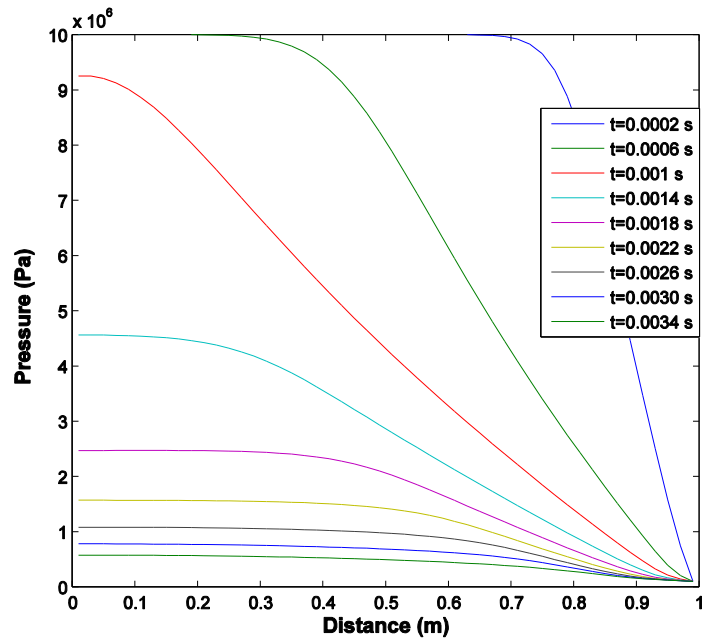


Figure 5.12 Pressure profiles at different times for Edward's pipe problem

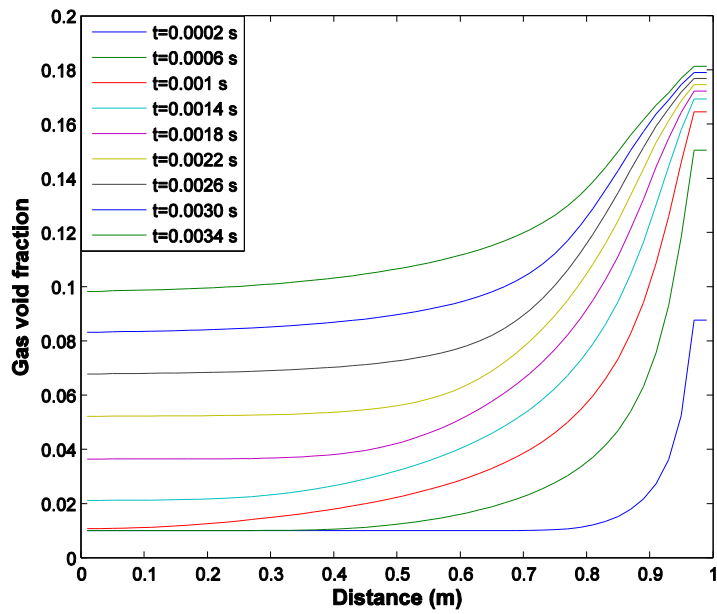


Figure 5.13 Gas void fraction at different times for Edward's pipe problem

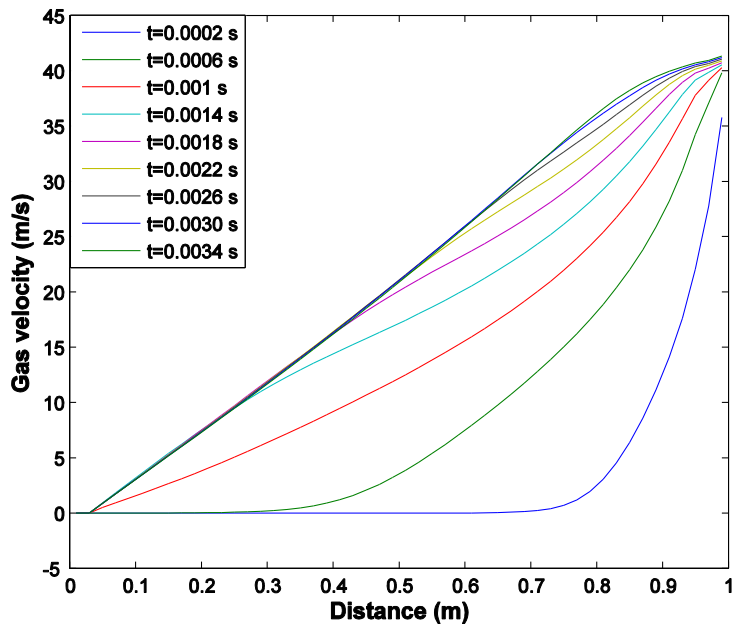


Figure 5.14 Gas velocity profiles at different times for Edward's pipe problem

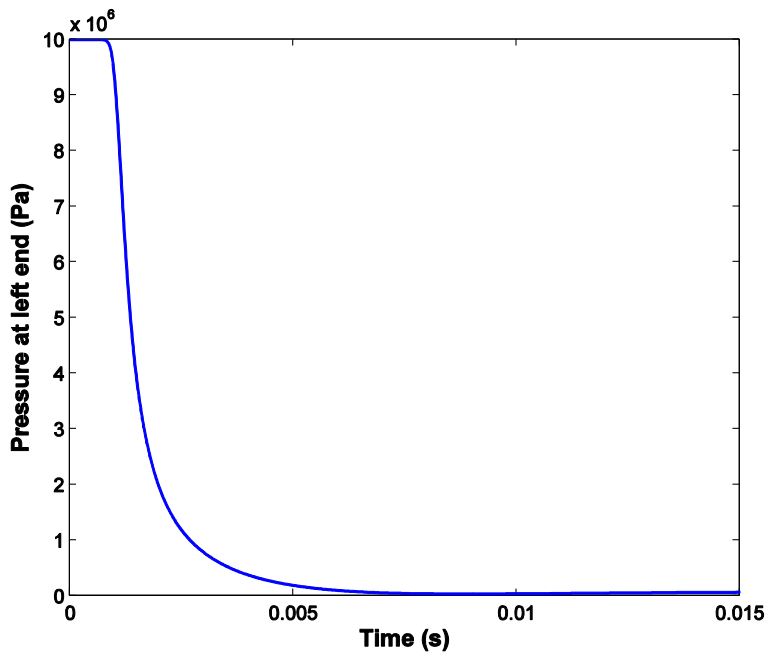


Figure 5.15 Left end pressure for Edward's pipe problem

Solution profiles for different variables were investigated for different mesh sizes (N=10, 20, 40 and 80). Solution profiles at t=0.0022 seconds for pressure, void fraction, gas velocity and pressure history at the closed end are shown in Figure 5.16, Figure 5.17, Figure 5.18 and Figure 5.19 respectively.

Time convergence was also investigated by changing the time step of the simulation. Three time steps were considered ($dt = 10^{-4}$, $2.5 * 10^{-5}$ and $6.25 * 10^{-6}$ seconds). Results for pressure, void fraction, gas velocity and pressure history at the closed end are shown in Figure 5.20, Figure 5.21, Figure 5.22 and Figure 5.23 respectively.

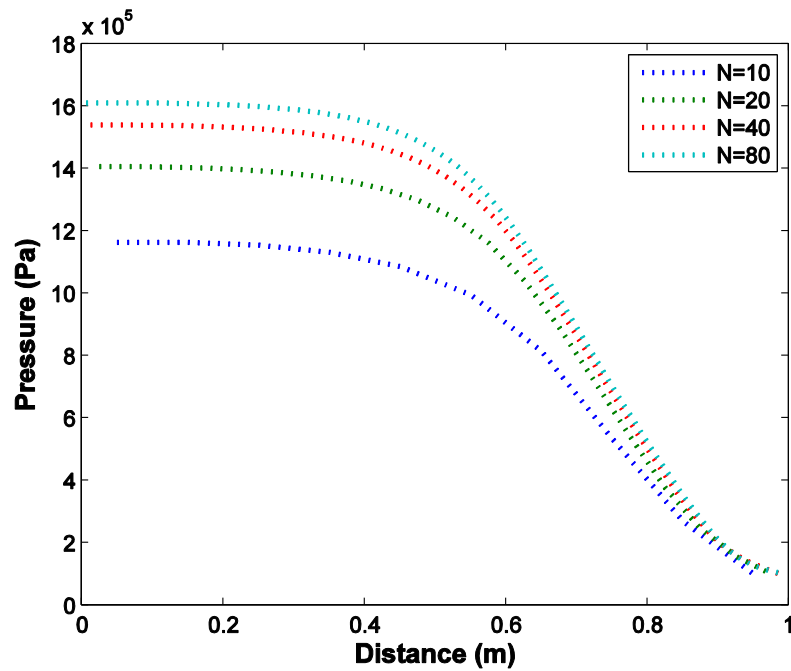


Figure 5.16 Pressure profile at t=0.0022 sec for different mesh sizes, $dt = 10^{-5}$

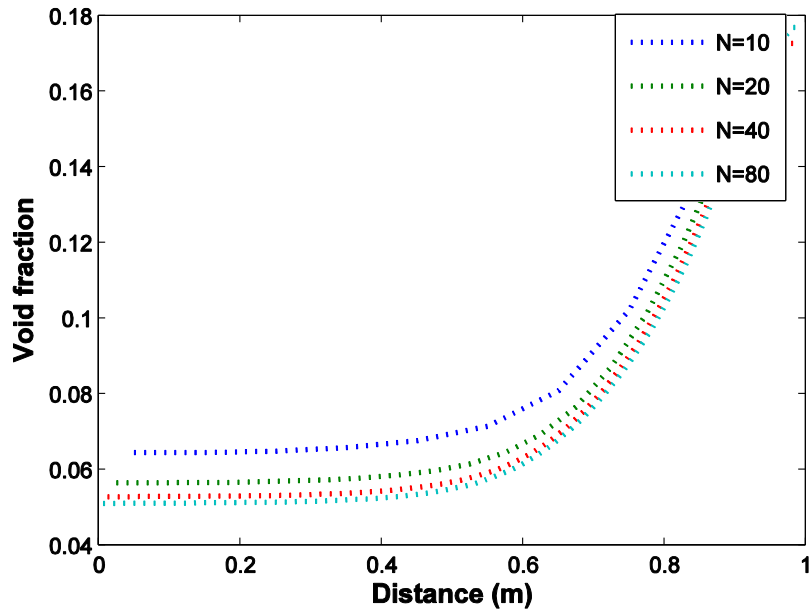


Figure 5.17 Void fraction profile at $t=0.0022$ sec for different mesh sizes, $dt = 10^{-5}$

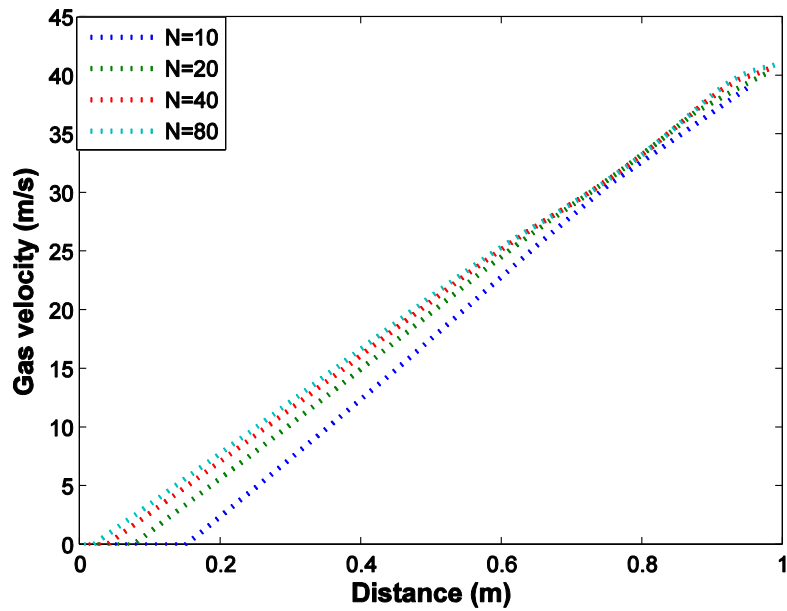


Figure 5.18 Gas velocity profile at $t=0.0022$ sec for different mesh sizes, $dt = 10^{-5}$

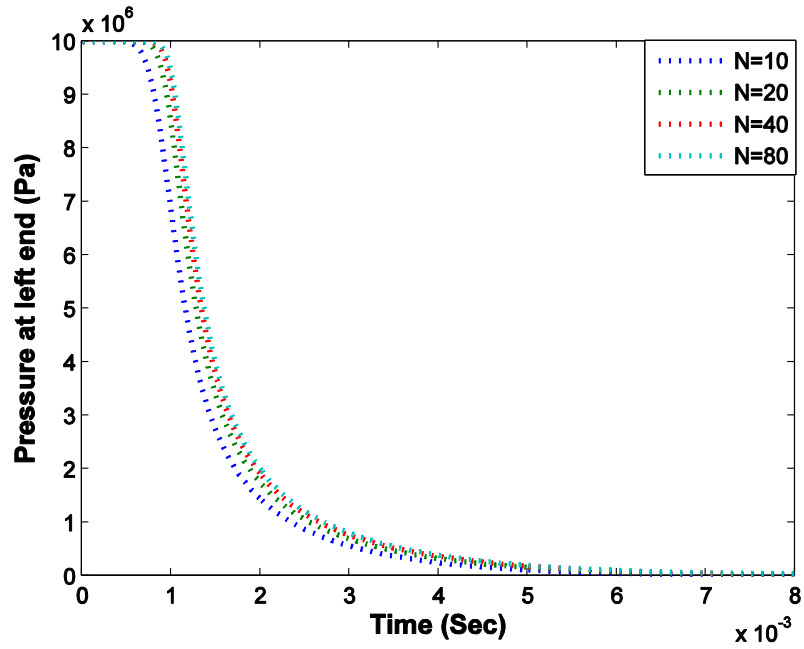


Figure 5.19 Pressure history at closed end for different mesh sizes, $dt = 10^{-5}$

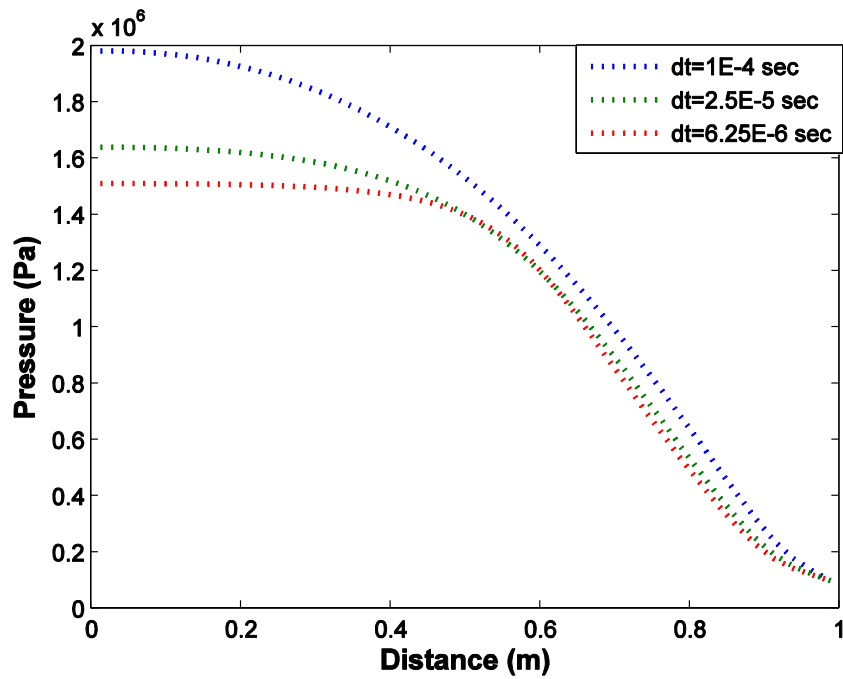


Figure 5.20 Pressure profile at $t=0.0022$ sec for different time steps, $N=40$

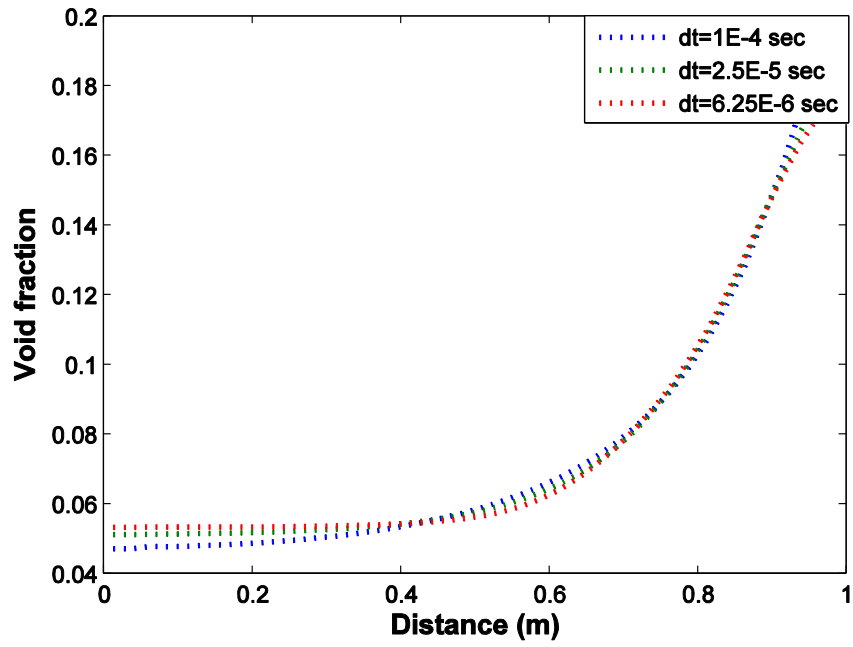


Figure 5.21 Void fraction profile at $t=0.0022$ sec for different time steps, $N=40$

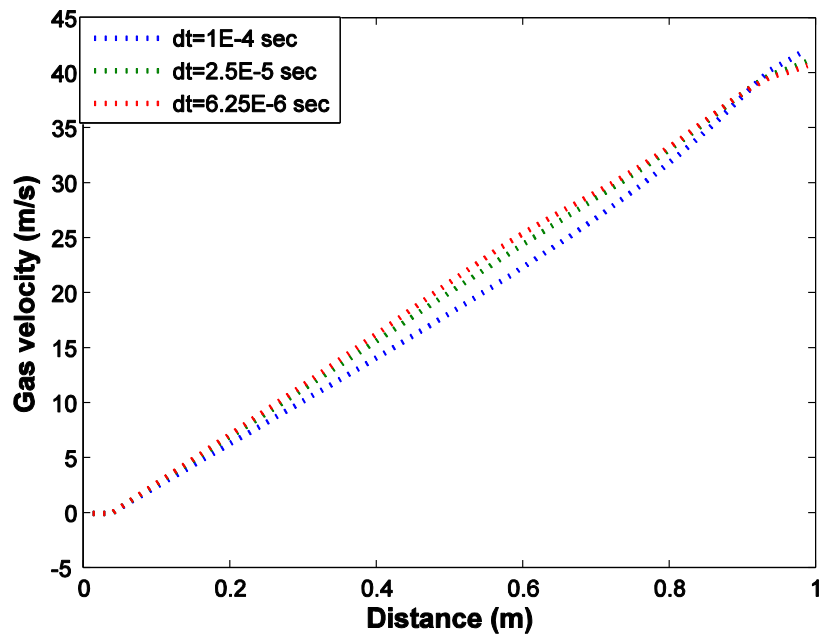


Figure 5.22 Gas velocity profile at $t=0.0022$ sec for different time steps, $N=40$

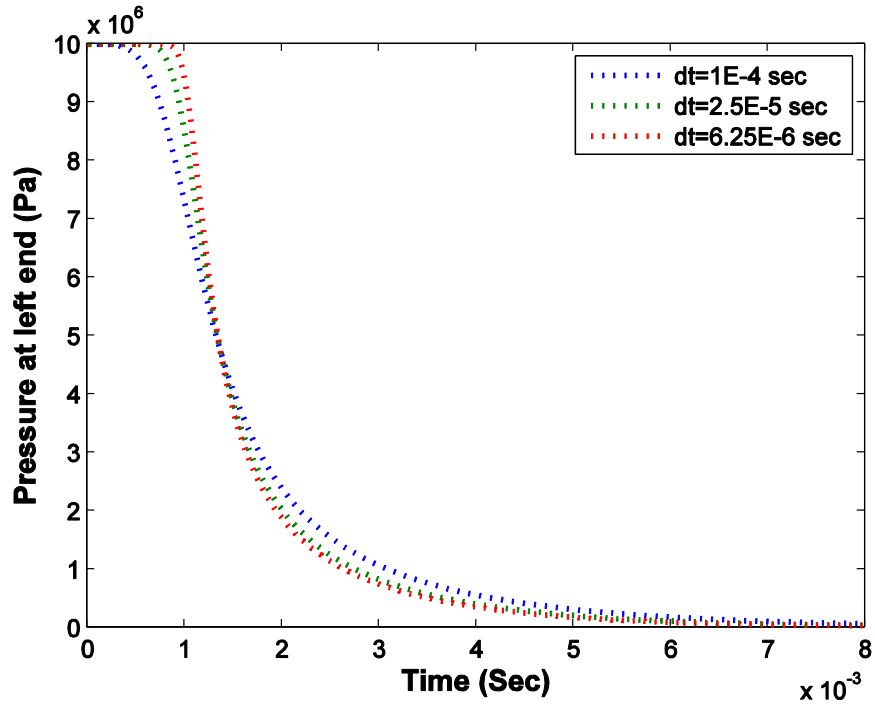


Figure 5.23 Pressure history at closed end for different time steps, $N=40$

At this point, it is important to mention that a quantitative comparison between the results of the new solver developed in this research and those of the nuclear thermal-hydraulic codes (TRACE and RELAP5) is not a fair comparison. This conclusion can be related to many reasons, which are basically differences between the two solvers. For example, some coefficients like the interfacial area between the two phases (a_{int}) and the interfacial friction coefficient (FI) are assumed constant in this research. On the other hand, TRACE and RELAP5 use some correlations to calculate these coefficients. Another important difference is the definition and implementation of the closure relations and the equations of state. Based on this, a quantitative comparison between the results of the new solver and those of the nuclear thermal-hydraulic codes (TRACE and RELAP5) should not be expected to yield a good level of quantitative agreement.

5.6.3 The Shock Tube Problem

This Riemann problem for the two-phase flow poses an example of shock formation during fast transients in the presence of phase change. Results from this problem are aimed to show the solver is able to handle large differences between temperatures of the two phases. The setup of this problem is a pipe containing water in its two different phases (gas and liquid). Initially the left and right halves of the tube have two different states at saturation and separated by a diaphragm. Different variations of this problem has been used for testing numerical methods by changing the initial left and right states of the fluid [39] [40]. The left and right states for this problem are defined in Table 5.3. Both ends of the pipe are kept closed, and the diaphragm is removed at the beginning of the simulation to start the transient. The domain of the problem was divided into 40 cells, and a time step of 10^{-5} seconds was used. Results from this simulation are compared to those from the nuclear thermal-hydraulics code TRACE. A schematic of the shock tube problem is shown in Figure 5.24.

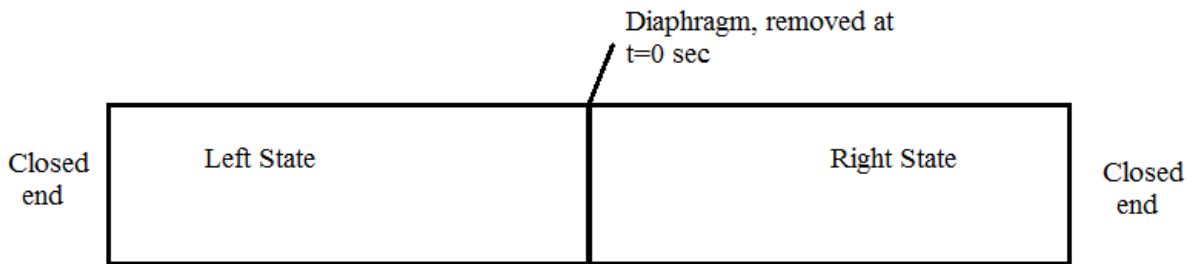


Figure 5.24 Schematic of the shock tube problem

Table 5.3 Initial conditions of the shock tube problem

Left side of the pipe	Right side of the pipe
$\alpha_g^L = 0.25$	$\alpha_g^R = 0.10$
$p^L = 20 \text{ MPa}$	$p^R = 10 \text{ MPa}$
$e_g^L = 2824 \text{ KJ/Kg}$	$e_g^R = 2836 \text{ KJ/Kg}$
$e_l^L = 1311 \text{ KJ/Kg}$	$e_l^R = 1330 \text{ KJ/Kg}$
$v_g^L = 0.0 \text{ m/s}$	$v_g^R = 0.0 \text{ m/s}$
$v_l^L = 0.0 \text{ m/s}$	$v_l^R = 0.0 \text{ m/s}$

Figure 5.25 shows the pressure profile in the pipe after 0.5 ms of the transient. A formation of a new constant state in the middle of the pipe can be observed. This constant state corresponds to an increasing pressure in the right half of the pipe, and decreasing pressure in the left half. Consequently, phase change happens in both halves, resulting in increasing gas void fraction in the left half, and decreasing gas void fraction in the right half, this is shown in Figure 5.26. Velocities and internal energies of the two phases are shown in Figure 5.27 and Figure 5.28, respectively. For both variables (velocity and internal energy), the gas phase is shown to have larger values than the liquid phase as expected. It can be seen that the results in these figures show a good quantitative agreement between the new solver and TRACE. This level of agreement is considered fortuitous and should not be expected for other types of problems as discussed in the previous section.

Results for gas density from the new solver is not as close to TRACE results as other variables. The transition between the two intermediate states of density is not as smooth as it is for the TRACE's solution. One reason behind this can be related to the implementation of closure relations in the new solver. The density of the gas phase, being highly compressible, is sensitive to any small change in pressure or temperature. The way this relation between density and other state variables (pressure and temperature) is implemented in the solver is based on a first-order linearization as discussed earlier.

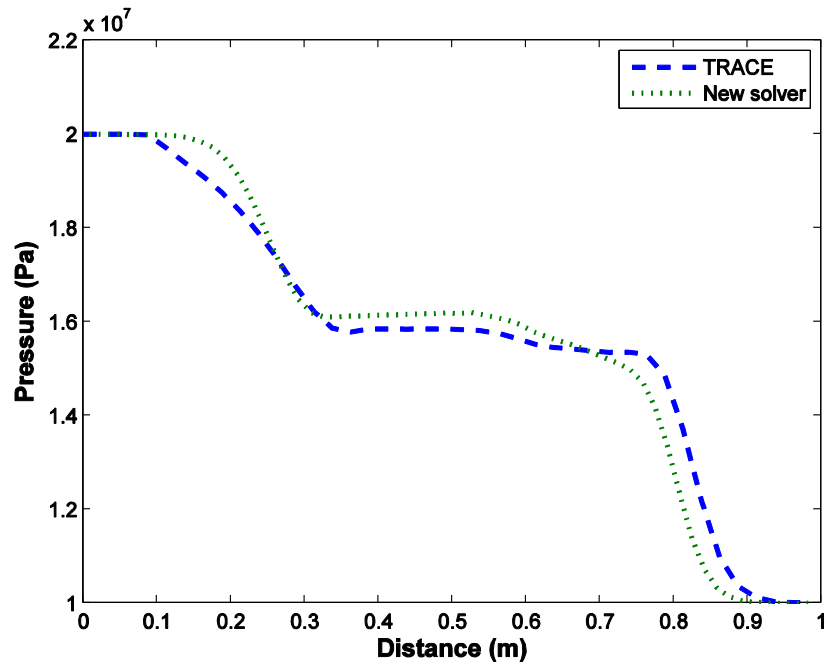


Figure 5.25 Pressure profile for shock tube problem at time=0.5 ms

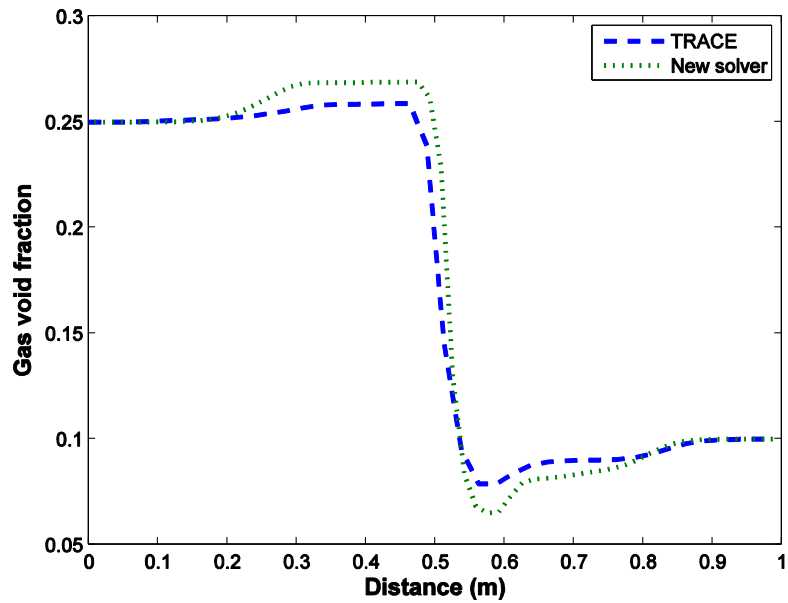


Figure 5.26 Gas void fraction profile for shock tube problem at time=0.5 ms

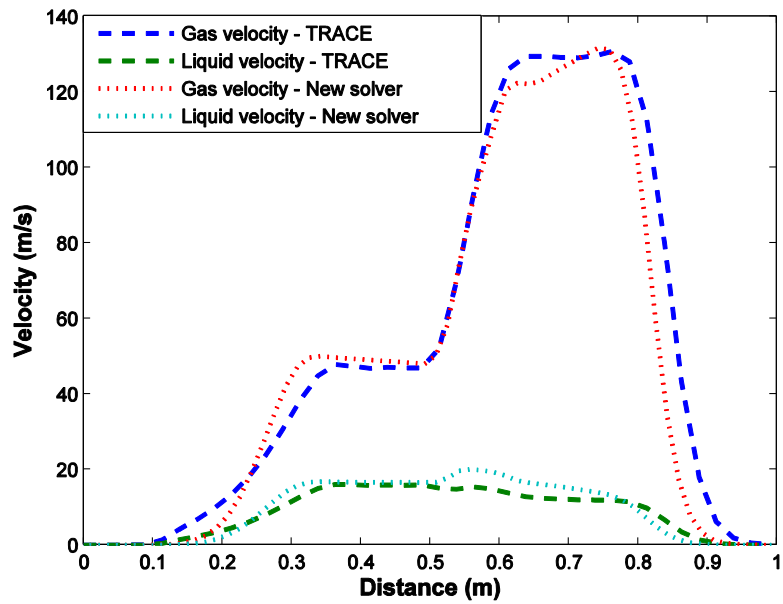


Figure 5.27 Velocity profiles for shock tube problem at time=0.5 ms

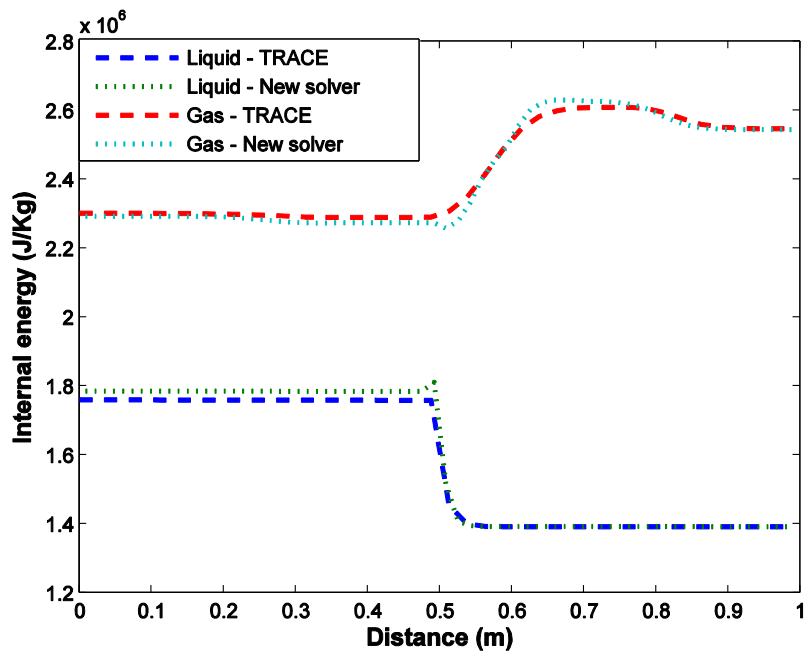


Figure 5.28 Internal energy profiles for shock tube problem at time=0.5 ms

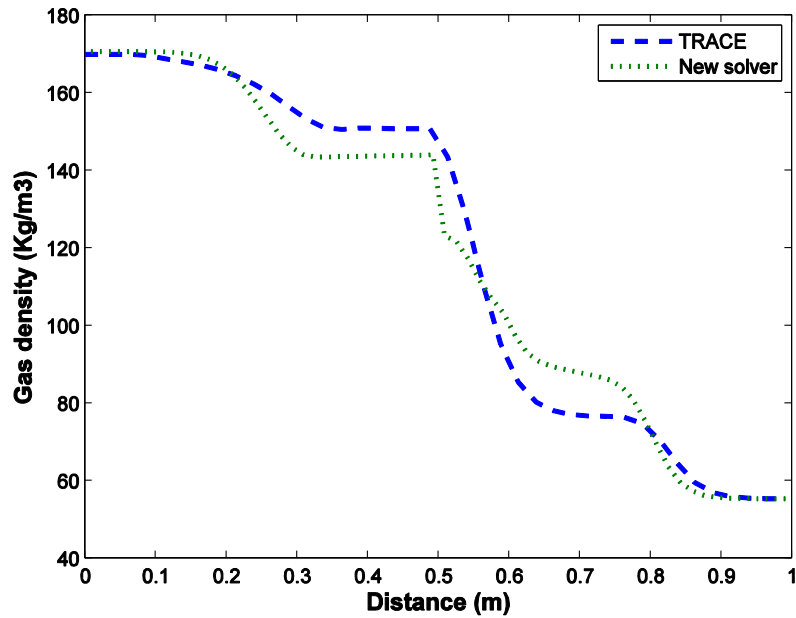


Figure 5.29 Gas density for shock tube problem at time=0.5 ms

Solution profiles for different variables were investigated for different mesh sizes ($N= 20, 40$ and 80). Solution profiles at $t = 0.5$ ms for pressure, void fraction and gas density are shown in Figure 5.30, Figure 5.31 and Figure 5.32 respectively.

Time convergence was also investigated by changing the time step of the simulation. Three time steps were considered ($dt = 10^{-4}, 2.5 * 10^{-5}$ and $6.25 * 10^{-6}$ seconds). Results for pressure, void fraction and gas density are shown in Figure 5.33, Figure 5.34 and Figure 5.35 respectively.

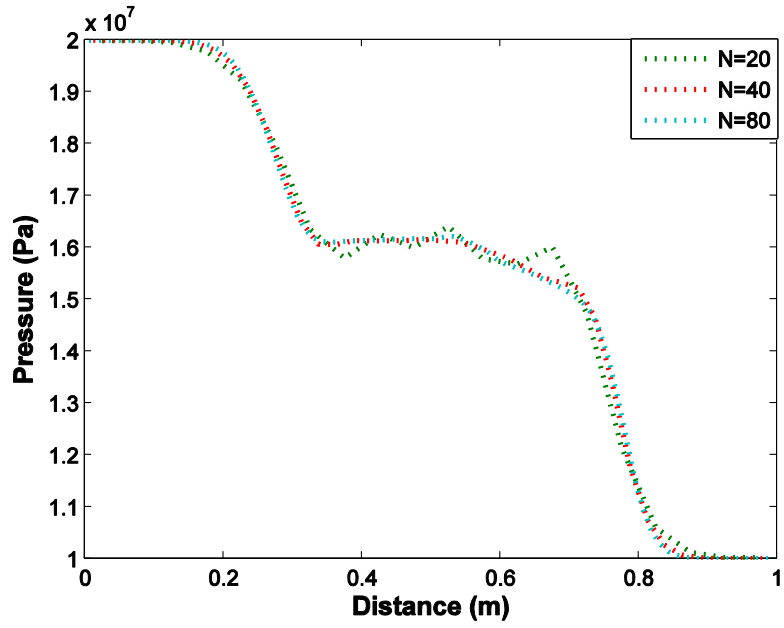


Figure 5.30 Pressure profile for shock tube problem at time=0.5 ms for different mesh sizes

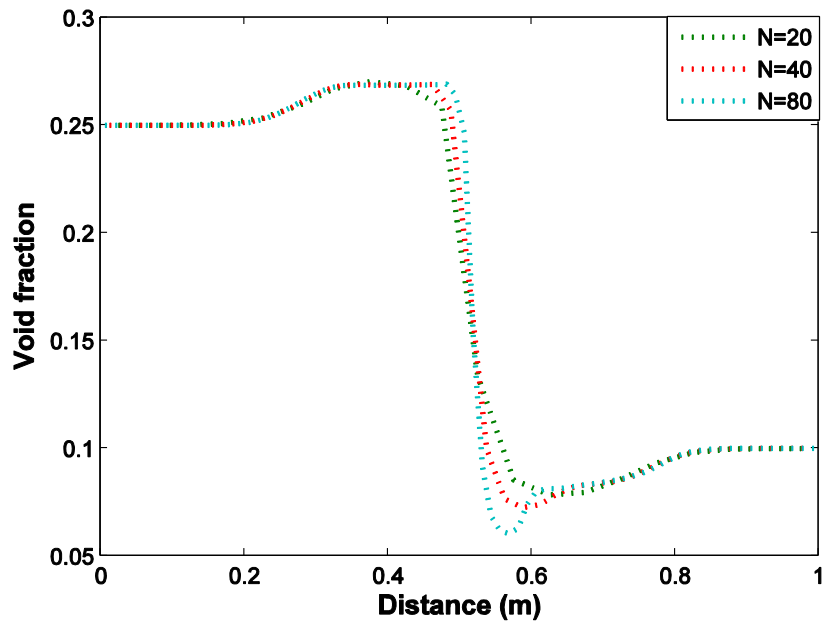


Figure 5.31 Void fraction profile for shock tube problem at time=0.5 ms for different mesh sizes

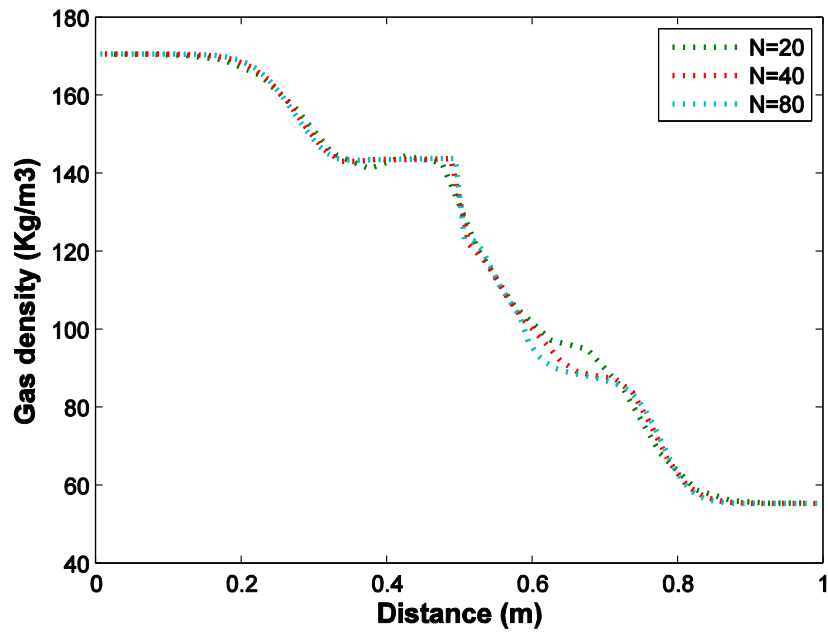


Figure 5.32 Gas density profile for shock tube problem at time=0.5 ms for different mesh sizes

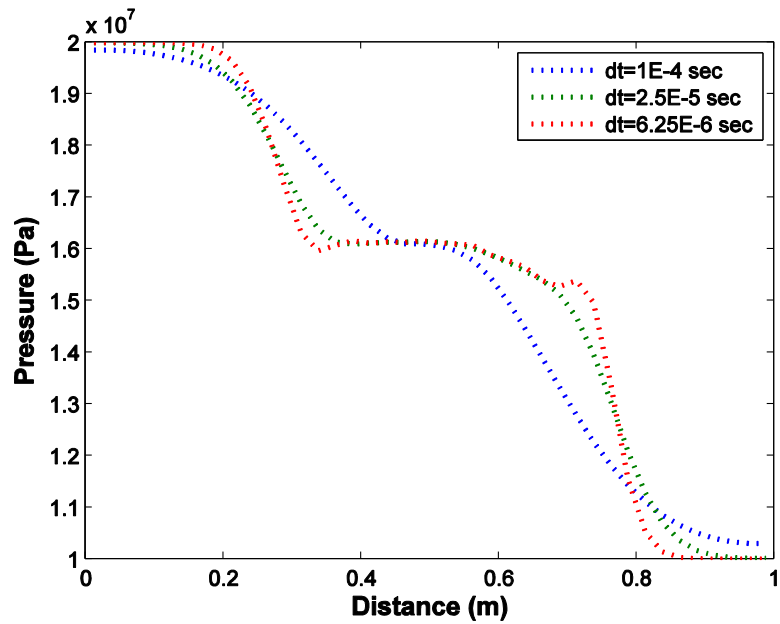


Figure 5.33 Pressure profile for shock tube problem at time=0.5 ms for different time steps

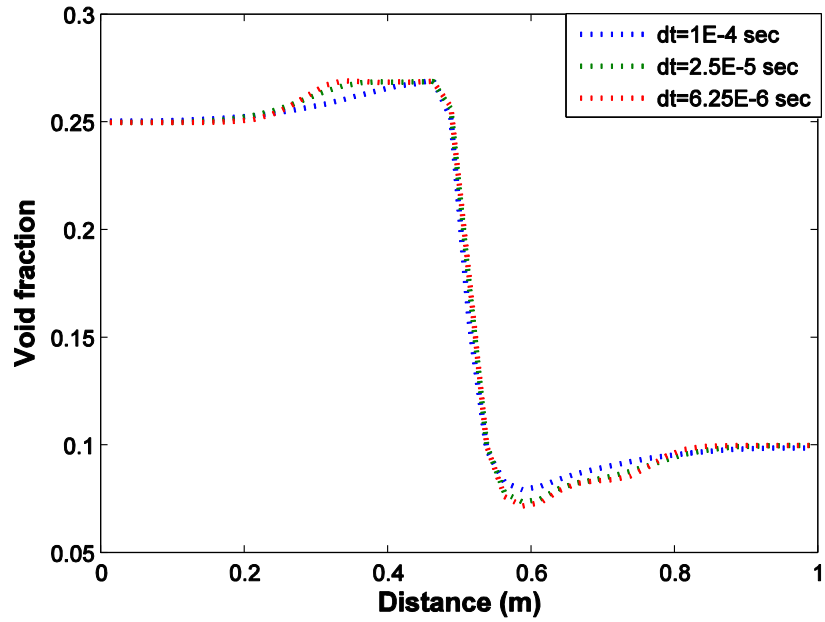


Figure 5.34 Void fraction profile for shock tube problem at time=0.5 ms for different time steps

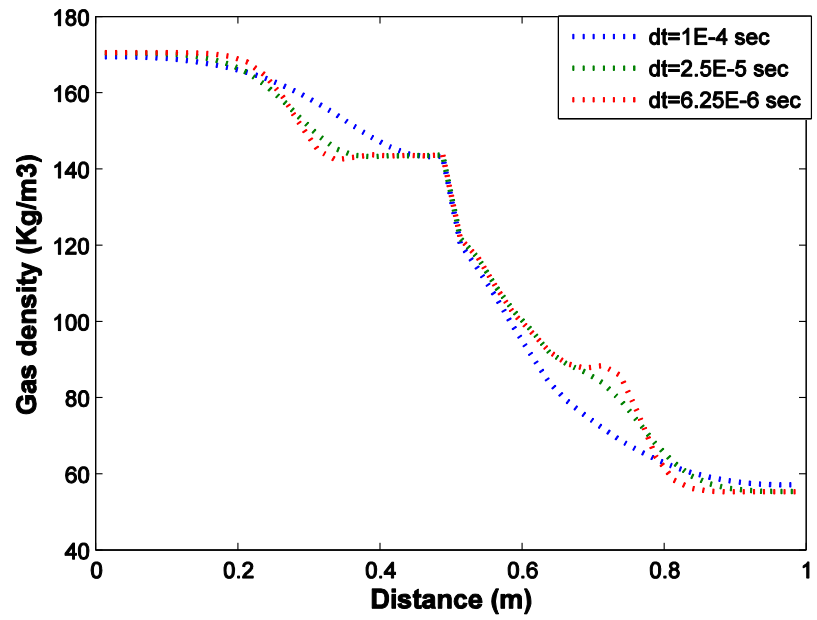


Figure 5.35 Gas density profile for shock tube problem at time=0.5 ms for different time steps

The two-phase shock tube problem is also used to compare the 1st-order upwind scheme to the new scheme developed in Chapter 4. This is done by comparing the mass error of the solver due to each scheme. Because both ends of the pipe are kept closed, the total mass of the system is ideally constant. Any change in the total mass of the system is considered a type of error. This error can be related to many sources, like the numerical scheme, the non-linear solver, or any other source in modeling the problem. To account for the error due to the numerical scheme, the mass error was observed by changing only the mesh size for the simulation. Three mesh sizes were examined: 40, 80 and 160 cells, corresponding to spatial step sizes of: 0.025, 0.0125 and 0.00625 m, respectively. Accuracy was assessed by calculating the percentage mass error as follows:

$$MassError = 100 * \frac{|M^f - M^i|}{M^i} \quad (5.42)$$

where M^f is the total mass of the system at the end of the transient and M^i is the total mass of the system at the beginning of the transient. The convergence rate is represented by a log-log plot of the mass error versus mesh size. Figure 5.36 shows the results of the spatial convergence of both schemes. We can observe that the solver with the new scheme exhibits better rate of convergence as compared to the 1st-order upwind scheme.

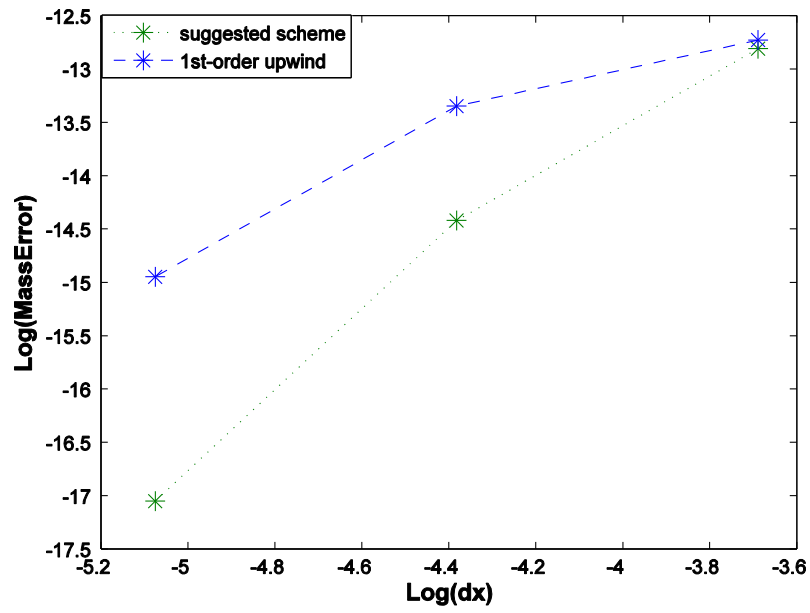


Figure 5.36 Convergence rate for the shock tube problem

CHAPTER 6. CONCLUSIONS AND RECOMMENDATIONS FOR FUTURE WORK

6.1 Summary and Conclusions

Modeling two-phase flows is a crucial topic in terms of safety and operation of nuclear reactors. There continues to be a significant amount of research dedicated to improvement of current methods and models for such simulations. Some of this work targets the ill-posed two-fluid model used in most nuclear thermal-hydraulics codes. Other work is targeted towards the numerical schemes used to discretize the mathematical model and the solvers used for the discretized non-linear system of equations. The scientific contribution presented in this dissertation is a new and original numerical method for the two-fluid model used in 1D system codes, with improved accuracy and stability relative to the currently available numerical schemes used in the two-phase simulation.

By adapting the flux limiters approach, a new high-resolution total variation diminishing scheme was derived by implementing a hybridization of the monotone 1st-order upwind scheme and the Quadratic Upstream Interpolation scheme (QUICK). The combination of the 1st-order upwind scheme and QUICK scheme was done by means of a flux limiting function, which depends on the smoothness of the solution. Constraints were imposed to make the resulting scheme TVD and high-order in smooth regions of the solution. For temporal discretization, the generalized Crank-Nicolson method characterized by the parameter θ was used.

Results from the proposed scheme were compared for the one-dimensional linear advection equation to classical and other popular high-resolution schemes. Convergence rate for the new scheme was investigated for smooth and discontinuous solutions. The new scheme was shown to exhibit better results as compared to other schemes. It is shown that high-resolution schemes based on 2nd-order Lax-Wendroff discretization (with Minbee and Superbee limiters) exhibit a convergence rate of about 1.0 for smooth solutions and 0.5

for discontinuous solutions. The new scheme developed in this thesis exhibits a convergence rate of about 1.3 for smooth solutions and 0.8 for discontinuous solutions. In the case of discontinuous solutions, the new method derived here showed better convergence rate compared to all schemes investigated in this research. In general, the parameter $\theta = 1/2$ (Crank-Nicolson method) yielded better results than the case of $\theta = 1$ (implicit method), with less numerical dissipation.

Finite volume techniques based on staggered mesh and different numerical schemes (including the new numerical scheme) were used to develop a high-order solver for the two-phase two-fluid model. Numerical derivatives for the linearized closure relations were calculated using water properties based on the IAPWS IF-97 standard. A numerical solver based on Newton's method with direct factorization of the Jacobian was used to solve the system of non-linear discrete equations. The new two-phase two-fluid model solver was tested for three benchmark problems: the faucet flow problem, Edward's pipe problem and the shock tube problem.

The analytical solution for the void fraction in the faucet flow problem exhibits propagation of a discontinuity. This is useful to test the solver for its abilities to handle discontinuities in realistic flow conditions. For the 1st-order upwind scheme, the results were smeared due to excessive numerical dissipation; this dissipation was minimum for the case of $\theta = 1/2$ (Crank-Nicolson method). For the 2nd-order upwind scheme, the results exhibited spurious oscillations near the discontinuity, as expected by the Godunov's theorem. Numerical results for the flux limiters schemes showed better agreement with the analytical solution and improved rate of convergence. Numerical solutions were less smeared and exhibited no oscillations near the discontinuity. Results due to the new scheme showed the best agreement with the analytical solution and the best convergence rate relative to the other schemes considered in this research.

The Edward's pipe problem was meant to examine the solver's abilities of handling fast transients with phase change. Results showed flashing of liquid water starting at the open end, and propagating towards the closed end in a form of a rarefaction wave.

The shock tube problem showed the solver's capability to handle fast transients with discontinuities and phase change. Results from this test were compared to those from the USNRC TRACE code, and good qualitative agreement between the two sets of results was observed. Errors in the system's total mass were calculated for two numerical schemes: 1st-order upwind scheme and the new scheme developed in this research. The new scheme showed better reduction in mass error as compared to the 1st-order upwind scheme.

6.2 Future Work

The effort done in this research can be improved and extended in different ways to tackle complicated problems associated with simulating two-phase flows in nuclear reactors in its multiple aspects. The first important improvement is conducting further testing of the numerical method and the solver by applying it to different benchmark problems. This provides better verification for the new numerical scheme and the solver, and serves as a tool to examine its capabilities to handle different types of physics and transients under a wide-range of conditions. This kind of work can be specific to nuclear reactor systems by choosing benchmark problems that mimic two-phase flows in operational and accident conditions of nuclear reactors. Results from this work can also be compared to those of the Loss-Of-Fluid Tests (LOFT) for validation.

The second important extension to this work is a multidimensional analysis of the problem (2D and 3D). As sufficient as 1D analysis is for many nuclear reactor systems, higher dimensions have to be considered to capture different physics and flow regimes. In this case one can account for interface tracking between the two phases and explicitly solve for different flow regimes rather than assuming a mixture of the two

phases at each cell. The new numerical scheme developed in this research can be combined with different interface tracking or capturing methods such as the front tracking method and the level set method to develop a high-order multidimensional solver. Before such implementation can be done, a study has to be carried out to prove the feasibility of the new scheme in terms of stability and accuracy if implemented in higher dimensions.

The third extension is to include core neutronics modeling in the solver. This means adding the neutron diffusion or transport equation to the model as well as the point kinetics model and performing proper coupling with the energy equation. By doing so, the solver will be able to handle a wider variety of problems and physics related to nuclear reactor systems, and coupling with external neutronics codes would not be needed. However, one should pay attention for the large difference in the time scales of the two physics. Neutronics physics occur at much smaller time scales than those of the thermal-hydraulics ones.

APPENDIX A.

MODIFIED EQUATION ANALYSIS FOR THETA METHOD

Taylor's series expansion:

$$q(z) = q(0) + z \frac{\partial q}{\partial z} + z^2 \frac{\partial^2 q}{\partial z^2} + \frac{z^3}{6} \frac{\partial^3 q}{\partial z^3}$$

We first assume:

$$x = x_0 + \alpha_0 z \rightarrow \alpha_0 = (x - x_0)/z$$

$$t = t_0 + \alpha_1 z \rightarrow \alpha_1 = (t - t_0)/z$$

$$q(x, t) = q(z)$$

Using the chain rule:

$$\frac{\partial q}{\partial z} = \frac{\partial x}{\partial z} \frac{\partial q}{\partial x} + \frac{\partial t}{\partial z} \frac{\partial q}{\partial t} = \left(\alpha_0 \frac{\partial q}{\partial x} + \alpha_1 \frac{\partial q}{\partial t} \right)$$

$$\frac{\partial^2 q}{\partial z^2} = \left(\alpha_0^2 \frac{\partial^2 q}{\partial x^2} + 2\alpha_0 \alpha_1 \frac{\partial^2 q}{\partial x \partial t} + \alpha_1^2 \frac{\partial^2 q}{\partial t^2} \right)$$

$$\frac{\partial^3 q}{\partial z^3} = \left(\alpha_0^3 \frac{\partial^3 q}{\partial x^3} + 3\alpha_0^2 \alpha_1 \frac{\partial^3 q}{\partial x^2 \partial t} + 3\alpha_0 \alpha_1^2 \frac{\partial^3 q}{\partial x \partial t^2} + \alpha_1^3 \frac{\partial^3 q}{\partial t^3} \right)$$

Now plugging the derivatives from the chain rule into Taylor's series, and using the definitions above, one can expand:

$$\begin{aligned}
q(x_0 + \Delta x, t_0 + \Delta t) &= q(x_0, t_0) + \left(\Delta x \frac{\partial q}{\partial x} + \Delta t \frac{\partial q}{\partial t} \right) \\
&+ \frac{1}{2} \left(\Delta x^2 \frac{\partial^2 q}{\partial x^2} + 2\Delta x \Delta t \frac{\partial^2 q}{\partial x \partial t} + \Delta t^2 \frac{\partial^2 q}{\partial t^2} \right) \\
&+ \frac{1}{6} \left(\Delta x^3 \frac{\partial^3 q}{\partial x^3} + 3\Delta x^2 \Delta t \frac{\partial^3 q}{\partial x^2 \partial t} + 3\Delta x \Delta t^2 \frac{\partial^3 q}{\partial x \partial t^2} + \Delta t^3 \frac{\partial^3 q}{\partial t^3} \right)
\end{aligned} \tag{A.1}$$

$$\begin{aligned}
q(x_0 - \Delta x, t_0 + \Delta t) &= q(x_0, t_0) - \Delta x \frac{\partial q}{\partial x} + \Delta t \frac{\partial q}{\partial t} + \frac{1}{2} \Delta x^2 \frac{\partial^2 q}{\partial x^2} - \Delta x \Delta t \frac{\partial^2 q}{\partial x \partial t} \\
&+ \frac{1}{2} \Delta t^2 \frac{\partial^2 q}{\partial t^2} - \frac{1}{6} \Delta x^3 \frac{\partial^3 q}{\partial x^3} + \frac{1}{2} \Delta x^2 \Delta t \frac{\partial^3 q}{\partial x^2 \partial t} - \frac{1}{2} \Delta x \Delta t^2 \frac{\partial^3 q}{\partial x \partial t^2} \\
&+ \frac{1}{6} \Delta t^3 \frac{\partial^3 q}{\partial t^3}
\end{aligned} \tag{A.2}$$

$$\begin{aligned}
q(x_0 - 2\Delta x, t_0 + \Delta t) &= q(x_0, t_0) + \left(-2\Delta x \frac{\partial q}{\partial x} + \Delta t \frac{\partial q}{\partial t} \right) \\
&+ \frac{1}{2} \left(4\Delta x^2 \frac{\partial^2 q}{\partial x^2} - 4\Delta x \Delta t \frac{\partial^2 q}{\partial x \partial t} + \Delta t^2 \frac{\partial^2 q}{\partial t^2} \right) \\
&+ \frac{1}{6} \left(-8\Delta x^3 \frac{\partial^3 q}{\partial x^3} + 12\Delta x^2 \Delta t \frac{\partial^3 q}{\partial x^2 \partial t} - 6\Delta x \Delta t^2 \frac{\partial^3 q}{\partial x \partial t^2} \right. \\
&\left. + \Delta t^3 \frac{\partial^3 q}{\partial t^3} \right)
\end{aligned} \tag{A.3}$$

$$q(x_0, t_0 + \Delta t) = q(x_0, t_0) + \Delta t \frac{\partial q}{\partial t} + \frac{1}{2} \Delta t^2 \frac{\partial^2 q}{\partial t^2} + \frac{1}{6} \Delta t^3 \frac{\partial^3 q}{\partial t^3} \tag{A.4}$$

$$q(x_0 - \Delta x, t_0) = q(x_0, t_0) - \Delta x \frac{\partial q}{\partial x} + \frac{1}{2} \Delta x^2 \frac{\partial^2 q}{\partial x^2} - \frac{1}{6} \Delta x^3 \frac{\partial^3 q}{\partial x^3} \quad (\text{A.5})$$

$$q(x_0 - 2\Delta x, t_0) = q(x_0, t_0) - 2\Delta x \frac{\partial q}{\partial x} + 2\Delta x^2 \frac{\partial^2 q}{\partial x^2} - \frac{4}{3} \Delta x^3 \frac{\partial^3 q}{\partial x^3} \quad (\text{A.6})$$

A.1 Modified equation for theta method with 1st-order upwind (positive velocity):

Starting with the conservative form of the numerical scheme:

$$q_i^{n+1} = q_i^n - \lambda \left(\mathcal{F}_{i+\frac{1}{2}}^n - \mathcal{F}_{i-\frac{1}{2}}^n \right) \quad (\text{A.7})$$

Using the definition of the numerical flux of 1st-order upwind scheme in Eq. (3.27):

$$q_i^{n+1} = q_i^n - \frac{\bar{u}\Delta t}{\Delta x} [\theta(q_i^{n+1} - q_{i-1}^{n+1}) + (1 - \theta)(q_i^n - q_{i-1}^n)] \quad (\text{A.8})$$

This can be written as:

$$\begin{aligned} q(x, t + \Delta t) = & q(x, t) - \frac{\bar{u}\Delta t}{\Delta x} [\theta(q(x, t + \Delta t) - q(x - \Delta x, t + \Delta t)) \\ & + (1 - \theta)(q(x, t) - q(x - \Delta x, t))] \end{aligned} \quad (\text{A.9})$$

Using the expansion:

$$\begin{aligned} \frac{\partial q}{\partial t} + \bar{u} \frac{\partial q}{\partial x} = & \frac{\bar{u}\Delta x}{2} \frac{\partial^2 q}{\partial x^2} - \bar{u}\Delta t\theta \frac{\partial^2 q}{\partial x\partial t} - \frac{1}{2}\Delta t \frac{\partial^2 q}{\partial t^2} - \frac{\bar{u}\Delta x^2}{6} \frac{\partial^3 q}{\partial x^3} + \frac{\bar{u}\Delta t\Delta x\theta}{2} \frac{\partial^3 q}{\partial x^2\partial t} \\ & - \frac{\bar{u}\Delta t^2\theta}{2} \frac{\partial^3 q}{\partial x\partial t^2} - \frac{1}{6}\Delta t^2 \frac{\partial^3 q}{\partial t^3} \end{aligned} \quad (\text{A.10})$$

From the original equation:

$$\frac{\partial q}{\partial t} = -\bar{u} \frac{\partial q}{\partial x} \quad (\text{A.11})$$

$$\frac{\partial^2 q}{\partial t^2} = -\bar{u} \frac{\partial}{\partial t} \left(\frac{\partial q}{\partial x} \right) = -\bar{u} \frac{\partial}{\partial x} \left(\frac{\partial q}{\partial t} \right) = -\bar{u} \frac{\partial}{\partial x} \left(-\bar{u} \frac{\partial q}{\partial x} \right) = \bar{u}^2 \frac{\partial^2 q}{\partial x^2} \quad (\text{A.12})$$

$$\frac{\partial^3 q}{\partial t^3} = \frac{\partial}{\partial t} \left(\bar{u}^2 \frac{\partial^2 q}{\partial x^2} \right) = \bar{u}^2 \frac{\partial^2}{\partial x^2} \left(\frac{\partial q}{\partial t} \right) = \bar{u}^2 \frac{\partial^2}{\partial x^2} \left(-\bar{u} \frac{\partial q}{\partial x} \right) = -\bar{u}^3 \frac{\partial^3 q}{\partial x^3} \quad (\text{A.13})$$

If we substitute Eqs. (A.11)-(A.13) into Eq. (A.10), we get:

$$\begin{aligned} \frac{\partial q}{\partial t} + \bar{u} \frac{\partial q}{\partial x} &= \left(\frac{\bar{u} \Delta x}{2} + \bar{u}^2 \Delta t \left(\theta - \frac{1}{2} \right) \right) \frac{\partial^2 q}{\partial x^2} \\ &+ \left(\frac{\bar{u}^3 \Delta t^2}{6} - \frac{\bar{u} \Delta x^2}{6} - \frac{\bar{u}^2 \Delta t \Delta x \theta}{2} - \frac{\bar{u}^3 \Delta t^2 \theta}{2} \right) \frac{\partial^3 q}{\partial x^3} \end{aligned} \quad (\text{A.14})$$

A.2 Modified equation for theta method with 2nd-order upwind (positive velocity):

Using the definition of the numerical flux of 2nd-order upwind scheme (Eq. (3.32)) into Eq. (A.7):

$$\begin{aligned} q_i^{n+1} &= q_i^n - \lambda \bar{u} \left[\theta \left(\left(\frac{3}{2} q_i^{n+1} - \frac{1}{2} q_{i-1}^{n+1} \right) - \left(\frac{3}{2} q_{i-1}^{n+1} - \frac{1}{2} q_{i-2}^{n+1} \right) \right) \right. \\ &\quad \left. + (1 - \theta) \left(\left(\frac{3}{2} q_i^n - \frac{1}{2} q_{i-1}^n \right) - \left(\frac{3}{2} q_{i-1}^n - \frac{1}{2} q_{i-2}^n \right) \right) \right] \end{aligned} \quad (\text{A.15})$$

This can be rearranged and written as:

$$\begin{aligned} q(x, t + \Delta t) &= q(x, t) \\ &- \lambda \bar{u} \left[\theta \left(\frac{3}{2} q(x, t + \Delta t) - 2q(x - \Delta x, t + \Delta t) \right. \right. \\ &\quad \left. \left. + \frac{1}{2} q(x - 2\Delta x, t + \Delta t) \right) \right. \\ &\quad \left. + (1 - \theta) \left(\frac{3}{2} q(x, t) - 2q(x - \Delta x, t) + \frac{1}{2} q(x - 2\Delta x, t) \right) \right] \end{aligned} \quad (\text{A.16})$$

Using the expansion we get:

$$\begin{aligned}
& \Delta t \frac{\partial q}{\partial t} + \frac{1}{2} \Delta t^2 \frac{\partial^2 q}{\partial t^2} + \frac{1}{6} \Delta t^3 \frac{\partial^3 q}{\partial t^3} \\
&= -\lambda \bar{u} \left[\theta \left(\frac{3}{2} \left(q(x, t) + \Delta t \frac{\partial q}{\partial t} + \frac{1}{2} \Delta t^2 \frac{\partial^2 q}{\partial t^2} + \frac{1}{6} \Delta t^3 \frac{\partial^3 q}{\partial t^3} \right) \right. \right. \\
&\quad - 2 \left(q(x, t) - \Delta x \frac{\partial q}{\partial x} + \Delta t \frac{\partial q}{\partial t} + \frac{1}{2} \Delta x^2 \frac{\partial^2 q}{\partial x^2} - \Delta x \Delta t \frac{\partial^2 q}{\partial x \partial t} \right. \\
&\quad + \frac{1}{2} \Delta t^2 \frac{\partial^2 q}{\partial t^2} - \frac{1}{6} \Delta x^3 \frac{\partial^3 q}{\partial x^3} + \frac{1}{2} \Delta x^2 \Delta t \frac{\partial^3 q}{\partial x^2 \partial t} - \frac{1}{2} \Delta x \Delta t^2 \frac{\partial^3 q}{\partial x \partial t^2} \\
&\quad \left. \left. + \frac{1}{6} \Delta t^3 \frac{\partial^3 q}{\partial t^3} \right) \right. \\
&\quad + \frac{1}{2} \left(q(x, t) + \left(-2\Delta x \frac{\partial q}{\partial x} + \Delta t \frac{\partial q}{\partial t} \right) \right. \\
&\quad + \frac{1}{2} \left(4\Delta x^2 \frac{\partial^2 q}{\partial x^2} - 4\Delta x \Delta t \frac{\partial^2 q}{\partial x \partial t} + \Delta t^2 \frac{\partial^2 q}{\partial t^2} \right) \\
&\quad + \frac{1}{6} \left(-8\Delta x^3 \frac{\partial^3 q}{\partial x^3} + 12\Delta x^2 \Delta t \frac{\partial^3 q}{\partial x^2 \partial t} - 6\Delta x \Delta t^2 \frac{\partial^3 q}{\partial x \partial t^2} \right. \\
&\quad \left. \left. + \Delta t^3 \frac{\partial^3 q}{\partial t^3} \right) \right) \\
&\quad + (1 - \theta) \left(\frac{3}{2} q(x, t) \right. \\
&\quad - 2 \left(q(x, t) - \Delta x \frac{\partial q}{\partial x} + \frac{1}{2} \Delta x^2 \frac{\partial^2 q}{\partial x^2} - \frac{1}{6} \Delta x^3 \frac{\partial^3 q}{\partial x^3} \right) \\
&\quad \left. \left. + \frac{1}{2} \left(q(x, t) - 2\Delta x \frac{\partial q}{\partial x} + 2\Delta x^2 \frac{\partial^2 q}{\partial x^2} - \frac{4}{3} \Delta x^3 \frac{\partial^3 q}{\partial x^3} \right) \right) \right]
\end{aligned} \tag{A.17}$$

Equation (A.17) can be further simplified into:

$$\begin{aligned}
& \Delta t \frac{\partial q}{\partial t} + \frac{1}{2} \Delta t^2 \frac{\partial^2 q}{\partial t^2} + \frac{1}{6} \Delta t^3 \frac{\partial^3 q}{\partial t^3} \\
&= -\lambda \bar{u} \left[\theta \left(\Delta x \frac{\partial q}{\partial x} + \Delta x \Delta t \frac{\partial^2 q}{\partial x \partial t} - \frac{\Delta x^3}{3} \frac{\partial^3 q}{\partial x^3} + \frac{\Delta x \Delta t^2}{2} \frac{\partial^3 q}{\partial x \partial t^2} \right) \right. \\
&\quad \left. + (1 - \theta) \left(\Delta x \frac{\partial q}{\partial x} - \frac{2}{6} \Delta x^3 \frac{\partial^3 q}{\partial x^3} \right) \right]
\end{aligned} \tag{A.18}$$

Rearrange and substitute $\lambda = \Delta t/\Delta x$ to get:

$$\frac{\partial q}{\partial t} + \bar{u} \frac{\partial q}{\partial x} = \frac{\bar{u}\Delta x^2}{3} \frac{\partial^3 q}{\partial x^3} - \Delta t \bar{u} \theta \frac{\partial^2 q}{\partial x \partial t} - \bar{u} \frac{\Delta t^2 \theta}{2} \frac{\partial^3 q}{\partial x \partial t^2} - \frac{\Delta t}{2} \frac{\partial^2 q}{\partial t^2} - \frac{\Delta t^2}{6} \frac{\partial^3 q}{\partial t^3} \quad (\text{A.19})$$

Using Eqs. (A.11)-(A.13) with some simplification yields the following modified equation:

$$\frac{\partial q}{\partial t} + \bar{u} \frac{\partial q}{\partial x} = \bar{u}^2 \Delta t \left(\theta - \frac{1}{2} \right) \frac{\partial^2 q}{\partial x^2} + \left(\frac{\bar{u}\Delta x^2}{3} - \frac{\bar{u}^3 \Delta t^2}{2} \left(\theta - \frac{1}{3} \right) \right) \frac{\partial^3 q}{\partial x^3} \quad (\text{A.20})$$

APPENDIX B.

ALGEBRAIC WORK FOR THE NEW TVD SCHEME

B-1. Finding the TVD region for $u < 0$

For $u < 0$, if we substitute the numerical fluxes of the 1st-order upwind and the QUICK schemes into Eq. (4.1) and then into Eq. (3.42), and use $\theta = 0$, we obtain the following scheme:

$$q_i^{n+1} = q_i^n - \frac{\Delta t}{\Delta x} u \left[q_{i+1} - q_i + \frac{1}{8} \varphi_{i+\frac{1}{2}} [3q_i - 3q_{i+1} + q_{i+1} - q_{i+2}] - \frac{1}{8} \varphi_{i-\frac{1}{2}} [-3q_i + 3q_{i-1} + q_i - q_{i+1}] \right] \quad (\text{B.1})$$

Equation (B.1) can be rearranged:

$$q_i^{n+1} = q_i^n - \frac{\Delta t}{\Delta x} u \left[1 - \frac{\varphi_{i+\frac{1}{2}}}{8} \left[3 + \frac{(q_{i+2} - q_{i+1})}{(q_{i+1} - q_i)} \right] + \frac{\varphi_{i-\frac{1}{2}}}{8} \left[3 \frac{(q_i - q_{i-1})}{(q_{i+1} - q_i)} + 1 \right] \right] (q_{i+1} - q_i) \quad (\text{B.2})$$

No we define the smoothness parameter:

$$r_i = \frac{(q_{i+2} - q_{i+1})}{(q_{i+1} - q_i)} \quad (\text{B.3})$$

Substituting Eq. (B.3) into Eq. (B.2) yields:

$$q_i^{n+1} = q_i^n - \frac{\Delta t}{\Delta x} u \left[1 - \frac{\varphi_{i+1/2}}{8} [3 + r_i] + \frac{\varphi_{i-1/2}}{8} \left[\frac{3}{r_{i-1}} + 1 \right] \right] (q_{i+1} - q_i) \quad (\text{B.4})$$

Let $v = \frac{-u\Delta t}{\Delta x} > 0$. This is a numerical scheme written in an incremental form (Eq. (3.8)) with the following parameters:

$$C_{i+1/2} = \left(v \left[1 + \frac{\varphi_{i+1/2}}{8} \left[\frac{3}{r_i} + 1 \right] - \frac{\varphi_{i-1/2}}{8} [3 + r_{i-1}] \right] \right), \quad D_{i-1/2} = 0 \quad (\text{B.5})$$

Implementing the conditions for the scheme to be *TVD* (Eq. (3.20)), we obtain the following inequality:

$$0 \leq v \left[1 - \frac{\varphi_{i+1/2}}{8} [3 + r_i] + \frac{\varphi_{i-1/2}}{8} \left[\frac{3}{r_{i-1}} + 1 \right] \right] \leq 1 \quad (\text{B.6})$$

This can be written as:

$$-8 \leq \varphi_{i-1/2} \left[\frac{3}{r_{i-1}} + 1 \right] - \varphi_{i+1/2} [3 + r_i] \leq 8 \left(\frac{1-v}{v} \right) \quad (\text{B.7})$$

At this point we impose the restriction $0 \leq v \leq 1/2$. This yields the following:

$$\left| \varphi_{i-1/2} \left[\frac{3}{r_{i-1}} + 1 \right] - \varphi_{i+1/2} [3 + r_i] \right| \leq 8 \quad (\text{B.8})$$

One condition we require for the limiter function is:

$$\varphi(r) = 0 \text{ for } r < 0$$

This condition yields the following:

$$0 \leq \left(\varphi_{i-\frac{1}{2}} \left[\frac{3}{r_{i-1}} + 1 \right], \varphi_{i+\frac{1}{2}} [3 + r_i] \right) \leq 8 \quad (\text{B.9})$$

From which we obtain the two inequalities:

$$0 \leq \varphi_{i-\frac{1}{2}} \leq \left[\frac{8r_{i-1}}{3 + r_{i-1}} \right] \rightarrow 0 \leq \varphi \leq \frac{8r}{3 + r} \quad (\text{B.10})$$

$$0 \leq \varphi_{i+\frac{1}{2}} \leq \left[\frac{8}{3 + r_i} \right] \rightarrow 0 \leq \varphi \leq \left[\frac{8}{3 + r} \right]$$

This is the same result as found for the case with positive velocity.

B-2. Value of limiter function corresponding to 3rd-order upwind scheme

Starting from Eq. (4.11):

$$q_i^{n+1} = q_i^n - \frac{\Delta t}{\Delta x} u \left[\frac{(5q_i - q_{i-1} + 2q_{i+1})}{6} - \frac{(5q_{i-1} - q_{i-2} + 2q_i)}{6} \right] \quad (\text{B.11})$$

This can be written as follows:

$$q_i^{n+1} = q_i^n - \frac{\Delta t}{\Delta x} u \left[(q_i - q_{i-1}) + \frac{(2q_{i+1} - q_{i-1} - q_i)}{6} - \frac{(2q_i - q_{i-2} - q_{i-1})}{6} \right] \quad (\text{B.12})$$

On the other side, we simplify Eq. (4.5):

$$q_i^{n+1} = q_i^n - \frac{\Delta t}{\Delta x} u \left[1 + \frac{\varphi_{i+\frac{1}{2}}}{8} \left[\frac{3}{r_i} + 1 \right] - \frac{\varphi_{i-\frac{1}{2}}}{8} [3 + r_{i-1}] \right] (q_i - q_{i-1}) \quad (\text{B.13})$$

Substituting: $r_i = \frac{(q_i - q_{i-1})}{(q_{i+1} - q_i)}$ and $r_{i-1} = \frac{(q_{i-1} - q_{i-2})}{(q_i - q_{i-1})}$ into Eq. (B.13), we obtain:

$$q_i^{n+1} = q_i^n - \frac{\Delta t}{\Delta x} u \left[1 + \frac{\varphi_{i+\frac{1}{2}}}{8} \left[\frac{3(q_{i+1} - q_i)}{(q_i - q_{i-1})} + 1 \right] - \frac{\varphi_{i-\frac{1}{2}}}{8} \left[3 + \frac{(q_{i-1} - q_{i-2})}{(q_i - q_{i-1})} \right] \right] (q_i - q_{i-1}) \quad (\text{B.14})$$

This can be simplified as:

$$q_i^{n+1} = q_i^n - \frac{\Delta t}{\Delta x} u \left[(q_i - q_{i-1}) + \frac{\varphi_{i+\frac{1}{2}}}{8} [3q_{i+1} - 2q_i - q_{i-1}] - \frac{\varphi_{i-\frac{1}{2}}}{8} [3q_i - 2q_{i-1} - q_{i-2}] \right] \quad (\text{B.15})$$

To find the value for the limiter function that makes the two Eqs. (B.12) and (B.15) equivalent, we require the two following equations to hold:

$$\varphi_{i+\frac{1}{2}} \left[\frac{3q_{i+1} - 2q_i - q_{i-1}}{8} \right] = \frac{(2q_{i+1} - q_{i-1} - q_i)}{6} \quad (\text{B.16})$$

$$\varphi_{i-\frac{1}{2}} \left[\frac{3q_i - 2q_{i-1} - q_{i-2}}{8} \right] = \frac{(2q_i - q_{i-1} - q_{i-2})}{6} \quad (\text{B.17})$$

Solving for the limiter functions in both equations:

$$\varphi_{i+\frac{1}{2}} = \left[\frac{4(2q_{i+1} - q_{i-1} - q_i)}{3(3q_{i+1} - 2q_i - q_{i-1})} \right] \quad (\text{B.18})$$

$$\varphi_{i-\frac{1}{2}} = \left[\frac{4(2q_i - q_{i-1} - q_{i-2})}{3(3q_i - 2q_{i-1} - q_{i-2})} \right] \quad (\text{B.19})$$

If we consider Eq. (B.18):

$$\varphi_{i+\frac{1}{2}} = \frac{4(q_{i+1} - q_i) \left(2 + \frac{q_i - q_{i-1}}{q_{i+1} - q_i}\right)}{3(q_i - q_{i-1}) \left(3 \left(\frac{q_{i+1} - q_i}{q_i - q_{i-1}}\right) + 1\right)} \quad (\text{B.20})$$

Now we rewrite the expression above in terms of the smoothness parameter $r_i = \frac{(q_i - q_{i-1})}{(q_{i+1} - q_i)}$:

$$\varphi_{i+\frac{1}{2}} = \frac{4(2 + r_i)}{3(3 + r_i)} \quad (\text{B.21})$$

Following same steps for Eq. (B.19), we obtain:

$$\varphi_{i-\frac{1}{2}} = \frac{4(2 + r_{i-1})}{3(3 + r_{i-1})} \quad (\text{B.22})$$

Dropping the subscripts from both equations (Eq. (B.21) and Eq. (B.22)), we obtain the following:

$$\varphi = \frac{4(2 + r)}{3(3 + r)} \quad (\text{B.23})$$

APPENDIX C.

CODE STRUCTURE FOR THE TWO-PHASE TWO-FLUID MODEL SOLVER

The MatLab code developed for the two-phase two-fluid solver can be divided into 7 main blocks:

- 1- **Main code:** In this block, physical constants (Interface heat transfer coefficients, Interfacial friction coefficient, etc.) and numerical parameters (θ , number of spatial cells, time step size, etc.) are defined. It also contains declaration for all the variables in the problem (p, α_g, u_g, Γ , etc.). Initial conditions are also provided in this block. This block also is the main block to solve for the variables of the problem during the transient. It passes current variables to the block “Parafun” and receives a function in a residual form, then, this function is passed to the solver block “nsold” to solve for the new variables at current time step. After receiving back the solution, post processing is done as a final part of this block.
- 2- **Parafun:** This function receives its arguments from the “Main code”. It passes different variables and arrays to different functions, and returns to the “Main code” a function of the new variables in a residual form. Boundary conditions of the problem are also defined in this function.
- 3- **Nsold:** This function by Kelly [35] receives a residual form from the “Main code” along with an initial guess for the solution (Initial guess passed is the solution at previous time step). It also receives other arguments from the “Main code”. These parameters are the relative and absolute error tolerances (For more information about this function refer to Kelly’s book [35]). It returns to the main code the solution for all variables in the residual problem at new time step.
- 4- **State Variables block:** This block covers all functions used to calculate state variables from closure relations (Densities, temperatures, and enthalpies). In this block, there is also the function used to

calculate the interfacial mass transfer and the function used to calculate the numerical derivatives used in the closure relations.

- 5- **Numerical Scheme block:** This block includes all functions used calculate the numerical scheme parameters, like smoothness parameter, the minbee limiter, the superbee limiter, etc.
- 6- **Donored Quantities block:** This block contains all functions used to calculate the donored quantities appearing in the discrete equations of the problem.
- 7- **Numerical Fluxes block:** This block has all the functions used to calculate the numerical fluxes in the system of discrete equations (Equations (5.13), (5.14), (5.17), (5.18), (5.21) and (5.22)).

Tables C.1 – C5 contain a brief description of all functions in each block. The diagram in Figure C. shows the interaction between different blocks of the code.

Table C.1 Main Blocks

Function name	Description
Main_Code	Definition of physical constants, numerical parameters, initial conditions and post processing
ParaFun	Formation of the residual form of discrete equations, and implementation of boundary conditions
nsold	Solving the non-linear system of discrete equations [35]

Table C.2 Numerical Scheme block

Function name	Description
Limiter	Determines which limiter function to use, and which smoothness parameter ($r_{i+1/2}^R$ or $r_{i+1/2}^L$)
CalSP	Calculation of the smoothness parameter (Eq. (5.37) and Eq. (5.38))
Minbee	Calculation of the Minbee flux limiter function
Superbee	Calculation of the Superbee flux limiter function
Kumar	Calculation of Kumar's flux limiter function
Quick	Calculation of the new flux limiter function

Table C.3 State Variables Block

Function name	Description
CalRhog	Calculation of density of gas (Eq. (5.24))
CalRhol	Calculation of density of liquid (Eq. (5.25))
CalTs	Calculation of saturation temperature (Eq. (5.26))
CalTg	Calculation of gas temperature (Eq. (5.27))
CalTl	Calculation of liquid temperature (Eq. (5.28))
Calhgs	Calculation of gas saturation enthalpy (Eq. (5.29))
Calhls	Calculation of liquid saturation enthalpy (Eq. (5.30))
Calhg	Calculation of gas enthalpy (Eq. (5.31))
Calhl	Calculation of liquid enthalpy (Eq. (5.32))
CalGStar	Calculation of interfacial mass transfer and phasic mass transfer enthalpies (Eq. (5.3))
Rho_ders	Calculation of numerical derivatives used for densities closure relations
T_ders	Calculation of numerical derivatives used for temperatures closure relations
h_ders	Calculation of numerical derivatives used for enthalpies closure relations
XSteam	Evaluation of real properties of water [34]

Table C.4 Donored Quantities Block

Function name	Description
CalAlphaDotg	Calculation of donored gas void fraction ($\dot{\alpha}_g$) in Eq. (5.21)
CalAlphaDotl	Calculation of donored liquid void fraction ($\dot{\alpha}_l$) in Eq. (5.22)
CalAlphaRhoDotg	Calculation of the donored quantity $(\rho\dot{\alpha})_g$ in Eq. (5.13)
CalAlphaRhoDotl	Calculation of the donored quantity $(\rho\dot{\alpha})_l$ Eq. (5.14)
CalAlphaRhoEtDotg	Calculation of the donored quantity $(\rho\dot{\alpha}e)_g$ in Eq. (5.21)
CalAlphaRhoEtDotl	Calculation of the donored quantity $(\rho\dot{\alpha}e)_l$ in Eq. (5.22)

Table C.5 Numerical Fluxes block

Function name	Description
CalFcg	Calculation of mass numerical fluxes for gas phase (Eq. (5.13))
CalFel	Calculation of mass numerical fluxes for liquid phase (Eq. (5.14))
CalFeg	Calculation of energy numerical fluxes for gas phase (Eq. (5.21))
CalFel	Calculation of energy numerical fluxes for liquid phase (Eq. (5.22))
CalFmg	Calculation of momentum numerical fluxes for gas phase (Eq. (5.17))
CalFml	Calculation of momentum numerical fluxes for liquid phase (Eq. (5.18))

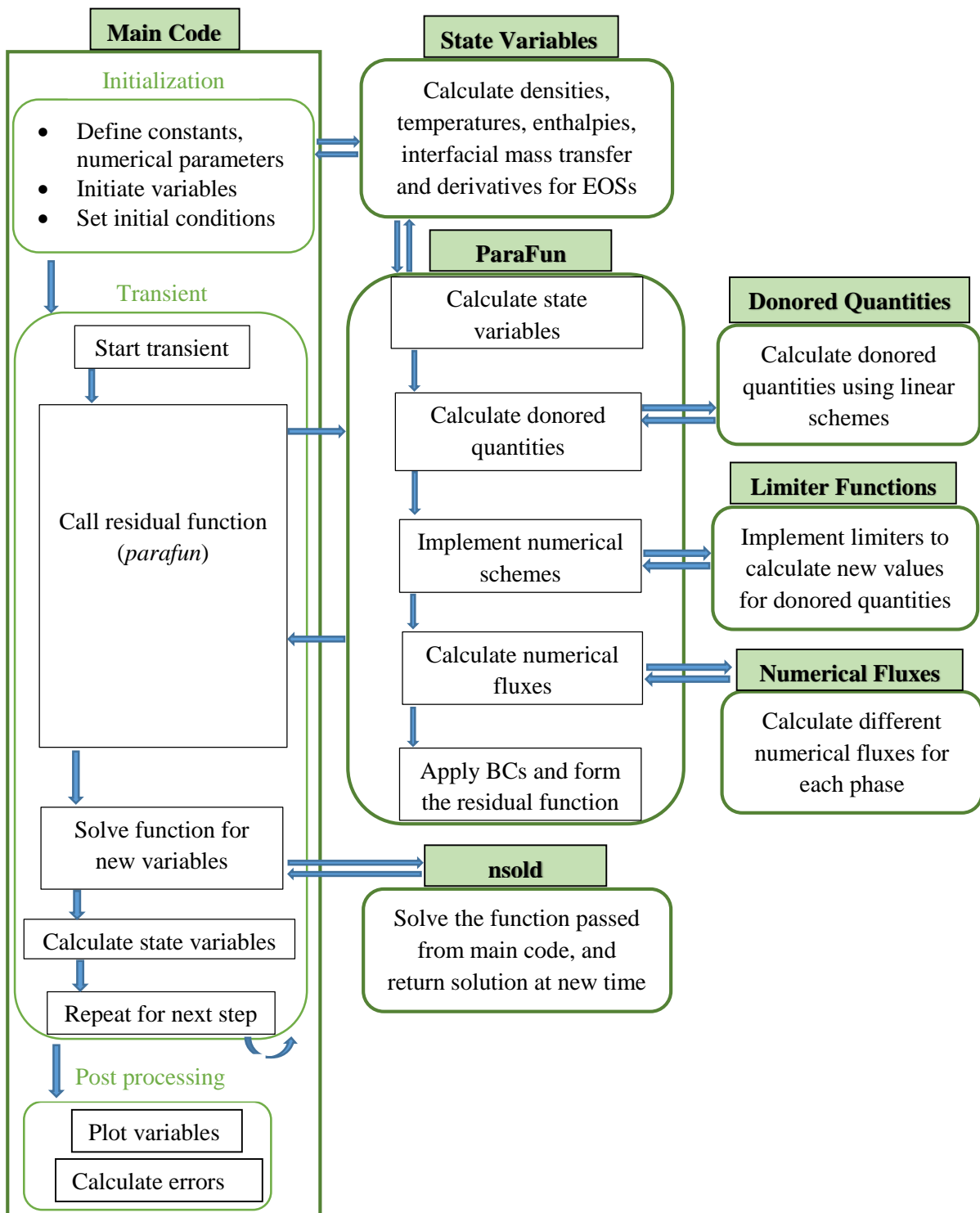


Figure C.1 Interaction between different blocks of the solver code

References

1. Mousseau, V.A., “Implicitly Balanced Solution of the Two-Phase Flow Equations Coupled to Nonlinear Heat Conduction,” *Journal of Computational Physics*, v. 200, 104-132, 2004.
2. Fullmer, W.D., Lopez De Bertodano, M.A. and Zhang, X., “Verification of a High-Order Finite Difference Scheme for the One-Dimensional Two-Fluid Model,” *Journal of Computational Multiphase Flows*, v. 5, 139-156, 2013.
3. Sokolowski, L., Koszela, Z., “RELAP5 Capability to Predict Pressure Wave Propagation Phenomena in Single- and Two-Phase Flow Conditions,” *Journal of Power Technologies*, v. 92, 150-165, 2012.
4. Balcazar, N., Jofre, L., Lehmkuhl, O., Castro, J. and Rigola, J., “A Finite-Volume/ Level-Set Method for Simulating Two-Phase Flows on Unstructured Grids,” *International Journal of Multiphase Flow*, v. 64, 55-72, 2014.
5. Bonometti, T., Magnaudet, J., “An Interface-Capturing Method for Incompressible Two-Phase Flows. Validation and Application to Bubble Dynamics,” *International Journal of Multiphase Flow*, v. 33, 109-133, 2007.
6. Brooks, C.S., Hibiki, T., Ishii, M., “Interfacial Drag Force in One-Dimensional Two-Fluid Model,” *Progress in Nuclear Energy*, v. 61, 57-68, 2012.
7. Yeom, G. S., Chang, K. S., “Numerical Simulation of Two-Fluid Two-Phase Flows by HLL Scheme Using an Approximate Jacobian Matrix,” *Numerical Heat Transfer, Part B: Fundamentals: An International Journal of Computation and Methodology*, v. 49, 155–177, 2006.
8. Wulff, W., “Computer Simulation of Two-Phase Flow in Nuclear Reactors,” *Nuclear Engineering and Design*, v. 141, 303–313, 1993.
9. Division of Systems Research, Office of Nuclear Regulatory Research, US Nuclear Regulatory Commission, Washington, DC 20555-0001. RELAP5/MOD3.3 Code Manual, October 2010.

10. Division of Safety Analysis, Office of Nuclear Regulatory Research, US Nuclear Regulatory Commission, Washington, DC 20555-0001. TRACE V5.0 Theory Manual. Field Equations, Solution Methods, and Physical Models, June 2010.
11. Dinh, T.N., Nourgaliev, R.R., Theofanous, T.G., "Understanding the Ill-Posed Two-Fluid Model," *The 10th International Topical Meeting on Nuclear Reactor Thermal Hydraulics (NURETH-10)*, October 2003.
12. Talpaert, A., "Analysis of Interfacial Forces on the Physics of Two-Phase Flow and Hyperbolicity of the Two-Fluid Model," Master's Thesis, University of Illinois at Urbana-Champaign, 2013.
13. Singh, S., Mousseau, V.A., "On the Hyperbolicity of a One-Dimensional Two-Phase Flow Model for Nuclear Reactor Safety," *Transactions of the American Nuclear Society*, v. 99, 830-832, 2008.
14. Chang, C., et al., "Hyperbolicity, Discontinuities, and Numerics of the Two-Fluid Model," *Proceedings of the 5th Joint ASME/JSME Fluids Engineering Summer Conference, FEDSM 2007 1 SYMPOSIA (part A)*, 635-644, 2007.
15. Leveque, R.J., "Finite Volume Methods for Hyperbolic Problems," 10th edition, Cambridge University Press, 76-78, 109-110, 218, 227-228, 2011.
16. Courant, R., Friedrichs, K.O., Lewy, H., "On the Partial Difference Equations of Mathematical Physics," *IBM Journal*, v. 11, 215-234, 1967.
17. Harten, A., "High Resolution Schemes for Hyperbolic Conservation Laws," *Journal of Computational Physics*, v. 135, 260-278, 1997.
18. Sweby, P. K., Baines, M. J., "On Convergence of Roe's Scheme for the General Non-Linear Scalar Wave Equation," *Journal of Computational Physics*, v. 56, 135-148, 1984.
19. Courant, R., Issacson, E., Rees, M., "On the Solution of Nonlinear Hyperbolic Differential Equations by Finite Differences," *Communication on Pure and Applied Mathematics*, v. 5, 243-255, 1952.

20. Godunov, S. K., "A Difference Method for the Numerical Calculation of Discontinuous Solution of Hydrodynamic Equations," *Mat. Sbornik*, v. 47, 271-306, 1957. Translated as JPRS 7225 by U.S. Dept. of Commerce, pages 36, 41 and 106, 1960.
21. Lax, P.D., Wendroff, B., "Systems of Conservation Laws," *Communications on Pure and Applied Mathematics*, v. 13 (2), 217-237, 1960.
22. Leonard, B.P., "A Stable and Accurate Convective Modeling Procedure Based on Quadratic Upstream Interpolation," *Computer Methods in Applied Mechanics and Engineering*, v. 19 (1), 59-98, 1979.
23. Toro, E.F., "Riemann Solvers and Numerical Methods for Fluid Dynamics: a Practical Introduction," 3rd edition, *Springer Dordrecht Heidelberg*, 480, 512-514, 2009.
24. Colella, P., Woodward, P., "The Piecewise Parabolic Method (PPM) for Gas-Dynamical Simulations," *Journal of Computational Physics*, v. 54, 174-201, 1984.
25. Harten, A., Osher, S., "Uniformly High-Order Accurate Non-Oscillatory Schemes I," *SIAM Journal on Numerical Analysis*, v. 24, 279-309, 1987.
26. Harten A., "Uniformly High-Order Accurate Essentially Non-Oscillatory Schemes III," *Journal of Computational Physics*, v. 71, 231-303, 1987.
27. Liu, X. D., Osher, S., Chan, T., "Weighted Essentially Non-Oscillatory Schemes," *Journal of Computational Physics*, v. 115, 200-212, 1994.
28. Shu, C.W., Osher, S., "Efficient Implementation of Essentially Non-Oscillatory Shock-Capturing Schemes," *Journal of Computational Physics*, v. 77, 439-471, 1988.
29. Waterson, N.P., Deconinck, H., "Design Principles for Bounded Higher-Order Convection Schemes - A Unified Approach," *Journal of Computational Physics*, v. 224, 182-207 (2007).
30. Sweby, P.K., "High Resolution Schemes Using Flux Limiters for Hyperbolic Conservation Laws," *SIAM Journal on Numerical Analysis*, v. 21, 995-1011, Oct. 1984.

31. Kadalbajoo, M. K., Kumar, R., "A High Resolution Total Variation Diminishing Scheme for Hyperbolic Conservation Law and Related Problems," *Applied Mathematics and Computation*, v. 175, 1556-1573, 2006.
32. Higham, D. J., "Mean-Square and Asymptotic Stability of the Stochastic Theta Method," *SIAM Journal for Numerical Analysis*, v. 38, 753-769, 2000.
33. Farago, I., "Convergence and Stability Constant of the Theta Method," *Proc. Of Conference of Applications of Mathematics*, Prague, 2013.
34. Holmgren, M., "XSteam – Properties of Water and Steam for MatLab," 2006, Retrieved November 3, 2012 from <http://www.x-eng.com/>.
35. C.T. Kelley, "Solving Nonlinear Equations with Newton's Method," 1st edition, 27-55, Society for Industrial and Applied Mathematics (2003).
36. Qin, H. Q., "Numerical Benchmark Test 2.1: Faucet Flow," *Multiphase Science and Technology*, v. 6, 577-590, 1992.
37. Edwards, A. R., "Studies of Phenomena Connected with the Depressurization of Water Reactors," *Journal of the British Nuclear Energy Society*, v. 9, 125-135, 1970.
38. Nutter, D. W., O'Neal, D. L., "Modeling the Transient Outlet Pressure and Mass Flow During Flashing of HCFC-22 in a Small Non-Adiabatic Vessel," *Mathematical and Computer Modeling*, v. 29, 105-116, 1999.
39. Toumi, I., "An Upwind Numerical Method for Two-Fluid Two-Phase Flow Models," *Nuclear Science and Engineering*, v. 123, 147-168, 1996.
40. Coquel, F., El Amine, K., Godlewski, E., Perthame, B. and Rascle, P., "A Numerical Method Using Upwind Schemes for the Resolution of Two-Phase Flows," *Journal of Computational Physics*, v. 136, 272-288, 1997.